THE ANALYSIS OF TURBULENT SENSIBLE HEAT FLUXES WITHIN A HETEROGENEOUS BLACK SPRUCE BOREAL FOREST IN ALASKA

By

Derek P. Starkenburg

RECOMMENDED:

_____
Dr. Jordi Cristóbal

_____
Dr. Rudiger Gens

_____
Dr. Douglas L. Kane

_____
Dr. Anupma Prakash
Advisory Committee Co-Chair

_____
Dr. Gilberto J. Fochesatto
Advisory Committee Co-Chair

_____
Dr. Uma Bhatt
Chair, Department of Atmospheric Sciences

APPROVED:

_____
Dr. Paul Layer
Dean, College of Natural Science and Mathematics

_____
Dr. John Eichelberger
Dean of the Graduate School

_____
Date

AN ANALYSIS OF TURBULENT SENSIBLE HEAT FLUXES WITHIN A HETEROGENEOUS BLACK SPRUCE BOREAL FOREST IN ALASKA

A

DISSERTATION

Presented to the Faculty

of the University of Alaska Fairbanks

In Partial Fulfillment of the Requirements

for the Degree of

DOCTOR OF PHILOSOPHY

By

Derek Starkenburg, M.A.

Fairbanks, AK

May 2015

Abstract

Turbulent sensible heat fluxes within the heterogeneous canopy of a black spruce boreal forest in Interior Alaska are evaluated at three different scales in order to assess their spatial variability, and to determine the feasibility of upscaling locally measured flux values to the landscape scale for modeling applications and climate studies. The first evaluation is performed locally at a single micrometeorological tower in an area of the boreal forest with a mean canopy height of 4.7 m. The data were taken across winter, spring and summer of 2012 from two sonic anemometers, one below the canopy at 3 m above ground, and one above the canopy at 12 m above ground. A multiresolution analysis is used to isolate coherent structures from the turbulent temperature time series at both instruments. When mean global statistics of coherent structures are analyzed at the two levels independently, results show an average of 8 structures per period, a mean duration of 85 s, and a mean sensible heat flux contribution of 48%. A spectral version of the Stokes parameters is applied to the turbulent horizontal wind components to show that 31% of the coherent turbulent structures detected at 12 m, and 13% at 3 m, may be complicated by canopy waves due to the prevalence of stable flows at this high latitude location. A most remarkable finding is that less than 25% of the coherent structures detected at these two heights occur synchronously, which speaks robustly to the lack of flow interaction within only 9 vertical meters of the forest, and to the complexity of the vertical aggregation of sensible heat therein.

The second evaluation quantifies differences in turbulent sensible heat fluxes horizontally between two micrometeorological towers 600 m apart, one in a denser canopy (DC) and the other in a sparser canopy (SC), but under approximately similar atmospheric boundary layer

conditions. Results show that SC is ~ 3 ^{o}C cooler and more stably stratified than DC during nighttime. This suggests that changes in the height and density of the canopy impact local temperature and stability regimes. Most importantly, the sensible heat flux at DC is greater during midday periods, with that difference exceeding 30% of the measured flux and over 30 W m^{-2} in magnitude more than 60% of the time. This difference is the result of higher mechanical mixing due to the increased density of roughness elements at DC. Furthermore, the vertical distribution of turbulent heat fluxes verifies a maximum above the canopy crown when compared with the levels below and well above the canopy. These spatial variations of sensible heat flux result from the complex scale aggregation of energy fluxes over a heterogeneous canopy, and suggest that locally measured fluxes will likely differ from large-scale area averaged values.

The third evaluation compares locally measured sensible heat fluxes from a sonic anemometer atop a 24 m micrometeorological tower to those derived from a large aperture scintillometer (LAS) whose beam is centered near the tower at an average height of 36 m above ground, and over a path length of 1423 m. This analysis focuses on unstable daytime periods from June, July and August of 2013. The daytime is defined as 0700-2000 Alaska Standard Time, since local sensible heat flux values derived from the sonic anemometer (H_{EC}) are robust (above 50 W m^{-2}) during this time, and since this time also agrees with the minima in the mean diurnal pattern of C_n^2 from the LAS. For daytime periods with robust sensible heat flux values, H_{EC} and the large-scale flux from the LAS (H_{LAS}) correlate with R^2 = 0.68, while H_{EC} captures about 82% of H_{LAS} on average. The magnitude of H_{EC} and H_{LAS} are both strongly sensitive to incoming solar radiation, with H_{LAS} having a better correlation and regression slope, suggesting

that the local measurements are adjusting also to surface and/or flow conditions above the heterogeneous canopy. Evaluation of the magnitude of the ratio of H_{EC}/H_{LAS} for days with varying amounts of solar radiation suggests that while radiation affects the magnitude of H_{EC} and H_{LAS} independently, it does not affect their ratio. For daytime periods with lower fluxes (H_{EC} between 10 and 50 W m^{-2}), H_{EC} captures about 69% of H_{LAS} on average. However, local and large-scale fluxes during this low flux regime correlate poorly with incoming solar radiation ($R^2 = 0.42$ for H_{LAS} and $R^2 = 0.15$ for H_{EC}), and with one another ($R^2 = 0.27$), suggesting that local heterogeneities are not well-integrated into the large-scale flux. Therefore, low flux periods should be considered separately for the purposes of upscaling local to landscape scale flux values in the boreal forest. For the high flux regime, a finer resolution of upscaling can be provided based on the mean diurnal pattern of H_{EC}/H_{LAS} and the Obukhov length (L). Namely, as the boundary layer becomes less unstable in late afternoon, H_{EC}/H_{LAS} increases, supporting that the eddy covariance technique can capture more of the large-scale flux when the boundary layer is more shear-driven (less buoyancy driven).

Table of Contents

Page

Page

Page

List of Figures

Page

Page

List of Tables

Page

Chapter 1 Introduction

The purpose of this research is to improve the characterization of the exchange of energy between the Alaskan boreal forest and the atmosphere, since it is this exchange that drives the local climatology and connects this biome to the global climate system [*Chapin et al.,* 2000]. Understanding surface-atmosphere interactions at the present time will improve future predictions of precipitation and temperature regimes, both of which are strongly impacted by climate change via complex feedbacks and nonlinear interactions. Climate change is especially critical in the high latitudes where thawing permafrost dramatically affects the landscape and its biome [*Osterkamp et al.,* 2000, 2009; *Jorgenson et al.,* 2001, 2006]. Other impacts of climate warming include reduced snow cover [*Wendler and Shulski,* 2009], a growing number of wildfires [*Johnson*, 1996; *Randerson et al.,* 2006; *Duffy et al.,* 2007] and attendant alterations to the regional and large-scale hydrology [*Hinzman and Kane,* 1992; *Woo et al.,* 2008; *Rawlins et al.,* 2010], all of which impact the magnitude and timing of the fluxes of energy and moisture between the surface and the atmosphere. While sensible and latent heat fluxes drive local processes in the boreal forest, fluxes of carbon dioxide (CO_2) and methane (CH_4) have global impacts [*Chapin et al.,* 2000]. Some studies suggest that boreal forests may be sources of CO_2 during climate warming [*Chapin et al.,* 2006], however others suggest that increased plant productivity may draw down CO_2 [*Kimball et al.,* 2006]. The response of the boreal forest to climate forcing is therefore complex, and our research in this area is far from complete [*Chapin et al.,* 2000, 2005; *Wilmking et al.,* 2004; *Ueyama et al.,* 2010]. In particular, the high sensitivity of the boreal forest to changes in the climate system prompts feedbacks that require additional

study [*Chapin et al.*, 2000; *Chapin et al.*, 2006]. Given that the boreal forest comprises one third of all Alaskan vegetation [*Fleming*, 1997] and over 10% of the earth's land cover [*Bonan and Shugart*, 1989], a more in-depth understanding of the exchange of energy between the boreal forest and the atmosphere is critical.

Despite the importance of this research, the boreal forest can be a challenging environment to study. One reason is the high degree of thermal stratification of the boundary layer in interior of Alaska, owing to frequent high pressure combined with strong radiative surface cooling in winter [*Shulski and Wendler*, 2007; *Mayfield and Fochesatto*, 2013]. Furthermore, the blocking of winds by topography contributes to quiescent flows in Fairbanks, especially during the winter season [*Shulski and Wendler*, 2007]. Low winds and stable flows can complicate local scale measurements of surface-atmosphere energy exchange when using sonic anemometer data for traditional eddy covariance techniques [*Acevedo et al.*, 2006], and may also retard the vertical aggregation of energy and matter to larger spatial scales. This can complicate the assessment of the larger area-average sensible and latent heat fluxes, which are often the values required for model validation [*Ward et al.*, 2014].

Quantifying the exchanges of energy and matter in the boreal forest is further complicated by the variability of this ecosystem. In many locations, lakes and hills contribute to the heterogeneity of the boreal forest across the landscape scale. Such irregularities in surface conditions can alter the local turbulent flux regime by creating large, stationary circulation patterns that cannot be easily captured by traditional eddy covariance techniques [*Mahrt*, 1998; *Foken*, 2008; *Foken et al.*, 2010; *Eder et al.*, 2014 (and further citations therein)]. At smaller local scales, the surface of the forest contains discontinuities in permafrost which affect drainage

in organic and mineral soil layers, create complex micro-topographies, and cause abrupt changes in canopy height. Studies show that significant differences in sensible heat flux values can exist between regions representing a similar surface type [*Beyrich et al.,* 2006]. This same problem is likely to exist within the boreal forest, and it is critical to quantify this spatial variation in energy exchange. For instance, it has been shown that failure to account for variability in canopy architecture can lead to incorrect estimations of evapotranspiration rates in weather models [*Sellers et al.*, 1997]. In addition, *Barr et al.*, [2006] showed that the energy balance closure for boreal forests is sensitive to friction velocity, atmospheric stability and time of day. Since the spatial distribution of the forest canopy controls friction velocity, abrupt changes in canopy height and density will likely result in spatial variations in sensible heat flux values. Furthermore, scale gaps between instruments, and the inability of some models to resolve certain spatial scales, demands a clearer understanding of local variations in energy exchange within boreal forests. These local variations will in turn provide insight into the link between the ecosystem and larger scale processes, and their connection to climate and atmospheric modeling.

The remoteness of the high latitudes and the harsh climate in these locations pose a logistical challenge to data collection and intensive observing efforts. It is therefore not surprising that amidst the growing number of micrometeorological towers around the world, the high northern latitudes remain underrepresented. Landscape-scale fluxes can be estimated by remote sensing devices, but the varying spatial and temporal scales of the measuring systems can be problematic, so an improved network of local observations is still important. A variety of techniques have been explored to upscale local micrometeorological measurements to larger spatial scales [*Ueyama et al.*, 2014; *Samain et al.*, 2012; *Xiao et al.*, 2012]. However, the unique

surface and flow heterogeneities of the boreal forest ecosystem suggest that any upscaling approach should be attended by a thorough investigation of the turbulent energy exchange at a variety of scales.

Historically, dimensional analysis and empirical evaluation of the nature of turbulence over homogenous, evenly heated surfaces and within stationary flows has led to the well-adopted Monin-Obukhov similarity hypothesis, which considers a field of turbulent eddies that are stochastic but isotropically distributed in space such that surface layer fluxes have negligible variation with height for several tens of meters [*Arya*, 1988; *Stull*, 1988; *Holton*, 1992]. Such an analysis enables mathematical models of the expected behavior of turbulence by relating turbulent parameters to stability [*Wyngaard et al.*, 1971]. However, in the boreal forest where the canopy has sharp changes in height and density, and where the surface is unevenly heated and the flow complicated by surface roughness, the similarity hypothesis will not optimally apply. The degree of departure from this hypothesis is a key to understanding the lack of ergodicity inherent in boreal forest canopy turbulence, and is therefore a necessary exploration before any generalized methodology can be adapted for adequately modeling the large-scale fluxes.

This research takes a three tier approach for providing in-depth information regarding the nature of the turbulent surface energy exchange in the boreal forest at a variety of scales before ultimately assessing the feasibility of upscaling the local flux to the landscape scale. The focus of this paper is the sensible heat flux, since this is the turbulent flux that can be measured with the most confidence [*Mauder et al.*, 2006]. Chapter 2 presents an analysis of the local turbulent flux regime at a single micrometeorological tower via the behavior of coherent turbulent structures. A novel methodology is used to assess the degree of canopy wave activity due to flow

stratification, so as to evaluate the percentage of turbulent structures which may be complicated by wave-like behavior. The synchronicity of coherent structures between the sub- and above-canopy levels is then used to infer the ability of sensible heat to aggregate vertically. Chapter 3 expands this analysis in the horizontal direction to compare sensible heat fluxes between two micrometeorological towers located about 600 m apart in the west-east direction. These towers are under approximately the same atmospheric boundary layer flow regime, but are located in distinctly different canopy architectures. This provides an estimate to the degree of spatial heterogeneity of the fluxes within a complex canopy. Based on results gleaned from these studies, Chapter 4 compares local sensible heat fluxes derived from the eddy covariance method at a micrometeorological tower (H_{EC}) with the landscape-scale sensible heat fluxes derived from a large aperture scintillometer (H_{LAS}). To evaluate the difference between these values, a careful clustering of high flux daytime data is performed ($H_{EC} > 50$ W m^{-2}) in order to discern a relationship between the local and large-scale flux values under optimal conditions, and the sensitivity of the two fluxes to solar radiation is evaluated to see the effects of the heterogeneous surface on the response of both instruments to higher values of incoming solar energy. A smaller clustering of a lower flux regime where H_{EC} is between 10 and 50 W m^{-2} is also evaluated to elucidate the relationship between H_{EC} and H_{LAS} under conditions when local heterogeneities may not be well-integrated into the large-scale flux due to a weak fluxing regime. For the high flux regime, a finer resolution of upscaling is also presented which shows the mean diurnal pattern of H_{EC}/H_{LAS} as a function of dynamic stability.

Chapter 2 The Role of Coherent Flow Structures in the Sensible Heat Fluxes of an Alaskan Boreal Forest[1]

Abstract

Accelerations in the flow over forests generate coherent structures which locally enhance updrafts and downdrafts, forcing rapid exchanges of energy and matter. Here, observations of the turbulent flow are made in a highly heterogeneous black spruce boreal forest in Fairbanks, Alaska at ~2.6 h (12 m) and ~0.6 h (3 m), where h is the mean canopy height of 4.7 m. Wavelet analysis is used to detect coherent structures. The sonic temperature and wind data cover 864 half-hour periods spanning winter, spring and summer. When mean global statistics of structures are analyzed at the two levels independently, results are similar to other studies. Specifically, an average of 8 structures occurs per period, their mean duration is 85 s, and their mean heat flux contribution is 48%. However, this analysis suggests that 31% of the structures detected at 2.6 h, and 13% at 0.6 h, may be influenced by wave-like flow organization. Remarkably, less than 25% of the structures detected occur synchronously in the subcanopy and above canopy levels, which speaks robustly to the lack of flow interaction within only 9 vertical meters of the forest.

[1] Starkenburg, D., G. J. Fochesatto, A. Prakash, J. Cristóbal, R. Gens, and D. L. Kane (2013), *J. Geophys. Res. Atmos., 118* (15), 8140-8155.

2.1 Introduction

2.1.1 The Boreal Forest

The analysis of the surface energy balance in the subarctic Alaskan interior is critical for understanding current conditions, and for predicting future trends in surface biogeochemical and hydrological processes, water availability, and energy transfer. The boreal forest comprises 11% of Earth's land surface [*Bonan and Shugart*, 1989], and specifically, the boreal spruce forest accounts for 33% of Alaskan vegetation [*Fleming*, 1997]. Cold temperatures, discontinuous permafrost, and aridity make the boreal forest unique, but at the same time vulnerable to climate change [*Chapin et al.*, 2006]. In turn, this vulnerability can alter the forest directly or indirectly by promoting feedbacks to an extent not yet fully understood [*Chapin et al.*, 2000]. The boreal forest is coupled directly to its local environment through sensible and latent heat fluxes, and surface albedo; it is also coupled to global climate through the fluxes of carbon dioxide (CO_2) and methane (CH_4) [*Chapin et al.*, 2000]. Some studies have shown that boreal forests may be potential sources of CO_2 during climate warming [*Chapin et al.*, 2006], while others suggest that they may become sinks due to increasing plant productivity [*Kimball et al.*, 2006]. Ultimately, many studies elucidate the complexity of the boreal forest, suggesting a non-uniform response to large-scale forcing [*Chapin et al.*, 2000, 2005; *Wilmking et al.*, 2004; *Ueyama et al.*, 2010].

Quantification of exchanges of energy and matter in the boreal forest is difficult because of the extent and variability of this ecosystem, as well as the remoteness of the high latitudes. Remote sensing can provide estimates of large-area fluxes in remote locations, but those estimates are based on the spatial and temporal scales of the measuring systems and thus vary one from another. One solution is to upscale local micrometeorological measurements to larger

spatial scales in order to acquire an optimum representation of land-atmosphere interactions [*Samain et al.*, 2012]. However, any such upscaling process in the boreal forest needs to consider the heterogeneity of canopy density and height, as well as non-stationary flows. Spatial and temporal lags in the storage and release of heat from within the forest [*Arya*, 1988] are also critical. For example, *Turner et al.* [1994] compared a heat flux contour diagram produced via wavelet analysis for three levels above a boreal black spruce forest in Quebec, Canada during the month of August. They found that under stable conditions in early evening, fluxes were generally negative at most levels except for a few areas with a positive flux near the canopy top. They attributed this to the final release of daytime heat that had been held locally within the canopy.

Yet another factor impacting the storage term is the robust thermal stratification accompanied by persistent quiescent flows, both of which are signatures of interior Alaska. Thermal stratification of atmospheric boundary layer flows is common because long winters are characterized by a positive feedback between frequent high pressure systems reinforced by radiative ground cooling [*Shulski and Wendler*, 2007; *Mayfield and Fochesatto*, 2013]. Terrain features also protect local valleys from the stronger winds of adjacent regions, resulting for instance, in mean winds of less than 1 m s^{-1} during December-January in Fairbanks [*Shulski and Wendler*, 2007]. Cold air drainage is also a prominent characteristic in the Alaskan interior which can impact local fluxes [*Fochesatto et al.*, 2013]. For instance, *Lee* [1998] shows that exchange processes in tall canopies are affected by a commonly ignored mass flow component term which results from local rising (sinking) causing convergence (divergence) of a scalar. In this framework, he used observational data from a Canadian boreal forest to substantiate the argument of *Grace et al.* [1996], which states that cold air drainage reduces the local flux of CO_2

above the forest. Neglecting this mass flow of CO_2 will result in underestimates of locally fluxed CO_2, and therefore overestimates of the amount of CO_2 actually available for annual uptake by the forest [*Lee*, 1998]. Thus, extended periods of stratified flow may have unexpected effects on the vertical aggregation of energy and matter to larger spatial scales, effects which may not be visible to models or remote sensing instruments. This motivates further analysis of the trends of fluxes in the boreal forest of Alaska during both winter and the warm season, and reminds one that closure for energy balance models cannot be achieved if microscale processes are evaluated with complete disregard for larger-scale forcing [*Foken*, 2008b; *Foken et al.*, 2010].

2.1.2 Coherent Structures

Exchanges of heat and moisture are driven by the amount of energy available at the canopy-atmosphere interface [*Arya*, 1988]. Under stationary conditions, thermal and mechanical turbulence draw energy from that interface to build fluxes. This turbulence is considered to be dissipative, and therefore is composed of high frequency inertial eddies of stochastic nature [*Stull*, 1988]. In the specific case of forest-atmosphere interaction, however, much of the energy exchange between vegetation canopies and the overlying atmosphere may derive from distinct, intermittent upward (ejection) and downward (sweep) motions [*Raupach and Thom*, 1981; *Raupach*, 1981; *Raupach et al.*, 1996; *Finnigan*, 2000; *Foken*, 2008a]. Evidence of a sweep of warm air from aloft into the cooler forest on a stable night can be found as early as 1936 in the work of Siegel [*Foken*, 2008a]. Later, the ramp-shapes in a scalar series resulting from sweeps and ejections were studied in detail by *Taylor* [1958], who originally hypothesized these ramps to result from "organized thermal structures of considerable vertical extent." Later, *Antonia et al.*

[1979] showed that these ramp features were transported mainly by the local velocity and could therefore be independent of buoyancy forces. Confirming that shear can be their driving force, *Gao et al.* [1989] showed that in the absence of convection (i.e. during near-neutral conditions), ramps over a Canadian deciduous forest still appeared within the time series of water vapor. Furthermore, the ensemble averaged temperature and fluctuating velocity fields analyzed by *Gao et al.* [1989] revealed that these ramps are comprised of distinct (~ 50 s duration) ejection/sweep cycles that can act on a scalar gradient, such as temperature, to produce a miniature frontal boundary (i.e., a microfront). The literature commonly refers to these events as "coherent structures." Quoting *Serafimovich et al.* [2011], a coherent structure is: "… an aperiodic, three-dimensional well-organized low-frequency flow pattern with characteristic forms and lifetimes… which largely differs from the high-frequency turbulence…"

It has been shown that the shear necessary to generate coherent structures derives from the inflection point in the vertical profile of the streamwise velocity that exists due to canopy drag [*Raupach et al.*, 1996]. In the 1800s, Rayleigh showed that such a velocity inflection point makes an inviscid flow unstable, resulting in horizontal vortices whose axes are oriented in the spanwise direction (i.e., perpendicular to the streamwise direction of the flow) [*Bayly et al.*, 1988; *Morland et al.*, 1991]. Gusts in the boundary layer above the canopy can instigate the formation of spanwise vortices [*Finnigan*, 2000; *Finnigan et al.*, 2009]. The fact that spanwise vortices can become three-dimensional has been mentioned and/or investigated by many authors [*Raupach and Thom*, 1981; *Rogers and Moser*, 1992; *Raupach et al.*, 1996; *Finnigan*, 2000; *Finnigan et al.*, 2009]. Large eddy simulations over a canopy by *Finnigan et al.* [2009] suggest how Kelvin-Helmholtz waves at the vegetation-atmosphere interface may develop into

horizontal spanwise vortices that undergo a helical pairing which results in a hairpin-shape configuration; sweeps and ejections are concentrated within the bends of the hairpins, where vertical motion is favored. This enhanced vertical motion magnifies a scalar gradient (in the case of temperature, this forms a microfront). An artistic representation of the evolution of an idealized coherent structure via this process is shown in Figure 2.1. Recent research suggests that an asymmetrical stretching mechanism is what causes the spanwise roller to split and form a lower sweep-generating hairpin, and an upper ejection-generating hairpin that is transported into the above inertial sublayer [*Bailey and Stoll*, 2012]. As our understanding evolves, we find that coherent structures form a total story of canopy-atmosphere interactions; they are tenuous, rapidly-evolving three-dimensional vortex entities that form over roughness elements, the dynamics of which can assist in destroying the scalar gradients contained by the roughness elements themselves.

The significance of coherent structures lies in their ability to contribute to fluxes of energy and matter. *Barthlott et al.* [2007] provide a comprehensive summary of authors who have evaluated the sensible heat flux contribution specifically from coherent structures compared to the total heat flux. They show that heat flux contributions from coherent structures range from as low as 40% [*Lu and Fitzjarrald*, 1994] to almost 90% [*Bergström and Högström*, 1989]. Other forest studies such as Serafimovich et al. [2011] and Thomas and Foken [2007a] suggest even less than 40%. It is clear that as automated detection techniques are applied to larger datasets, the flux contribution from coherent structures becomes more representative of actual conditions, and declines from earlier studies where only a small data set during ideal circumstances was assessed [*Barthlott et al.*, 2007]. Despite that coherent structures are not always the dominant process for

turbulent transport [*Barthlott et al.*, 2007], their contributions can be important, and the degree to which such structures contribute to fluxes in the high latitudes is worth continued investigation.

Earlier, it was explained how shear may produce coherent structures. However, it has also been demonstrated that when convective conditions exist, the organization of turbulent motion can be enhanced by larger convective eddies, or "attached eddies" [*Poggi et al.*, 2004; *Thomas et al.*, 2006; *Thomas and Foken*, 2007b]. Therefore, under highly unstable conditions, any detection of coherent structures may result in a population with contributions from both convective and/or shear processes [*Thomas and Foken*, 2007b]. Furthermore, many authors have stressed that under stable conditions, ramp-like features in a temperature series may be gravity waves, or be strongly influenced by gravity waves [*Paw U. et al.*, 1992; *Lee et al.*, 1997; *Cava et al.*, 2004; *Thomas and Foken*, 2007b; *Serafimovich et al.*, 2010]. Gravity waves and turbulence can have similar frequency spectra, spatial scales, and/or geometric shapes in a scalar time series [*Finnigan et al.*, 1984; *Lee et al.*, 1997; *Cava et al.*, 2004]. The detection of coherent structures should therefore also be expected to be complicated by the presence of waves whenever the flow is stable. While linear waves cannot transport heat energy because vertical velocity is 90° out of phase with temperature, nonlinear waves can transport scalars [*Stull*, 1988], just as do coherent structures. Furthermore, gravity waves have been shown to feed kinetic energy into local turbulence; as such, waves and turbulence can be both synchronous and well correlated [*Finnigan et al.*, 1984; *Nappo*, 2002; *Lu et al.*, 2005]. Gravity waves may also alter the pattern of momentum flux contributions from the sweep and ejection phases of a coherent structure that is occurring at the same time as the wave [*Serafimovich et al.*, 2010]. Whether waves and/or turbulence contribute to sensible heat fluxes, separating these two phenomena is important for

establishing a more complete understanding of canopy layer physics, especially in the subarctic boreal forest where stratified flows are common.

Finally, another consideration regarding the significance of coherent structures is their ability to affect large vertical extents within and above a vegetation canopy synchronously. For cases over a forest canopy, coherent structures may force exchanges between the vegetation and the overlying atmosphere, and may therefore play a role in coupling above and below canopy flows [*Shaw et al.*, 1989; *Thomas and Foken*, 2007a]. Therefore, it is often added to the definition of a coherent structure that it must produce roughly synchronous temperature ramps at multiple levels within and above the forest canopy [*Bergström and Högström*, 1989; *Gao et al.*, 1989; *Shaw et al.*, 1989]. To this end, *Feigenwinter and Vogt* [2005] detect ramp features in three levels above an urban canopy independently, but statistically evaluate only the features that occur within ±25 s of one another at all heights (i.e., those that "dominate the exchange"). The work of *Lu and Fitzjarrald* [1994] locates ramps from anemometer data at one height above the Harvard forest, and then extrapolate that detection to the subcanopy anemometer. Their composited time series revealed that vertical velocity fluctuations were in phase at both levels, suggesting that coherent structures detected above the canopy generally extend into the subcanopy data in their forest.

The objective of this work is to use an automated detection algorithm to extract coherent structures from the turbulent temperature time series in an Alaskan black spruce boreal forest across three seasons at the above canopy and subcanopy levels. From this, we evaluate what physical properties of coherent structures detected in this study are unique to our higher latitude, and then we discern the importance these structures might have in the vertical aggregation of heat fluxes within the forest. The organization of this paper is as follows. Section 2.2 describes

the study site in detail. Section 2.3 describes the quality control procedure applied to the turbulent measurements, the signal processing method to extract turbulent components of the flow, the methodology used to determine turbulent data which may be under the influence of organized wave-like motion, and the multiresolution technique (i.e., wavelet transform) applied to extract the coherent structures themselves. Section 2.4 first treats both measurement levels independently and evaluates all detected structures, including their contributions to the total flux, and their transport efficiencies. Structures influenced by waves are then described. Next, the coherent structures which affect both the above-canopy and subcanopy simultaneously are located and evaluated. Section 2.5 discusses these results in the context of previous studies, and with regard to the environmental and climatic conditions of the subarctic Alaskan boreal forest. Section 2.6 summarizes the salient conclusions.

2.2 Study Area

Fairbanks is located in interior Alaska at 64°49'N latitude and 147°52'W longitude. This region is characterized by an arid continental climate that is isolated from both the wetter and more moderate regime south of the Alaska Range, and from the colder Arctic tundra north of the Brooks Range. The seasonality of the region is extreme (records range from -62°C to +38°C), but long severe winters statistically dominate the short warm summers, resulting in a sub-freezing annual average temperature [*Shulski and Wendler*, 2007]. The micrometeorological site for this analysis is the UAF north campus site. This site is located in the boreal forest north of the Geophysical Institute on the west ridge of the University of Alaska Fairbanks (UAF) at an altitude of 165 m above sea level (Figure 2.2). The overstory is predominantly black spruce

(*Picea mariana*), with a 60% cover density. The understory is composed of small trees, shrubs (*Vaccinium sp., Betula nana, Alnus incana*), and mosses (*Sphagnum sp*.) [*Kitamoto et al.*, 2007]. Soil profiles reveal an organic layer which ranges from 13 to 26 cm deep, underneath which is a mineral layer. The site is underlain by discontinuous permafrost [*Iwata et al.*, 2010].

A forest inventory (Figure 2.3) was undertaken using an aerial image to establish a 200 m grid surrounding the micrometeorological tower, within which 25 equal area transects were identified to perform a tree sampling. The total mean canopy height (h) is 4.7 m, with a standard deviation of ±3.14 m. The lowest mean canopy height is 2.6 m and the tallest is 10.9 m. Additionally, the number of trees within each sample varies greatly, from five to ninety-one. This variability in canopy height and tree density emphasizes the heterogeneity of the boreal forest, resulting from strong biological gradients determined by local factors such as permafrost, slope, and drainage. Within the forest, a micrometeorological tower is equipped with two R.M. Young Model 81000 3D ultrasonic anemometers mounted at 0.6 h (3 m) and 2.6 h (12 m). The anemometers sample at 20 Hz with a threshold of 0.01 m s^{-1} and provide the three velocity components of the air flow (u, v, and w), as well as sonic temperature (T).

2.3 Data Processing and Methods

2.3.1 Data Selection and Quality Control

Due to the extreme contrast between winter and summer in subarctic continental locations, we choose a seasonal clustering of data in lieu of classification by flow-specific conditions such as, for example, stability. From the most complete data sets with the least glaring quality issues, we select a sample of winter, spring and summer days from 2012 (Table 2.1) (at

the onset of this work, fall data was not yet available). Note that in Fairbanks, March is considered a winter month since the average monthly temperature is still well below freezing [*Shulski and Wendler*, 2007]. After selection, we break the set of measurements into half-hour periods for analysis. Despite the concern that varying period lengths are required for the analysis of turbulent fluxes based on differences in the flow regime [*Acevedo et al.*, 2006], 30 min is a generally accepted period of time to allow all turbulent processes to collectively contribute to the total flux, as shown from ogive tests [*Lee et al.*, 2004].

The sonic temperature and velocity time series are de-spiked using an algorithm based on *Vickers and Mahrt* [1997]. Also, periods with confirmed dropouts (sections of data abruptly removed from the local mean by instrument error) are rejected. Prior to extracting the turbulent properties, we perform the streamline coordinate rotation according to *Kaimal and Finnigan* [1994].

2.3.2 Identification of Wave-like Periods

Regarding the concern that gravity waves can complicate the detection of coherent structures, we seek a method to evaluate how wave-like is the flow regime for the periods we consider. *Vincent and Fritts* [1987] demonstrated that the partial correlation of the turbulent components of the horizontal flow (u’ and v’) is a mathematical proxy for the oscillations of gravity waves embedded within the wind field. As such, the traditional Stokes parameters can be adapted to evaluate the degree of polarization (δ) of u’ and v’, which provides a quantitative measure of the degree to which wave-like organization is contributing to the total fluctuation [*Eckermann*, 1996]. We evaluate whether waves act upon specific periods where coherent

structures have been detected, and as such focus our attention in the frequency range in which canopy waves and coherent structures are most likely to coexist (from 0.1 to 0.003 Hz, or event durations of 10 to 300 s) [*Barthlott et al.*, 2007, their Figure 6]. The form of the Stokes parameters used here is adapted from *Vincent and Fritts* [1987] and *Eckermann* [1996], and the set of equations (2.1) to (2.5) describe them:

$$I = A(u_R'^2 + u_I'^2 + v_R'^2 + v_I'^2) \quad \text{total variance} \quad \text{(Eq. 2.1)}$$

$$D = A(u_R'^2 + u_I'^2 - v_R'^2 - v_I'^2) \quad \text{axial anisotropy (difference in variance)} \quad \text{(Eq. 2.2)}$$

$$P = 2\,A(u_R'v_R' + u_I'v_I') \quad \text{linear polarization} \quad \text{(Eq. 2.3)}$$

$$Q = 2\,A(u_R'v_I' - u_I'v_R') \quad \text{circular polarization} \quad \text{(Eq. 2.4)}$$

$$\delta = (D^2 + P^2 + Q^2)^{1/2} / I \quad \text{total degree of polarization} \quad \text{(Eq. 2.5)}$$

Here, the subscripts R and I indicate the real and imaginary parts of the windowed Fourier transform of the turbulent velocity fields (u' and v') within the frequency interval from 0.1 to 0.003 Hz. The coefficient A scales the squared Fourier coefficients to power spectral densities [*Eckermann*, 1996], but its value is ignored here because it self-cancels when δ is calculated. Using this methodology, we evaluate the 30 min mean δ corresponding to each half-hour period in the analysis. Then, applying the criterion of *Lu et al.* [2005], we flag periods where $\delta > 40\%$ as being under possible wave influence, while those with $\delta \leq 40\%$ are flagged as primarily turbulent driven.

To evaluate whether this criterion produces reasonable results, we first note that δ clearly decreases at both the 2.6 h (12 m) and 0.6 h (3 m) levels from winter to summer (Table 2.2), and even has a diurnal cycle during warmer periods wherein larger values of δ occur at night (note

shown). This is logical because higher values of δ are expected during colder periods, where gravity waves are facilitated by the presence of stratified flow conditions [*Nappo*, 2002].

Evaluations of δ as a function of wind direction also corroborate that this criterion is reasonable for evaluating the wave-like behavior of the flow. Specifically, the data for all three seasons combined reveals that the mean wind direction for periods where δ > 40% is typically northerly or westerly. The foothills of the White Mountains rise from ~ 300 to 700 m to the north and west of the study site (Figure 2.2). As shown in *Fochesatto et al.* [2013], shallow cold air masses flow down the Goldstream Valley in winter, undercutting the stagnant air in the valley west of Fairbanks. Any such drainage type flows originating from the hills in any season may "bounce" as they enter the study site under stable conditions, potentially resulting in gravity waves.

2.3.3 Detection of Coherent Structures

Several methods for detecting coherent structures and evaluating the effects of their induced vertical velocity on scalars have been reported [*Shaw et al.*, 1989; *Collineau and Brunet*, 1993a, 1993b; *Thomas and Foken*, 2005; *Barthlott et al.*, 2007; *Thomas and Foken*, 2007a]. Visual identification of ramps in temperature works well for small data sets [*Gao et al.*, 1989; *Barthlott et al.*, 2007]. Alternatively, coherent structures can be analyzed by quadrant analysis whereby plots of a turbulent scalar (*x* axis) and vertical velocity (*y* axis) determine the sign and magnitude of fluxes with coherent ejection and sweep motions [*Raupach and Thom*, 1981; *Bergström and Högström*, 1989; *Gao et al.*, 1989]. While useful for evaluating flux contributions

from organized structures, quadrant analysis alone is inadequate for describing the coherent structures in space and time domains [*Thomas and Foken*, 2005].

Wavelet analysis was first used to detect coherent structures in turbulent flows above forest canopies by *Collineau and Brunet* [1993a], and has since become common practice over forests and other roughness elements [*Lu and Ftizjarrald*, 1994; *Feigenwinter and Vogt*, 2005; *Thomas and Foken*, 2005; *Barthlott et al.*, 2007]. Wavelet analysis has the ability to quantitatively determine the time when coherent structures occur, and also the approximate duration of the structures. For example, *Collineau and Brunet* [1993a] demonstrated that the Mexican-Hat wavelet (MHAT) exhibits a zero-crossing at the microfront location. *Barthlott et al.* [2007] also showed that the zero-crossing point of the MHAT wavelet coefficient, combined with the adjacent minima in the wavelet, can be used to determine the beginning and the end (i.e. the duration, D) of each ramp event. This method for detecting D differs from previous studies. For instance, *Gao et al.* [1989] use the vertical velocity to define D as the zone comprised by a continuous updraft, plus the subsequent continuous downdraft, located at the microfront; this has the weakness that the vertical velocity signal can be noisy and non-monotonic. Other studies use a single value of D that characterizes each period of analysis, centered on the microfront locations [*Lu and Fitzjarrald*, 1994; *Feigenwinter and Vogt*, 2005; *Thomas and Foken*, 2005; *Thomas and Foken*, 2007a, 2007b]. Typically, this value is calculated by time-integration of the wavelet transform to yield the global wavelet power spectrum, the first peak of which (F_{MAX}) characterizes the time scale of the structures that provide the most energy to the turbulent processes, i.e. coherent structures [*Collineau and Brunet*, 1993a]. Then, the peak frequency of the wavelet associated with F_{MAX} is used in conjunction with the time resolution of the data to

generate a single value of D for each period [*Thomas and Foken*, 2005, 2007a, 2007b]. Similarly, [*Lu and Fitzjarrald*, 1994] use twice the dominant wavelet scale associated with F_{MAX}. Using a single value of D for each period, however, will not capture the variations in duration that each ramp feature can possess within an evaluation period. To this end, we find the procedure of *Barthlott et al.* [2007] most appealing and employ this method on our data.

After data quality control (Section 3.1), we proceed as described in steps 1 through 4 in Section 2.3 of *Barthlott et al.* [2007]. The wavelet transform is given by:

$$W_n(s) = \frac{1}{s}\int_{-\infty}^{+\infty} T(t)\Psi\left(\frac{t-n}{s}\right)dt \qquad \text{(Eq. 2.6)}$$

Here, $W_n(s)$ is the continuous wavelet transform of the temperature time series $T(t)$, by the MHAT wavelet, $\Psi(t,s)$, and s is the scale dilation of the wavelet transform. Similarly, n is a position translation [*Collineau and Brunet*, 1993a; *Barthlott et al.*, 2007]. The global wavelet power spectrum, $W(s)$, used to find F_{MAX} as described above, is then given by:

$$W(s) = \int_{-\infty}^{+\infty} |W_n(s)|^2 dn \qquad \text{(Eq. 2.7)}$$

Since small, insignificant changes in temperature can be detected by this procedure, it is necessary to screen the resulting wavelet function so as to eliminate the MHAT wavelets whose amplitudes are less than a prescribed amount [*Barthlott et al.*, 2007]. Based on a series of tests, *Barthlott et al.* [2007] chose to eliminate all wavelets whose amplitudes were not 40% or more of the largest amplitude in that particular series. In this study, threshold values of 20%, 40% and 60% were tested to confirm that the 40% threshold is also reasonable for our study site.

Dynamic stability plays a role in evaluating the duration of each temperature ramp because it determines whether the microfront proceeds or precedes the ejection [*Barthlott et al.*, 2007]. To evaluate dynamic stability, *Barthlott et al.* [2007] use the Obukhov Length (L_*), a

value which determines the relative importance of buoyancy versus mechanical mixing [*Stull*, 1988]. The sign of L_* will be positive for stable flows, and negative for unstable conditions. The concern here is that our data is from a forest canopy, wherein the Monin-Obukhov Similarity Hypothesis on which L_* is predicated may be violated due to heterogeneous conditions and non-stationary flows. Furthermore, since we are calculating L_* as a mean value for each half-hour, it is possible for stability to transition during that time. Therefore, a visual inspection was performed on the results of the boreal forest data to discern if the use of the sign of L_* is valid for determining the duration of the ramp features. After testing 48 half-hour periods, we conclude that using the sign of L_* is a reasonable approach in the present study site (Figure 2.4).

2.4 Contribution to the Total Turbulent Flux by Coherent Structures

The study area is heterogeneous regarding canopy height and density (Figure 2.3), and often experiences quiescent winds and stratified flows. Due to these conditions, we evaluate turbulent data from within and above the canopy with no presupposition that coherent structures at the two heights should necessarily be part of the same event. A qualitative review of the data suggests that while ramp features sometimes occur synchronously in both levels, often they do not. Therefore, we assume that it is possible for coherent structures to be initiated at different canopy heights. Since stratified flow may limit the three-dimensional development of turbulence [*Finnigan et al.*, 1984], coherent structures may not always mature enough to penetrate the entire forest. To this end, we first detect and analyze the properties of all detected structures at each level in the forest independently, including their heat flux contributions and transport efficiencies.

Using the results from the multiresolution wavelet analysis (Section 3.3), the sensible heat flux contribution from coherent structure (F_{COH}) compared to the total eddy-covariance derived sensible heat flux (F_{TOT}), is determined from *Lu and Fitzjarrald* [1994]. Here, F_{COH} is defined as the sum total of sensible heat fluxes from all coherent structures during the entire 1800 s period analyzed according to Eq. 2.8:

$$F_{COH} = \frac{\left\{\sum_1^{N_{COH}} \overline{w'T'} \cdot t|_{COH}\right\}}{\left(\overline{w'T'} \cdot t\right)} \qquad \text{(Eq. 2.8)}$$

where N_{COH} is the number of coherent structures, t is 1800 s, and the subscript (COH) refers to values corresponding only to coherent structures. Note that due to the method for evaluating D, t_{COH} will vary for each coherent structure. Similarly, the value $\overline{w'T'}_{COH}$ for any single coherent structure k is indicated in Eq. 2.9, in which the temporal means of w and T are calculated based on the mean values over the entire analyzed period:

$$\overline{w'T'}_{COH} = \frac{1}{t_{COH}} \sum_k (w_k - \overline{w}) \cdot (T_k - \overline{T})\,|_{COH} \qquad \text{(Eq. 2.9)}$$

The total sensible heat flux including coherent structures and stochastic components (F_{TOT}) is:

$$F_{TOT} = \frac{1}{t} \sum_k (w_k - \overline{w}) \cdot (T_k - \overline{T}) \qquad \text{(Eq. 2.10)}$$

2.4.1 Characteristics of Coherent Structures in the Study Area

Before analyzing the effects of coherent structures on turbulent flow exchanges, it is instructive to review the mean global properties of all of the detected events. Results show that the average number of coherent structures at both levels and across three seasons is about 8 per half-hour period, with seasonal means at the two levels ranging from ~ 7 to 9 (Figure 2.5). This

result aligns with Steiner et al. [2011] who find a median of 5 to 9 events per half-hour period within a mid-latitude deciduous forest. Our results are also similar to *Barthlott et al.* [2007], who find an average of 7 to 11 structures per half-hour period over an open field, and to those of *Feigenwinter and Vogt* [2005], whose analysis above an urban canopy during unstable conditions reveals around 7 to 10 per half-hour period. For this study, the mean number of coherent structures and the standard deviations are both slightly larger during spring (Figure 2.5). Overall, the difference in the mean number of structures between seasons and between the two forest levels is relatively consistent for this study area.

On average, the duration of a coherent structure (D) for both levels and across three seasons is about 85 s, with a slightly higher mean value for summer than for winter or spring (Figure 2.6). Overall, D is consistent between the two levels and across seasons. Other literature had typically shown D to be shorter for forested locations, for instance about 50 s [*Gao et al.*, 1989], 53 to 54 s [*Lu and Fitzjarrald*, 1994], and 10 to 30 s [*Serafimovich et al.*, 2011; *Eder et al.*, 2013]. However, *Steiner et al.* [2011], who also used the *Barthlott et al.* [2007] method over a forest, found large median values of D as well (i.e., 91 to 116 s). Possibly, the dynamic method of determining a unique D for each coherent structure [*Barthlott et al.*, 2007] might be one reason for the statistically larger durations in this and the work of *Steiner et al.* [2011]. Recall that *Gao et al.* [1989] also used a dynamic method, but their analysis was based on vertical velocity. *Eder et al.* [2013] and *Serafimovich et al.* [2011] used a single value of D for each period, as described previously.

When extending this comparison to non-forested sites, one notes that *Barthlott et al.* [2007] found a range of durations over the open field, specifically means of 61 to 65 s for stable

conditions and 83 to 98 s for unstable periods. Similarly, *Feigenwinter and Vogt* [2005] found larger event durations of 90 s over an urban canopy during unstable conditions (again, they used a fixed value of D). Based on this comparison, the mean duration of coherent structures in this study area is larger than for some other forest studies, despite our low mean canopy height. Whether the methodology, the flow conditions and/or the canopy architecture play a role would require further investigation.

Frequency distributions reveal that the range of coherent structure durations becomes slightly smaller in summer (Figure 2.6). This, coupled with the slightly higher means for summer, suggests a subtle shift to consistently longer events during warmer periods where conditions are more likely to be unstable. *Barthlott et al.* [2007] showed that as conditions become unstable, the probability of having longer coherent structures increases. However, for our data this shift is not robust, which implies that the duration of coherent structure in our forest may be less sensitive to stability that in other locations. Frequency distributions also show some bimodality, particularly in the winter data (Figure 2.6a). One reason could be that our data clustering was by season rather than by flow-specific classifications. During winter, we note significant changes in D within the same day, with some periods dominated by lower frequency temperature fluctuations and others with higher frequencies. This variation appears to be related to the presence of breaking gravity waves (low frequencies) and inertial oscillations (higher frequencies), coupled with their ability to penetrate (or not) multiple forest levels.

2.4.2 Flux Contribution and Fluxing Efficiency of Coherent Structures

As previously mentioned, automated detection techniques and larger data sets reveal smaller heat flux contributions than earlier studies [*Barthlott et al.*, 2007], so now it becomes crucial to compare the modern studies across varying landscapes to ascertain if there is a universal importance in coherent structures to the local energy balance. One problem in comparing the heat flux contribution of coherent structures to the total heat flux (F_{COH}/F_{TOT}) is that when turbulence is very low, this quantity can exceed 100% [*Barthlott et al.*, 2007]. *Feigenwinter and Vogt* [2005] also encountered this issue, and attributed it in part to the outward and inward interactions (i.e., noncoherent motions) that can occur in concert with coherent structures. In addition, we also find a high number of small values of F_{COH}/F_{TOT} (i.e., less than 5% at 0.6 h). We isolated the periods where the flux contribution from coherent structures was very small or very large (i.e., 5% and less, or 100% and above). This data, hereafter denoted as $F_{COHextreme}$, clearly populates the tails of the distribution with very low mean fluxes (Table 2.5). Eliminating $F_{COHextreme}$ leaves 748 periods at 2.6 h (12 m), and 657 periods at 0.6 h (3 m) for all subsequent analyses regarding flux contributions and fluxing efficiency.

Results show that the mean flux contribution from coherent structures ranges from about 44% to 53% between the two levels over the seasons (Figure 2.7), which is consistent with the statistical formulation of some larger data sets. For example, *Lu and Fitzjarrald* [1994] found the mean contribution to be about 40% and Steiner et al. [2011] found 44% to 48%, both over mid-latitude deciduous forests. While the mean flux contribution from coherent structures in this study is similar at both the 2.6 h (12 m) and 0.6 h (3 m) levels for summer, there is actually a slightly larger mean heat flux contribution at the 0.6 h (3 m) level during winter and spring (and

overall). Most interesting, however, is the frequency distributions which indicate that the dominant value of coherent flux contributions shifts seasonally from being largest at 0.6 h (3 m) in winter to being largest at 2.6 h (12 m) in summer (Figure 2.7).

Dividing the time that coherent structures were present during a half-hour period (in s), by the total length of a half-hour period (1800 s), provides the time coverage of coherent structures. Across three seasons, we find that coherent structures occupy an average of 36% of each period at both levels. This is similar to the 34 to 38% time coverage found across stability classes by *Barthlott et al.* [2007]. Related to the time coverage is the fluxing efficiency of coherent structures, which is a ratio of their heat flux contribution during a given half-hour period, divided by the percentage of time that they exist within that period; values above (below) 1.0 are considered efficient (inefficient) [*Barthlott et al.*, 2007]. From Figure 2.8, it can be seen that at 2.6 h (12 m), the dominant value of efficiency for coherent structures exceeds 1.0 during all three seasons, while at 0.6 h (3 m), the dominant value of efficiency only exceeds 1.0 during spring (Figure 2.8).

To summarize, we include Table 2.3, which compares our results with those of other studies where wavelet analysis was also used to detect coherent structures. Rows one through six are studies done within forests, the first two of which use the method of *Barthlott et al.* [2007]. The last two rows, shaded in gray, were done in non-forest environments. One finding is that the number of coherent structures is similar for both forest and non-forest regions. This may result from the fact that, despite the types of roughness elements over which the flow travels, coherent structures are self-limiting in that their negative momentum fluxes ultimately destroy the vertical velocity gradients that initiate them.

A primary difference amongst these studies is the duration of structures (D), as was previously discussed. The heat flux contribution by coherent structures also varies, but all are well below the larger values of 75 to 90% given from earlier studies on smaller data sets [*Gao et al.*, 1989; *Bergström and Högström*, 1989]. It is worth mentioning that differences in heat flux contribution may also result from methodology. Specifically, *Eder et al.* [2013] note that studies who use the method of *Lu and Fitzjarrald* [1994] to determine F_{COH}/F_{TOT} (rows 1, 2, 6 and 7) will count all the fluxing within the duration of a structure as a coherent flux, whereas studies who use the method of *Collineau and Brunet* [1993b] (rows 3-5) will average out the turbulent fluxes at scales significantly below the event duration, D. Furthermore, differences in determining D can also impact the amount of flux provided by coherent structures (i.e., longer events yield greater flux contributions). In general, the length of the datasets, season(s) during which the data was collected, data screening criteria, detection/analysis techniques, canopy characteristics and precise measurement heights will scatter results across studies. Considering these differences, results across authors are reasonably consistent. However, the data for this study site contains a strong influence from the wave-like flows associated with stratified regimes, and also a large number of coherent structures that are isolated at only one level.

2.4.3 Analysis of Periods Under the Influence of Wave-like Flow

Frequency distributions for δ at both levels confirm that most of the periods are more turbulent than wave-like, especially during the warmer seasons (Figure 2.9). However, the fraction of actual half-hour periods influenced by waves is significant: 29% at 2.6 h (12 m), and 18% at 0.6 h (3 m) across seasons (Table 2.4). Also, we assume that if a given half-hour period is

wave-like, then all coherent structures detected therein are potentially waves or turbulent features influenced by waves. Based on this assumption, the fraction of actual coherent structures determined to be under a wave influence is about 31% for the 2.6 h (12 m) level and 13% in the 0.6 h (3 m) level across seasons (Table 2.4). Clearly, the 2.6 h (12 m) level consistently shows a higher polarization, implying more wave-like organization of the flow at that level. These results suggest that a significant portion of the coherent structures detected in the boreal forest could be complicated by waves and/or wave-turbulence interactions. As a comparison, *Cava et al.* [2004] evaluated nighttime data over a pine forest in North Carolina and found that while almost 50% of a given night's data may contain canopy waves, a mean of only 6% for the 21 summer evening periods they analyzed were determined to be dominated by canopy waves.

We use this polarization criterion to cluster the flux contributions from coherent structures that are more likely to be purely turbulent (F_{COH}), and contributions from structures more likely to be under the influence of waves (F_{WAVE}) (Figure 2.10). Results across three seasons indicate that the mean flux contributions for F_{WAVE} is about 43% at 2.6 h (12 m) and 55% at 0.6 h (3 m). For F_{COH} the means are 46% at 2.6 h (12 m) and 49% at 0.6 h (3 m). These mean values are not largely different from one another, nor are they much different from the previous evaluation of mean flux contributions of all structures combined (recall Figure 2.7). The standard deviation for F_{WAVE}, however, is more than a 20% increase over the standard deviation of F_{COH} at both levels. This is particularly evident at the 0.6 h (3 m) level (Figure 2.10a), and suggests a slightly broader range of values for F_{WAVE}. This would be consistent with the conclusions of *Cava et al.* [2004], who found that canopy waves broaden the spectrum of the scalar time series in their data.

Clustering all data by δ shows that periods under the influence of waves typically have low mean sensible heat flux values. Table 2.5 compares the statistical parameters regarding the total heat flux for all periods classified as F_{WAVE} ($\delta > 40\%$), and also the same statistical summary for all periods classified as $F_{COHextreme}$ (F_{COH}/F_{TOT} is $\leq 5\%$ or $\geq 100\%$). We note that these two populations are not the same, but they do overlap (i.e., at the 12 m level 22% of F_{WAVE} also meet the criteria of $F_{COHextreme}$; at the 3 m level 48% of F_{WAVE} meet the criteria of $F_{COHextreme}$). What is remarkable is that the mean flux contributions by coherent structures is not much different during wave-influenced periods, when the mean total flux is small, than it is for more turbulent periods when the mean total flux is greater. Thus, we find that the flux contribution by coherent structures is insensitive to the magnitude of the total flux, and therefore does not necessarily assess the importance of the individual structures.

2.4.4 Analysis of Synchronous Coherent Structures

In response to the concern that coherent structures may be of greater importance when they can impact multiple levels within a forest at once [*Gao et al.*, 1989; *Bergström and Högström*, 1989; *Shaw et al.*, 1989], we evaluate our data to see how many of the ramps we detected in the two levels are synchronous. If ramps shapes occur synchronously at both levels, then we assume this implies the presence of a coherent structure that was capable of penetrating from one level of the forest to the other. To do this, one must first define what synchronous means in terms of flows within a canopy. Since the microfront tends to appear first in upper levels and lags slightly in time at lower levels [*Taylor*, 1958; *Gao et al.*, 1989], some amount of offset between events at different levels is required. For the Canadian forest analyzed by *Gao et*

al. [1989], the mean canopy height is 18 m. They determined that within the canopy, temperature changes took about 10 s to descend 12 m, which translates to 7.5 s for the 9 m difference in this study. *Feigenwinter and Vogt* [2005] considered structures synchronous when they occurred within ±25 s at three levels above their 24 m urban canopy. We compromise between these two studies and use a lag time window of ±0 to 10 s (closer to *Gao et al.*, [1989]). The reason for the plus or minus is to account for slight inaccuracies in the zero-crossing of the MHAT wavelet which sometimes do not occur precisely at the end of a microfront. To explore whether or not this time lag is appropriate, we also flag cases where the microfronts are within ±10 to 20 s (closer to *Feigenwinter and Vogt* [2005]), and then compare the results.

Scanning the data with the ±0 to 10 s criteria confirms the hypothesis that ramps are rarely synchronous in both levels. Specifically, the percent of the total ramps detected whose microfronts occur within ±0 to 10 s of one another are about 16.5% in winter, 21.5% in spring, and 22% in summer (Table 2.6). Despite a small increase through spring and summer, the data suggest that on average less than one quarter of the events we detect in the two levels occur within 0 to 10 s of one another. When we analyze cases where microfronts are within ±10 to 20 s, the percentage of cases is even lower. Since the anemometers are only 9 m apart in the vertical, this speaks robustly to the difference in flow regimes that can occur within a shallow layer of our forest, even during warmer seasons.

If we evaluate the mean flux contribution from synchronous ramps only, and compare this to the mean flux contributions for all ramps as shown in Figure 2.7, there is a noticeable decline in this value. Across three seasons, the mean flux contribution from synchronous ramps which are ±0 to 10 s apart is 9 - 14%, and for cases that are ±10 to 20 s apart the flux contribution

drops to around 5 - 10% (Table 2.7). Thus, the heat flux contribution from only the coherent structures that were determined to be synchronous in this analysis is small, despite that the flux contributions from all detected structures at any one level are similar to what has been shown in other locations.

2.5 Discussion

Similarities in mean global statistics for all detected structures between ours and other studies suggest that structures have somewhat universal properties. Where our results differ from others who used wavelet analysis on large datasets in forests is first in the slightly longer durations (D) of our coherent structures. Recall also that D was larger in the work of *Steiner et al.* [2011]. One reason could be that both studies used the method of *Barthlott et al.* [2007] to derive D, which scales more dynamically with individual structures. However, the canopy height for *Steiner et al.* [2011] was 22.5 m and our canopy was only 4.7 m. Since the size and spacing of eddies generated from shear at the canopy should scale in proportion to the canopy height [*Raupach et al.*, 1996], one might expect shorter durations for our study area. However, based on Taylor's hypothesis [*Stull*, 1988], this evaluation has to be tempered with the fact that a lower wind speed would move structures more slowly, resulting in longer durations as measured from a stationary tower. *Barthlott et al.* [2007] showed that for stable conditions, coherent structures were more likely to be shorter; for this study, event duration only grows slightly from winter to summer, suggesting that other parameters besides stability control their duration. All of these hypotheses should be considered in light of the fact that the strong heterogeneity of our canopy height may be adding complexity to the formation of structures, such that structures of varying

scales may interact at once. Further analysis is required to investigate what other physical parameters might be involved. Finally, recall that using the sign of the Obukhov Length (L_*) occasionally results in inaccuracies when measuring the duration of a ramp. The detection algorithm will also sometimes group a few less well-defined ramps together as one feature. Thus, some imperfections in the detection process may also contribute to the slightly longer duration times in this study.

Another difference between this and other studies is in regard to the flux contribution of the coherent structures to the total 30 min heat flux (F_{COH}/F_{TOT}). Our results for F_{COH}/F_{TOT} were similar to other forested and non-forested regions, especially the ones which used the *Barthlott et al.* [2007] method for determining event duration and/or the *Lu and Fitzjarrald* [1994] method for calculating F_{COH}/F_{TOT} (Table 2.3). However, the fact that the dominant values of F_{COH}/F_{TOT} transition from being higher at 0.6 h (3 m) in winter to being higher at 2.6 h (12 m) in summer was a notable finding in our results (Figure 2.7). This, combined with the high standard deviation in tree heights for the boreal forest, suggests that coherent structures detected by the two sonic anemometers may sometimes come from separate events initiated at different canopy heights. Since coherent structures are often initiated near the top of a canopy where shear instability is highest [*Raupach et al.,* 1996], it follows then that F_{COH}/F_{TOT} should be largest within the upper half of the canopy at which the structures are initiated, and weaker above and below this height as shown by *Gao et al.* [1989, their Figure 11]. For the black spruce forest, the upper portion of the canopy near the micrometeorological tower is about 2 to 4 m in height. Thus, we should consistently see higher values of F_{COH}/F_{TOT} at 0.6 h (3 m) if coherent structures are initiated locally there. If we consider only mean values of F_{COH}/F_{TOT}, this is generally true because the

mean value of F_{COH}/F_{TOT} tends to be higher at 0.6 h (3 m), except for summer (Figure 2.7). However, the density distribution of F_{COH}/F_{TOT} is not always normal, and so the dominant value does not reflect that F_{COH}/F_{TOT} is consistently higher at 0.6 h (3 m). We hypothesize that during winter, coherent structure might be more frequently initiated within the lower canopy, local to the site. During summer, coherent structures might be more often initiated from the higher canopy at the periphery of our study site. Further, we could be seeing a combination of coherent structures whose physical sizes vary, but which become superimposed as they enter the forest. More detailed investigations of the scale of the detected structures and their synchronicity would be required to determine this.

Another critical element is the stratification within the boreal forest, which clearly makes the flow susceptible to gravity waves. In this study, we used an adaptation of the Stokes parameters to suggest that almost one third of the structures we detect at 2.6 h (12 m, i.e. above the canopy) could be complicated by wave-like behavior (Table 2.4); at the sub-canopy level 0.6 h (3 m), this value was lower. Since we expect waves to be ducted within layers of comparable stratification, the fact that there are considerably more waves in the 2.6 h (12 m) flow suggests that even a 9 m vertical difference is significant when considering the flow regime in our forest. It is important to note that in this study, we include daytime periods and periods during warmer, potentially more convective regimes when evaluating the wave-like nature of the flow, in contrast to other studies on gravity waves which focus only on nighttime data. Despite this, we still find a high number of wave-influenced cases, emphasizing the importance of stratification on the analysis of any kind of organized structures in the black spruce boreal forest.

Finally, we showed that less than a quarter of the features we detect at the subcanopy and above canopy levels are synchronous, i.e. produced by the same coherent structure. As a result, F_{COH}/F_{TOT} from only the synchronous events is significantly less than when all structures are included in each level independently (Table 2.7). This was a most remarkable finding, because it suggests that most of the time, coherent structures may not be the dominant mechanism in the vertical aggregation of sensible heat within our boreal forest. Furthermore, the vertical distance over which we are evaluating the flow is only 9 m; the lack of synchronous ramps between these two levels speaks robustly to the lack of interaction between the subcanopy and above canopy levels in our black spruce forest. Ultimately, implications of this finding are that when upscaling heat fluxes within the boreal forest, one must also be concerned with other modes besides organized motion. Clearly, low flow conditions could be influencing this result. We also note that the first maximum in the global wavelet power spectrum (F_{MAX}), which is used to define the range of frequencies for organized turbulence, can often be broad and hard to define [*Barthlott et al.*, 2007]. Imposing a criterion on the kurtosis of the global wavelet spectrum might help with this analysis, as it would provide a quantitative manner of rejecting periods where this value is not robust enough to be reliable.

2.6 Conclusions

In conclusion, we detect coherent structures in the turbulent temperature time series for 864 half-hour periods spanning winter, spring and summer of 2012, using an automated wavelet analysis technique at both the above canopy (2.6 h or 12 m) and subcanopy (0.6 h or 3 m) levels within an Alaskan black spruce boreal forest whose mean canopy height (h) is 4.7 m. When

analyzed at each of these two levels independently, global mean statistics for all detected structures show that the number of structures per half-hour period, their durations, their heat flux contributions, and their fluxing efficiencies are not largely different from other studies in diverse locations. Specifically, considering all the structures we detected at both levels and across all three seasons, we find an average of 8 coherent structures every thirty minutes and a mean duration of 85 s. Eliminating events with extreme flux contribution values during times of low total fluxing ($F_{COHextreme}$), we find a mean heat flux contribution of 48%, and a mean fluxing efficiency of around 1.5.

However, our analysis shows that as much as 31% of the structures detected at 2.6 h (12 m), and 13% of those detected at 0.6 h (3 m), may be complicated by a wave-influenced flow regime, and therefore may not be purely coherent turbulent structures. These wave-influenced periods are often characterized by low total heat fluxes, but when analyzed separately, the flux contributions from structures during these periods is similar to our pervious values. This suggests that flux contributions from wave-influenced events may be similar to that from more turbulent events, despite differences in the total heat flux. Most importantly, we find that less than 25% of structures affect both levels simultaneously, a finding that speaks robustly to the lack of flow interaction in only 9 vertical meters of our forest. This result suggests that the vertical aggregation of sensible heat fluxes within a black spruce boreal forest is complicated, and that other modes of fluxing besides organized motion (e.g. stochastic or dispersive fluxes) are important.

Acknowledgements

This research was supported by the Alaska NASA EPSCoR program award NNX10NO2A, and by the Alaska Space Grant Program. Authors would also like to thank Dr. Glenn Juday from the School of Natural Resources and Agricultural Sciences of the University of Alaska Fairbanks for his support in the forestry inventory section of this paper. We thank the very positive comments and feedbacks from reviewers.

The following authors contributed work on this manuscript as noted:

D. Starkenburg: Collected, processed, and evaluated data; primary writer/editor

G. J. Fochesatto: Assisted in collecting data, scripting codes, and guiding research; secondary editor

A. Prakash, J. Cristóbal, R. Gens, and D. L. Kane: Secondary editors

2.7 References

Acevedo, O. C., O. L. L. Moraes, G. A. Degrazia, and L. E. Medeiros (2006), Intermittency and exchange of scalars in the nocturnal surface layer, *Boundary-Layer Meterol., 119*(1), 41-55, doi: 10.1007/s10546-005-9019-3.

Antonia, R. A., A. J. Chambers, C. A. Friehe, and C. W. Van Atta (1979), Temperature ramps in the atmospheric surface layer, *J. Atmos. Sci., 36*(1), 99-108, doi: 10.1175/1520-0469(1979)036<0099:TRITAS>2.0.CO;2

Arya, S. P. (1988), *Introduction to micrometeorology*, Academic, San Diego, CA.

Bailey, B. N., and R. Stoll (2012), Coherent turbulence structure detection in plant canopies using a coupled Eulerian-Lagrangian detection method, paper presented at 2012 Fall Meeting, AGU, San Francisco, Calif., 3-7 Dec.

Barthlott, C., P. Drobinski, C. Fesquet, T. Dubos, and C. Pietras (2007), Long-term study of coherent structures in the atmospheric surface layer, *Boundary-Layer Meterol., 125*(1), 1-24, doi: 10.1007/s10546-007-9190-9.

Bayly, B. J., S. A. Orszag, and T. Herbert (1988), Instability mechanisms in shear-flow transition. *Annu. Rev. Fluid Mech., 20*(1), 359-391, doi: 10.1146/annurev.fl.20.010188.002043.

Bergström, H., and U. Högström (1989), Turbulent exchange above a pine forest II. Organized structures, *Boundary-Layer Meterol., 49*(3), 231-263, doi: 10.1007/BF00120972.

Bonan, G. B., and H. H. Shugart (1989), Environmental factors and ecological processes in boreal forests, *Annu. Rev. Ecol. Syst., 20*(1), 1-28, doi: 10.1146/annurev.es.20.110189.000245.

Cava, D., U. Giostra, M. Siqueira, and G. Katul (2004), Organized motion and radiative perturbations in the nocturnal canopy sublayer above an even-aged pine forest, *Boundary-Layer Meterol.*, *112*(1), 129-157, doi: 10.1023/B:BOUN.0000020160.28184.a0.

Chapin III, F. S., A. D. McGuire, J. Randerson, R. Pielke Sr., D. Baldocchi, S. E. Hobbie, N. Roulet, W. Eugster, E. Kasischke, E. B. Rastetter, S. A. Zimov, and S. W. Running (2000), Arctic and boreal ecosystems of western North America as components of the climate system, *Global Change Biology*, *6*(S1), 211–223, doi: 10.1046/j.1365-2486.2000.06022.x.

Chapin III, F. S., M. Sturm, M. C. Serreze, J. P. McFadden, J. R. Key, A. H. Lloyd, A. D. McGuire, T. S. Rupp, A. H. Lynch, J. P. Schimel, J. Beringer, W. L. Chapman, H. E. Epstein, E. S. Euskirchen, L. D. Hinzman, G. Jia, C.-L. Ping, K. D. Tape, C. D. C. Thompson, D. A.Walker, and J. M. Welker (2005), Role of land-surface changes in Arctic summer warming, *Science*, *310*(5748), 657-660, doi: 10.1126/science.1117368.

Chapin III, F. S., M. W. Oswood., K. Van Cleve., L. A. Viereck, and D. L. Verbyla (2006), *Alaska's Changing Boreal Forest,* Oxford University, New York, N.Y.

Collineau, S., and Y. Brunet (1993a), Detection of turbulent coherent motions in a forest canopy part I: Wavelet analysis, *Boundary-Layer Meterol.*, *65*(4), 357-379, doi: 10.1007/BF00707033.

Collineau, S., and Y. Brunet (1993b), Detection of turbulent coherent motions in a forest canopy part II: Time-scales and conditional averages, *Boundary-Layer Meterol.*, *66*(1-2), 49-73, doi: 10.1007/BF00705459.

Eckermann, S. D. (1996), Hodographic analysis of gravity waves: relationships among Stokes parameters, rotary spectra and cross-spectral methods. *J. Geophys. Res.-Atmos, 101*(D14), 19169-19174, doi: 10.1029/96JD01578.

Eder, F., Serafimovich, A., and T. Foken (2013), Coherent structures at a forest edge: properties, coupling and impact of secondary circulations. *Boundary-Layer Meteorol., 148*(2), 285-308, doi: 10.1007/s10546-013-9815-0.

Feigenwinter, C., and R. Vogt (2005), Detection and analysis of coherent structures in urban turbulence, *Theor. Appl. Climatol., 81*(3-4), 219-230, doi: 10.1007/s00704-004-0111-2.

Finnigan, J. J., F. Einaudi, and D. Fua (1984), The interaction between an internal gravity wave and turbulence in the stably-stratified nocturnal boundary layer, *J. Atmos. Sci., 41*(16), 2409-2436, doi: 10.1175/1520-0469(1984)041<2409:TIBAIG>2.0.CO;2.

Finnigan, J. J. (2000), Turbulence in plant canopies, *Annu. Rev. Fluid Mech., 32*(1), 519-571.

Finnigan, J. J., R. H. Shaw, and E. G. Patton (2009), Turbulence structure above a vegetation canopy, *J. Fluid Mech., 637*, 387-424, doi: 10.1017/S0022112009990589.

Fleming, M. D. (1997), A statewide vegetation map of Alaska using phenological classification of AVHRR data, in *Proceedings of the Second Circumpolar Arctic Vegetation Mapping Workshop and the CAVM-North America Workshop*, Arendal, Norwary, pp. 25-26.

Fochesatto, G., J. Mayfield, D. Starkenburg, M. Gruber, and J. Connor (2013), Occurrence of shallow cold flows in the winter atmospheric boundary layer of interior Alaska, *Meteorol. Atmos. Phys.*, in press.

Foken, T. (2008a), *Micro-meteorology*, Springer-Verlag, Berlin, Heidelberg.

Foken, T. (2008b), The energy balance closure problem: an overview, *Ecol. Appl.*, *18*(6), 1351-1367, doi: 10.1890/06-0922.1.

Foken, T., M. Mauder, C. Liebethal, F. Wimmer, F. Beyrich, J.-P. Leps, S. Raasch, H. A. R. DeBruin, W. M. L. Meijninger, and J. Bange (2010), Energy balance closure for the LITFASS-2003 experiment, *Theor. Appl. Climatol.*, *101*(1-2), 149-160, doi: 10.1007/s00704-009-0216-8.

Gao, W., R. H. Shaw, and K. T. Paw U. (1989), Observation of organized structure in turbulent flow within and above a forest canopy, *Boundary-Layer Meterol.*, *47*(1-4), 349-377, doi: 10.1007/BF00122339.

Grace, J., Y. Malhi, J. Lloyd, J. McIntyre, A. C. Miranda, P. Meir, and H. S. Miranda (1996), The use of eddy covariance to infer the net carbon dioxide uptake of Brazilian rain forest, *Glob. Change Biol.*, *2*(3), 209-217, doi: 10.1111/j.1365-2486.1996.tb00073.x.

Iwata, H., Y. Harazono, and M. Ueyama (2010), Influence of source/sink distributions on flux–gradient relationships in the roughness sublayer over an open forest canopy under unstable conditions, *Boundary-Layer Meterol.*, *136*(3), 391-405, doi: 10.1007/s10546-010-9513-0.

Kaimal, J. C., and J. J. Finnigan (1994), *Atmospheric Boundary Layer Flows: Their Structure and Measurement*, Oxford University, New York, N.Y.

Kimball, J. S., M. Zhao, K. C. McDonald, and S.W. Running (2006), Satellite remote sensing of terrestrial net primary production for the Pan-Arctic Basin and Alaska, *Mitig. Adapt. Strateg. Glob. Clim. Change*, *11*(4), 783-804, doi: 10.1007/s11027-005-9014-5.

Kitamoto, T., M. Ueyama, Y. Harazono, T. Iwata, and S. Yamamoto (2007), Applications of NOAA/AVHRR and observed fluxes to estimate 3 regional carbon fluxes over black spruce forests in Alaska, *J. Agr. Meteorol.*, *63*(4), 171-183.

Lee, X., W. Massman, and B. Law (2004), *Handbook of Micrometeorology: A Guide for Surface Flux Measurement and Analysis*, Kluwer Academic, Dordrecht, Netherlands.

Lee, X. (1998), On micrometeorological observations of surface-air exchange over tall vegetation, *Agr. and For. Meteorol.*, *91*(1), 39-49, doi: 10.1016/S0168-1923(98)00071-9.

Lee, X., H. H. Neumann, G. Hartog, R. E. Mickle, J. D. Fuentes, T. A. Black, P. C. Yang, and P. D. Blanken (1997), Observation of gravity waves in a boreal forest, *Boundary-Layer Meterol.*, *84*(3), 383-398, doi: 10.1023/A:1000454030493.

Lu, C.-H., and D. R. Fitzjarrald (1994), Seasonal and diurnal variations of coherent structures over a deciduous forest, *Boundary-Layer Meterol.*, *69*(1-2), 43-69, doi: 10.1007/BF00713294.

Lu, C., S. E. Koch, and N. Wang (2005), Stokes parameter analysis of a packet of turbulence-generating gravity waves, *J. Geophys. Res.-Atm.*, *110*(D20), D20105, doi: 10.1029/2004JD005736.

Mayfield, J. A., and G. J. Fochesatto (2013), The Layered Structure of the Winter Atmospheric Boundary Layer in the Interior of Alaska, *J. Appl. Meteorol. Climatol.*, *52*(4), 953-973 doi: 10.1175/JAMC-D-12-01.1.

Morland, L. C., P. G. Saffman, and H. C. Yuen (1991), Waves generated by shear layer instabilities, paper presented at Proceedings of the Royal Society of London, *Series A: Mathematical and Physical Sciences*, *433*(1888), 441-450, doi: 10.1098/rspa.1991.0057.

Nappo, C. J. (2002), *An Introduction to Atmospheric Gravity Waves*, Academic Press, San Diego, CA.

Paw U., K. T., Y. Brunet, S. Collineau, R. H. Shaw, T. Maitani, J. Qiu, and L. Hipps (1992), On coherent structures in turbulence above and within agricultural plant canopies, *Agr.and For. Meteorol.*, *61*(1-2), 55-68, doi: 10.1016/0168-1923(92)90025-Y.

Poggi, D, A. Porporato, L. Ridolfi, J. D. Albertson, and G. G. Katul (2004), The effect of vegetation density on canopy sub-layer turbulence, *Boundary-Layer Meterol.*, *111*(3), 565-587, doi: 10.1023/B:BOUN.0000016576.05621.73.

Raupach, M. R. (1981), Conditional statistics of Reynolds stress in rough-wall and smooth-wall turbulent boundary layers. *J. Fluid Mech.*, *108*, 363-382, doi: 10.1017/S0022112081002164.

Raupach, M. R., J. J. Finnigan, and Y. Brunet (1996), Coherent eddies and turbulence in vegetation canopies: the mixing layer analogy, *Boundary-Layer Meterol.*, *78*(3-4), 351-382, doi: 10.1007/BF00120941.

Raupach, M. R., and A. S. Thom (1981), Turbulence in and above plant canopies, *Ann. Rev. Fluid Mech.*, *13*(1), 97-129, doi: 10.1146/annurev.fl.13.010181.000525.

Rogers, M. M., and R. D. Moser (1992), The three-dimensional evolution of a plane mixing layer: the Kelvin-Helmholtz rollup, *J. Fluid Mech.*, *243*, 183-226, doi: 10.1017/S0022112092002696.

Samain, B., G. W. H. Simons, M. P. Voogt, W. Defloor, N.-J. Bink, and V. Pauwels (2012), Consistency between hydrological model, large aperture scintillometer and remote

sensing based evapotranspiration estimates for a heterogeneous catchment, *Hydrol. Earth Syst. Sci.*, *16*(7), 2095 - 2107, doi: 10.5194/hess-16-2095-2012.

Serafimovich, A., C. J. Nappo, and T. Foken (2010), Impact of gravity waves on the turbulent exchange above a forest site, paper presented at 19th Symposium on Boundary Layers and Turbulence, *Am. Meteorol. Soc.*, Keystone, CO.

Serafimovich, A., C. Thomas, and T. Foken (2011), Vertical and horizontal transport of energy and matter by coherent motions in a tall spruce canopy, *Boundary-Layer Meterol.*, *140*(3), 429-451, doi: 10.1007/s10546-011-9619-z.

Shaw, R.H., K. T. Paw U., and W. Gao (1989), Detection of temperature ramps and flow structures at a deciduous forest site, *Agri. and For. Meteorol.*, *47*(2-4), 123-138, doi: 10.1016/0168-1923(89)90091-9.

Shulski, M., and G. Wendler (2007), *The Climate of Alaska*, University of Alaska, Fairbanks, AK.

Steiner, A. L., Pressley, S. N., Botros, A., Jones, E., Chung, S. H., and S. L. Edburg (2011), Analysis of coherent structures and atmospherr-canopy coupling strength curing the CABINEX field campaign. *Atmos. Chem. Phys.*, 11, 11921-11936, doi: 10.5194/acp-11-11921-2011.

Stull, R. B. (1988), *An Introduction to Boundary Layer Meteorology*, Kluwer Academic, Dordrecht, Netherlands.

Taylor, R. J. (1958), Thermal structures in the lowest layers of the atmosphere, *Aust. J. Phys.*, *11*(2), 168-176, doi: 10.1071/PH580168.

Thomas, C., and T. Foken (2005), Detection of long-term coherent exchange over spruce forest using wavelet analysis, *Theor. Appl. Climatol.*, *80*(2-4), 91-104, doi: 10.1007/s00704-004-0093-0.

Thomas, C., J.-C. Mayer, F. X. Meixner, T. Foken (2006), Analysis of low-frequency turbulence above tall vegetation using a Doppler sodar, *Boundary-Layer Meterol., 119*(3), 563-587. doi: 10.1007/s10546-005-9038-0.

Thomas, C., and T. Foken (2007a), Flux contribution of coherent structures and its implications for the exchange of energy and matter in a tall spruce canopy, *Boundary-Layer Meterol.*, *123*(2), 317-337, doi: 10.1007/s10546-006-9144-7.

Thomas, C., and T. Foken (2007b), Organized motion in a tall spruce canopy: temporal scales, structure spacing and terrain effects, *Boundary-Layer Meterol.*, *122*(1), 123-147, doi: 10.1007/s10546-006-9087-z.

Turner, B. J., M. Y. Leclerc, M. Gauthier, K. E. Moore, and D. R. Fitzjarrald (1994), Identification of turbulence structures above a forest canopy using a wavelet transform, *J. Geophys. Res.-Atm.*, *99*(D1), 1919-1926, doi: 10.1029/93JD02260.

Ueyama, M., Y. Harazono, and K. Ichii (2010), Satellite-based modeling of the carbon fluxes in mature black spruce forests in Alaska: a synthesis of the eddy covariance data and satellite remote sensing data, *Earth Interactions*, *14*(13), 1-27, doi: 10.1175/2010EI319.1.

Vickers, D., and L. Mahrt (1997), Quality control and flux sampling problems for tower and aircraft data, *J. Atmos. Oceanic Tech.*, *14*(3), 512-526, doi: 10.1175/1520-0426(1997)014<0512:QCAFSP>2.0.CO;2.

Vincent, R. A., and D. C. Fritts (1987), A climatology of gravity wave motions in the mesopause region at Adelaide, Australia, *J. Atmos. Sciences*, *44*(4), 748-760, doi: 10.1175/1520-0469(1987)044<0748:ACOGWM>2.0.CO;2.

Wilmking, M., G. P. Juday, V. A. Barber, and H. S. J. Zald (2004), Recent climate warming forces contrasting growth responses of white spruce at treeline in Alaska through temperature thresholds, *Glob. Change Biol. 10*(10), 1724-1736, doi: 10.1111/j.1365-2486.2004.00826.x.

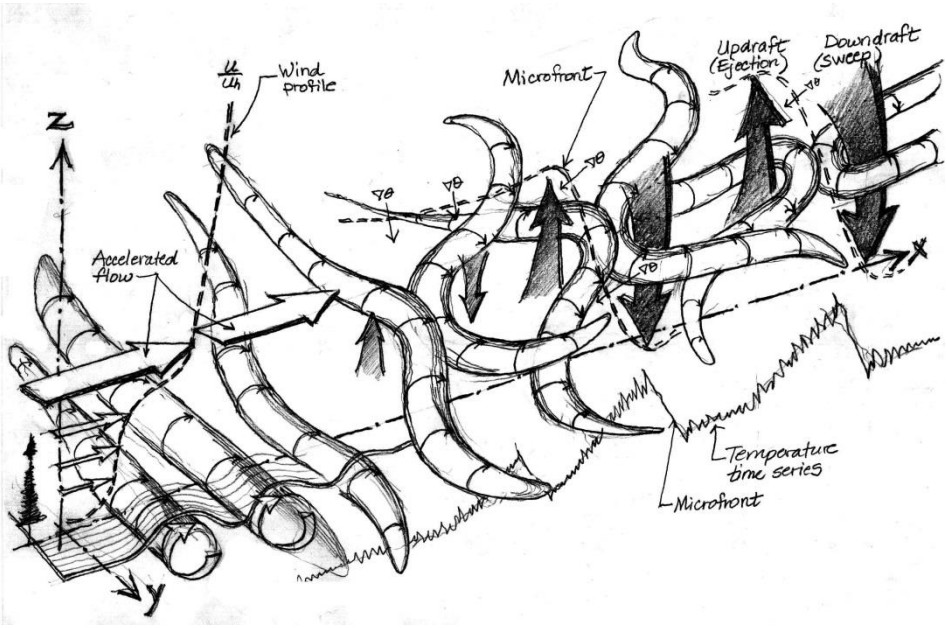

Figure 2.1 Author's artistic rendering of the development of a coherent structure by shear due to the vertical velocity gradient at a black spruce forest canopy; adapted from *Finnigan et al.* [2009, their Figure 14].

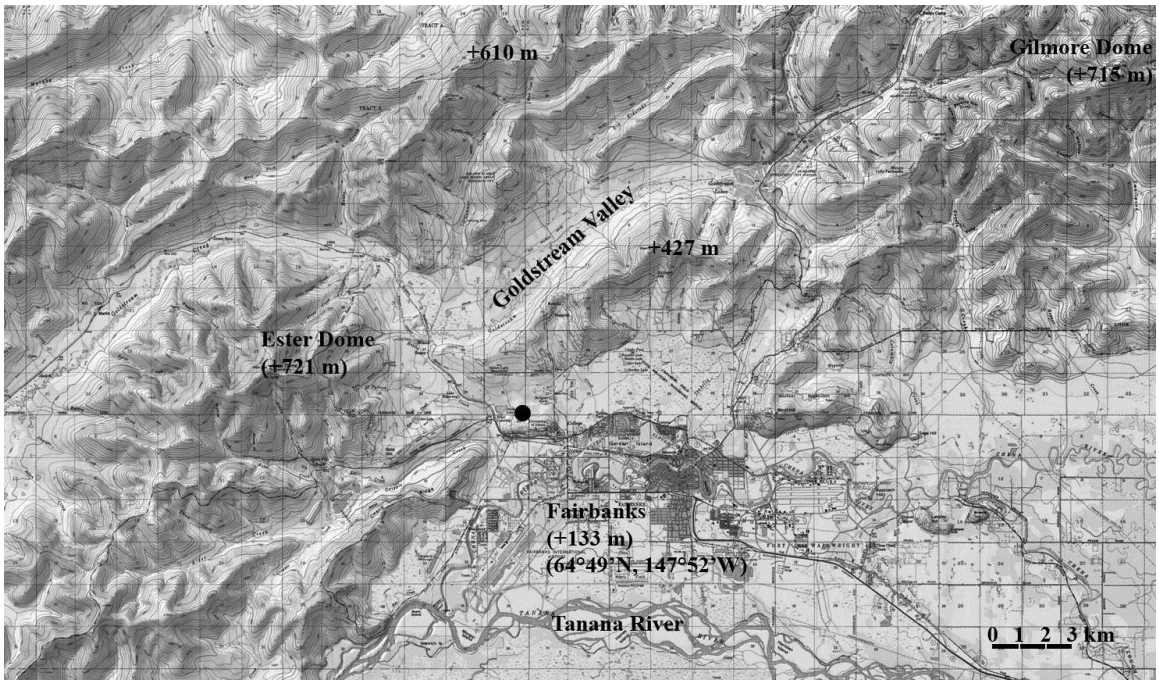

Figure 2.2 Topographical map showing terrain in the Fairbanks area. Approximate location of the UAF north campus site is indicated by the solid black dot. Approximate elevations of local terrain features are labeled in meters above sea level. Map generated from National Geographic USGS Mapping Software (powered by TOPO!).

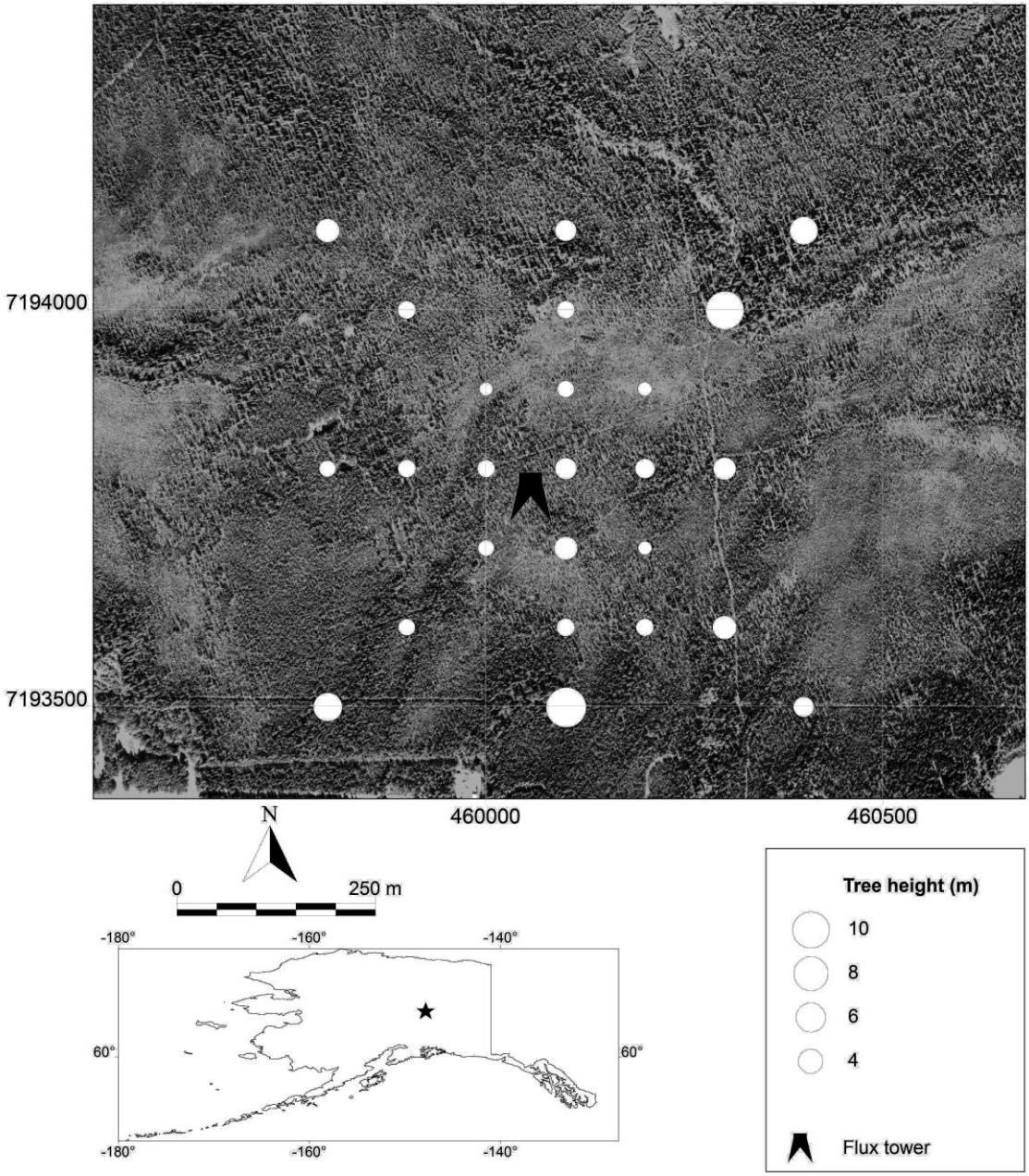

Figure 2.3 Aerial map of the UAF north campus site, showing the approximate range of mean canopy heights (white circles). Dark (light) gray indicates taller (lower) spruce. The numbers on the edges of the top image are Universal Transverse Mercator (UTM) coordinates in meters (Zone 6N, using the NAD83 datum).

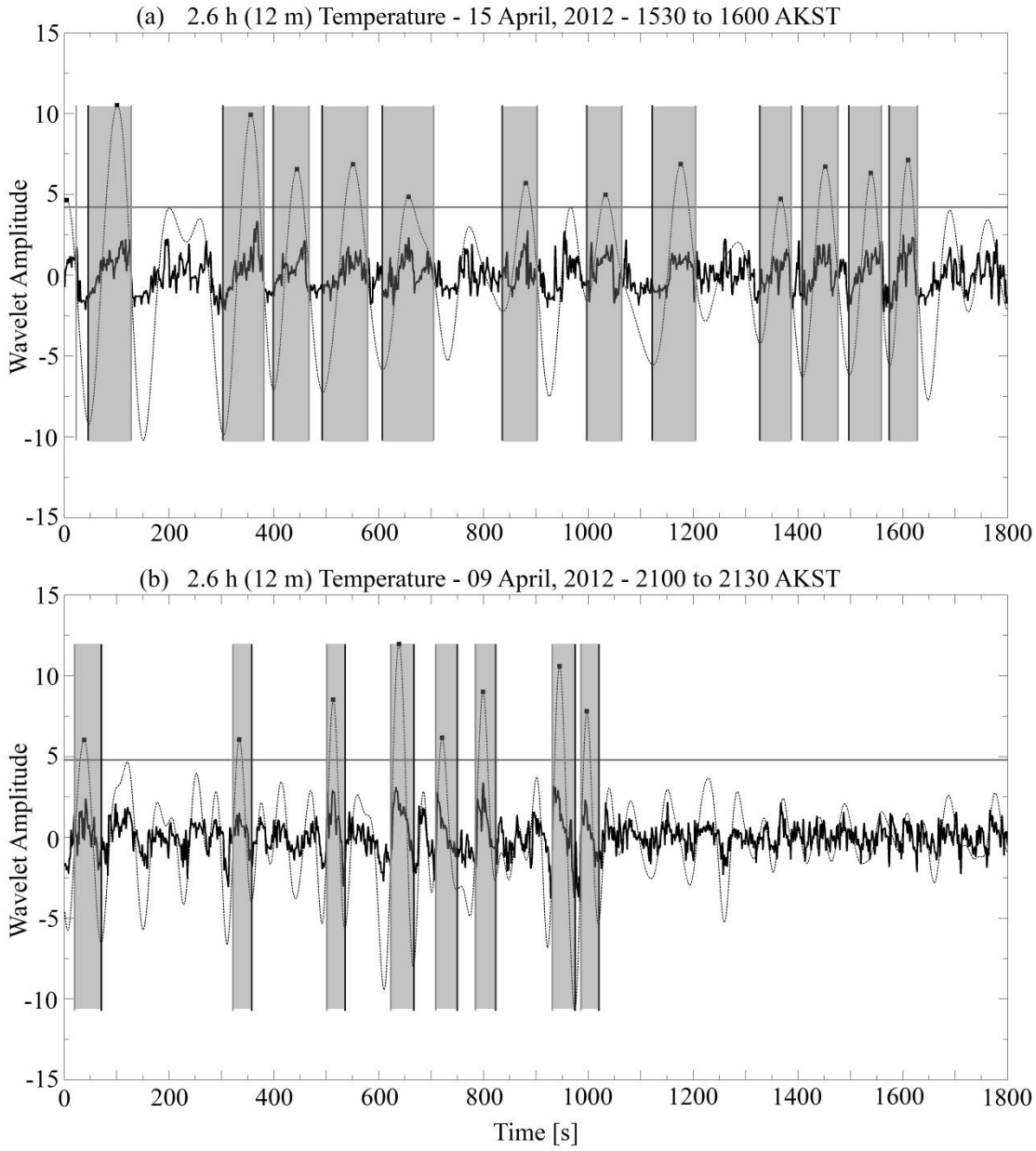

Figure 2.4 Wavelet detection of coherent structures for unstable conditions where $L_* < 0$ (a), and stable conditions where $L_* > 0$ (b). Oscillatory trace line is the wavelet function selected according to the local maximum in the wavelet power spectrum. Superimposed in black trace is the 1 sec. normalized temperature signal (zero mean, ±1 σ). Shading in gray indicates the duration of each detected structure. Solid squares at the wavelet peaks indicate structures whose contribution to the temperature power spectrum is at least 40% of the most energetic within the half-hour series. Horizontal line is the 40% threshold.

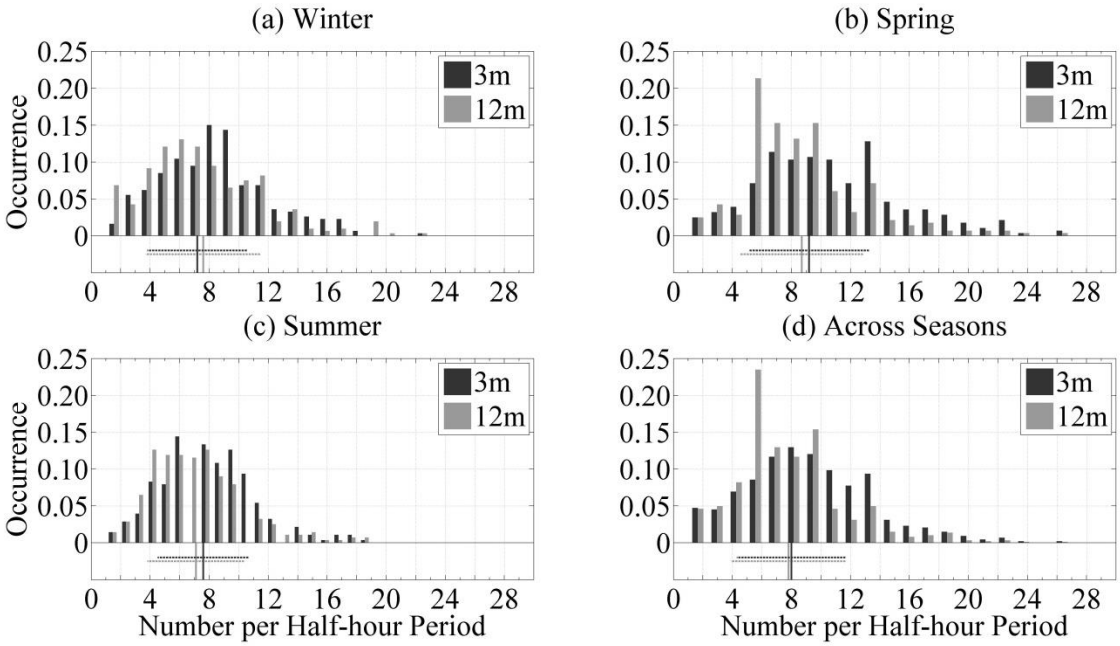

Figure 2.5 Number of coherent structures per half-hour period. Panel (a) winter (306 samples), (b) spring (281 samples), (c) summer (277 samples), and (d) across seasons (864 samples). Solid vertical (dashed horizontal) lines below the histograms are means (standard deviations). The bin size per histogram is 20.

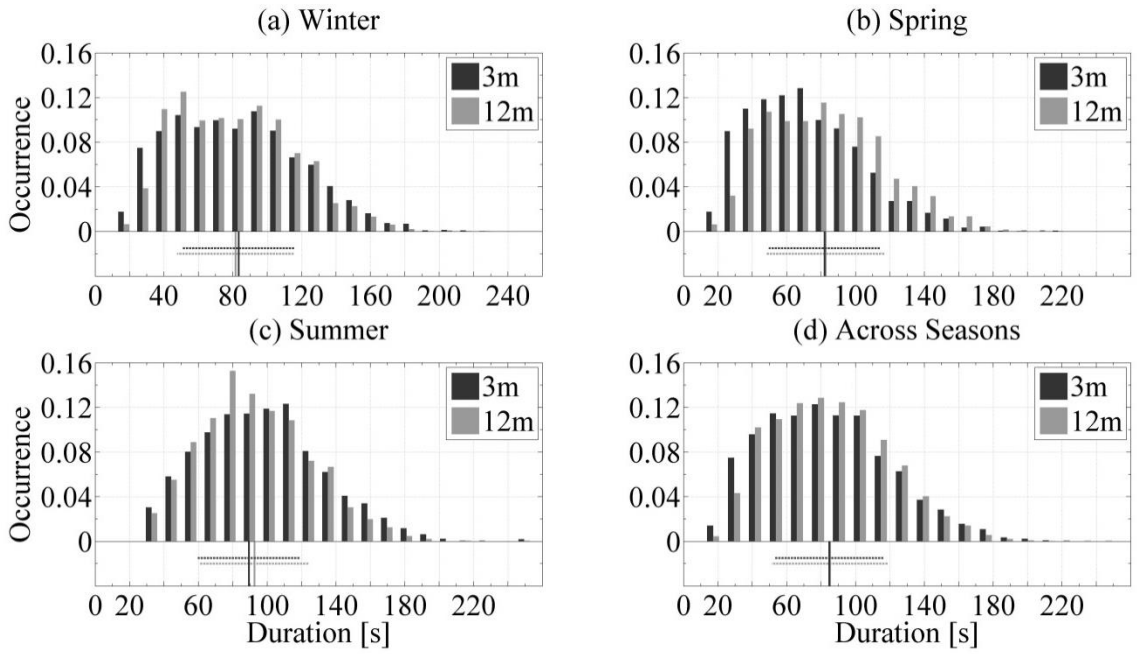

Figure 2.6. Duration of coherent structures. Panel (a) winter (2137 cases at 0.6 h; 2253 at 2.6 h), (b) spring (2525 cases at 0.6 h; 2366 at 2.6 h), (c) summer (2028 cases at 0.6 h; 1900 at 2.6 h), and (d) across seasons (6690 cases at 0.6 h; 6519 at 2.6 h).

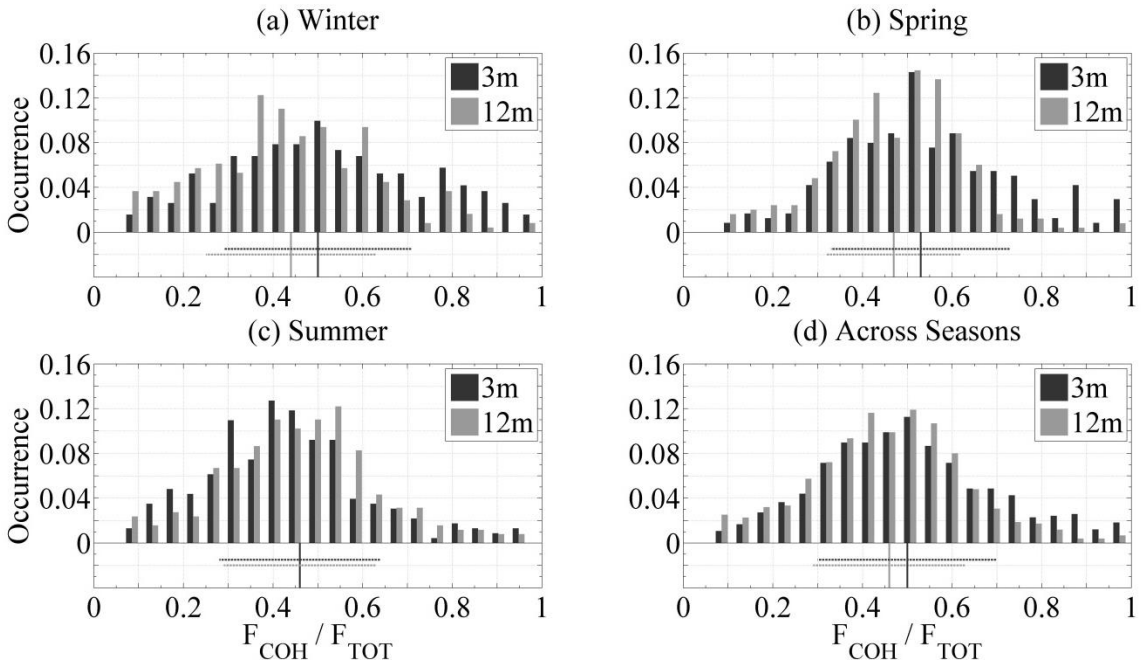

Figure 2.7 Flux contribution from coherent structures (i.e., F_{COH}/F_{TOT}, for contributions between 5% and 100%). Panel (a) winter (191 cases at 0.6 h; 245 at 2.6 h), (b) spring (238 at 0.6 h; 249 at 2.6 h), (c) summer (228 at 0.6 h; 254 at 2.6 h) and (d) across seasons (657 cases at 0.6 h; 748 at 2.6 h).

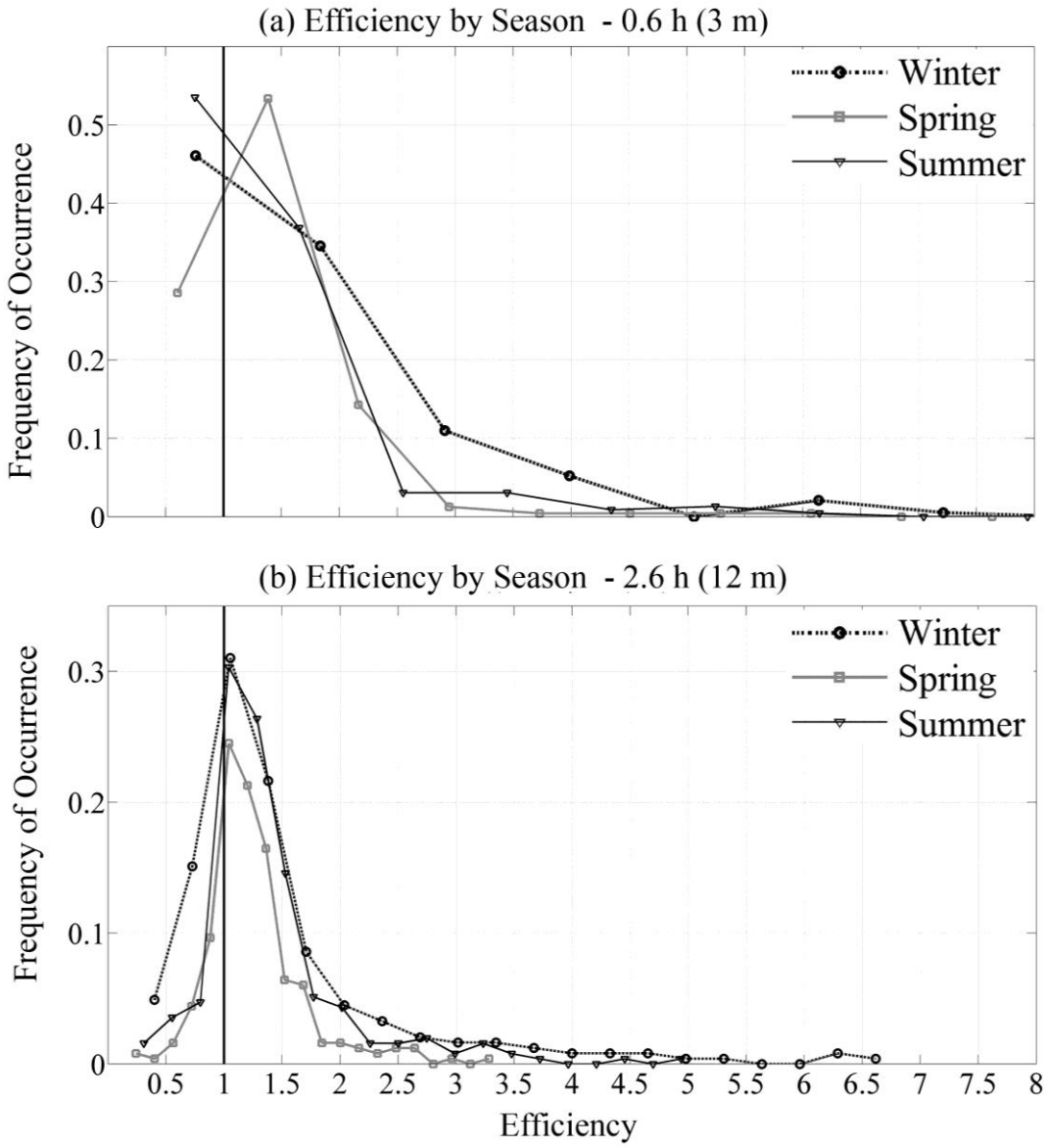

Figure 2.8 Fluxing efficiency of coherent structures whose flux contributions lie between 5% and 100% at (a) 0.6 h (657 cases), and (b) 2.6 h (748 cases). The vertical line denotes an efficiency of 1 (< 1 is inefficient; > 1 is efficient). The number of bins per histogram is 20.

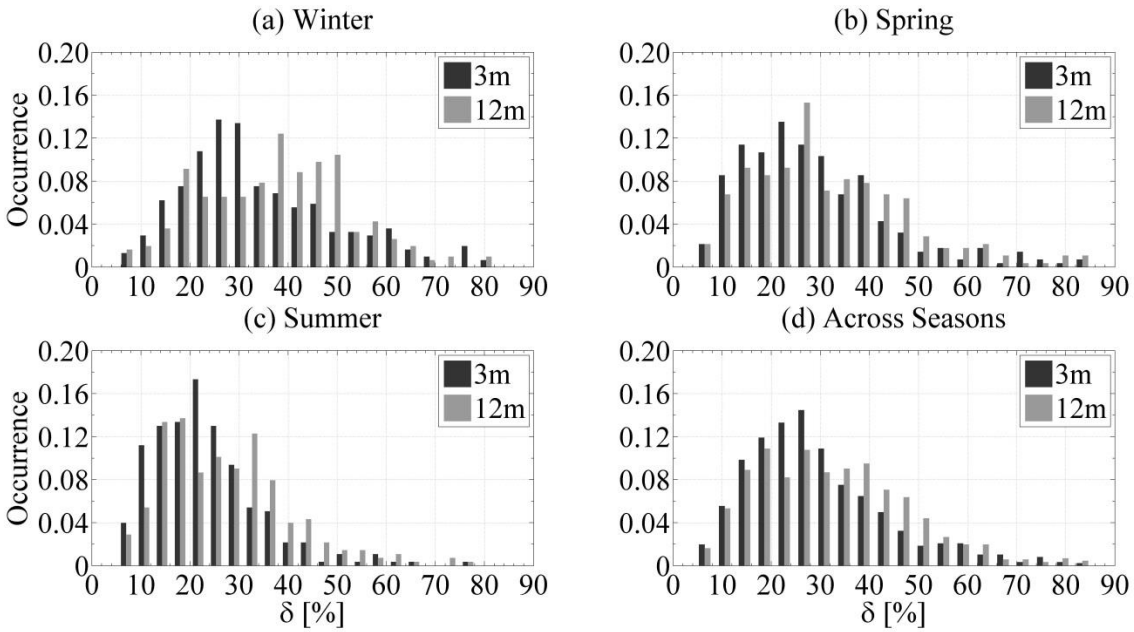

Figure 2.9 Thirty minute mean polarization (δ). Panel (a) winter (306 cases); (b) spring (281 cases); (c) summer (277 cases); and (d) across seasons (864 cases). The bin size per histogram is 20.

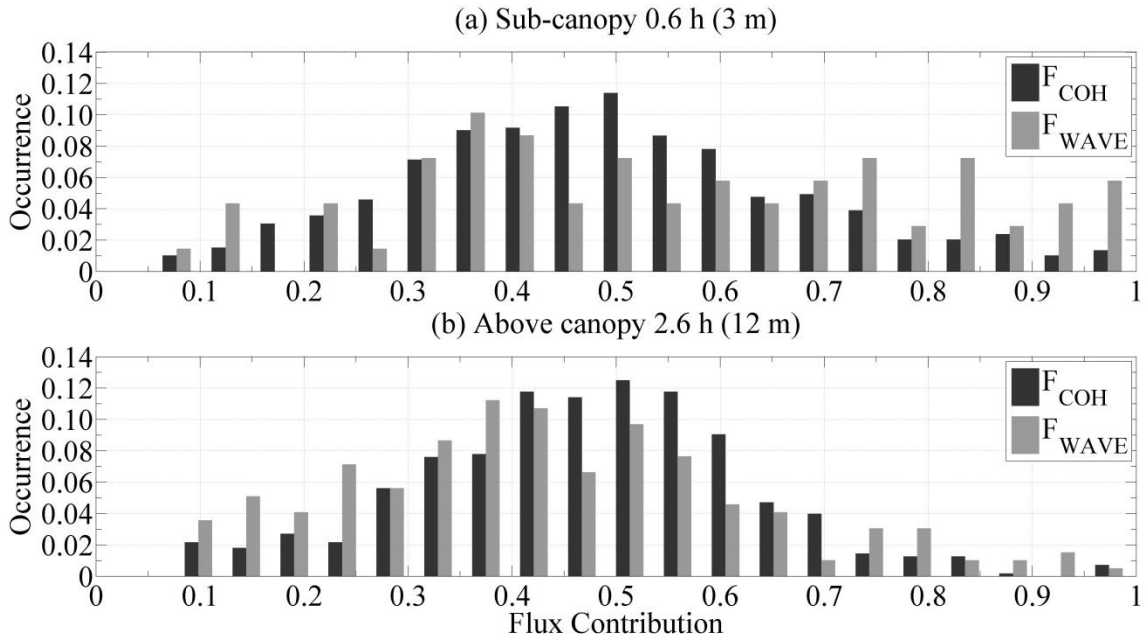

Figure 2.10 Flux contribution from coherent structures under a wave-like regime ($F_{WAVE,}$ 196 cases at 2.6 h; 69 cases at 0.6 h), and a more turbulent regime (F_{COH}, 552 cases at 2.6 h; 588 cases at 0.6 h). The bin size per histogram is 20.

Table 2.1 Selected diurnal cycles for this study covering winter, spring and summer of 2012 in UTC. Note that March is considered winter because in Fairbanks, the mean daily high for that month is still below freezing.

	Julian Day	Date		Julian Day	Date		Julian Day	Date
Winter	36	5 February	**Spring**	93	2 April	**Summer**	176	24 June
	43	12 February		94	3 April		187	5 July
	53	22 February		95	4 April		189	7 July
	61	1 March		100	9 April		190	8 July
	63	3 March		101	10 April		193	11 July
	64	4 March		106	15 April		194	12 July
	65	5 March						

Table 2.2 Summary of the mean half-hour wave-like polarization indicator coefficient (δ, in %), for three seasons and for the ensemble across seasons.

Season	2.6 h (12 m)	0.6 h (3 m)
winter	37.5	30.6
spring	31.9	27.1
summer	27.2	23.6
TOTAL	32.4	27.2

Table 2.3 Summary of literature review in which wavelet analysis is used to detect and evaluate coherent structures. Columns 3-7 are: number of structure per half-hour period; duration (D) of structures in seconds; time coverage (%) of structures; flux contribution from structures (%); fluxing efficiency. Gray shading indicates non-forested study sites.

Authors	Study site	Number	Duration	Coverage	F_{COH}/F_{TOT}	Efficiency
Starkenburg et al. (this work)†	Alaskan boreal spruce	7 to 9	82 to 93	31 to 43	44 to 53	1.3 to 1.8
Steiner et al. (2011)‡	Michigan deciduous	5 to 9	91 to 116	–	44 to 48	1.2 to 1.3
Eder et al. (2013)‡	German spruce forest	–	15 to 30	–	24 to 29	–
Serafimovich et al. (2011)‡	German spruce forest	–	10 to 30	–	~ 30	–
Thomas and Foken (2007a)†	German spruce forest	–	–	–	26	0.53
Lu and Fitzjarrald (1994)†	Massachusettes deciduous	–	53	42 to 45	35 to 45	1.00 to 1.03
Barthlott et al. (2007)†	Suburban open field	7 to 11	61 to 98	34 to 38	42 to 51	1.05 to 1.66
Feigenwinter and Vogt (2005)†	Urban canopy	7 to 10	90	45	49 to 124	

† = data means

‡ = data medians

– data unavailable

Table 2.4 Summary of the seasonal occurrence of wave-like periods. Columns 3 and 5 show the number of half-hour periods (or, in the last row, the number of coherent structures) determined to be under a wave-like influence. Columns 4 and 6 show the corresponding percentages.

Season		**2.6 h (12 m)**		**0.6 h (3 m)**	
winter	periods with waves	134		72	
	total periods analyzed	306	44%	306	24%
spring	periods with waves	76		40	
	total periods analyzed	281	27%	281	14%
summer	periods with waves	42		21	
	total periods analyzed	277	15%	277	8%
TOTAL	periods with waves	252		133	
	total periods analyzed	864	29%	864	15%
	wave influenced structures	2052		901	
	total structures detected	6715	31%	6899	13%

Table 2.5 Statistical summary of sensible heat flux values ($W \cdot m^{-2}$) under conditions of extreme fluxing contribution ($F_{COHextreme}$), and also under the influence of wave-like motion (F_{WAVE}).

	$F_{COHextreme}$		F_{WAVE}	
	2.6 h (12) m	**0.6 h (3 m)**	**2.6 h (12 m)**	**0.6 h (3 m)**
Minimum	-10.7	-24.8	-50.7	-43.1
Maximum	25.9	11.4	387.6	51.3
Mean	-0.1	-0.6	-0.35	-1.2
Standard Deviation	4.5	2.9	30	10.4

Table 2.6 Percentages of coherent events that are synchronous between both levels, for each day and for the season ("Total"). Time lags are ±0 to 10 s ("10 s"), and ±10 to 20 s ("20 s"). Note that the number of synchronous temperature ramps is identical in both levels, but the total number of ramps detected varies between levels (therefore the percentages are slightly different between levels).

Winter																
Julian Day	**36**		**43**		**53**		**61**		**63**		**64**		**65**		**Total**	
	10s	20s	10s	20s	10s	20s	10s	20s	10s	20s	10s	20s	10s	20s	10s	20s
2.6h (12 m)	15	8	22	8	12	8	18	10	14	9	18	12	10	8	16	9
0.6h (3 m)	15	8	23	9	12	8	17	9	14	9	22	14	11	9	17	10
Spring																
Julian Day	**93**		**94**		**95**		**100**		**101**		**106**				**Total**	
	10s	20s	10s	20s	10s	20s	10s	20s	10s	20s	10s	20s			10s	20s
2.6h (12 m)	28	15	20	16	18	17	19	13	21	16	20	16			21	15
0.6h (3 m)	25	14	21	16	17	17	18	12	19	14	18	14			20	15
Summer																
Julian Day	**176**		**187**		**189**		**190**		**193**		**194**				**Total**	
	10s	20s	10s	20s	10s	20s	10s	20s	10s	20s	10s	20s			10s	20s
2.6h (12 m)	27	18	24	16	25	15	18	16	19	13	24	15			23	15
0.6h (3 m)	25	17	21	14	21	13	17	16	20	13	23	15			21	14

Table 2.7 Fraction of coherent flux contribution (F_{COH}/F_{TOT}) for synchronous events compared to all detected events. Synchronous structures are defined by the time lag intervals of ±0 to 10 s and ±10 to 20 s, and are compared with the (F_{COH}/F_{TOT}) contribution of all events ("All").

	2.6 h (12 m**)**			**0.6 h (**3 m**)**		
Season	All	±0 to10 s	±10 to 20 s	All	±0 to10 s	±10 to 20 s
Winter	44	9	5	50	12	6
Spring	47	12	9	53	14	10
Summer	46	11	9	46	12	8
TOTAL	46	11	8	50	12	8

Chapter 3 Temperature Regimes and Turbulent Heat Fluxes Across a Heterogeneous Canopy in an Alaskan Boreal Forest[1]

Abstract

We evaluate local differences in thermal regimes and turbulent heat fluxes across the heterogeneous canopy of a black spruce boreal forest on discontinuous permafrost in interior Alaska. The data were taken during an intensive observing period in the summer of 2013 from two micrometeorological towers 600 m apart in a central section of boreal forest, one in a denser canopy (DC) and the other in a sparser canopy, but under approximately similar atmospheric boundary layer (ABL) flow conditions. Results suggest that on average 34% of the half-hourly periods in a day are non-stationary, primarily during night and during ABL transitions. Also, thermal regimes differ between the two towers; specifically between midnight and 0500 AKST it is about 3 ^{o}C warmer at DC. On average, the sensible heat flux at DC was greater. For midday periods, the difference between those fluxes exceeded 30% of the measured flux and over 30 W m^{-2} in magnitude more than 60% of the time. These differences are due to higher mechanical mixing as a result of the increased density of roughness elements at DC. Finally, the vertical distribution of turbulent heat fluxes verifies a maximum atop the canopy crown (2.6 h) when compared with the sub-canopy (0.6 h) and above canopy (5.1 h), where h is the mean canopy height. We argue that these spatial and vertical variations of sensible heat fluxes result from the complex scale aggregation of energy fluxes over a heterogeneous canopy.

[1] Starkenburg, D., G. J. Fochesatto, J. Cristóbal, A. Prakash, R. Gens, J. G. Alfieri, H. Nagano, Y. Harazono, H. Iwata, and D. L. Kane (2015), *J. Geophys. Res. Atmos.*, *120*(4), 1348-1360.

3.1 Introduction

Boreal forests represent approximately 33% of the world's forested ecosystems and are a critical component of the global climate system [*Leblanc et al.,* 2005; *Euskirchen et al.,* 2010; *Barr et al.,* 2012]. Previously, large-scale field campaigns such as the Boreal Ecosystem-Atmosphere Study (BOREAS) have shown that land-atmosphere exchange processes are unique for high latitude conifer forests. For instance, boreal conifer forests have low albedos and high sensible heat fluxes compared with other forest biomes at lower latitudes [*Sellers et al.,* 1997; *Eugster et al.,* 2000]. As described in the recent report for the Arctic Boreal-Vulnerability Experiment, the role and complexity of surface-atmosphere interaction in high-latitude ecosystems remains an open question that can be answered only by combining field observations, modeling, and satellite remote sensing [*Kasischke et al.,* 2010]. Therefore, boreal ecosystems remain poorly understood.

The coniferous boreal forest in interior Alaska is characterized by local heterogeneities such as canopy architecture, micro topographies, and subsoil profiles that include organic layers and discontinuous permafrost. It also consists of landscape scale variations owing to lakes and sometimes hilly terrain. As such, the analysis of turbulent processes is particularly challenging in this environment. For instance, large-scale surface heterogeneities can promote stationary updrafts and other secondary circulations that cannot always be captured by the eddy covariance instruments when evaluating local sensible and latent heat fluxes [*Mahrt,* 1998; *Foken,* 2008b; *Foken et al.,* 2010; *Eder et al.,* 2014, and citations therein]. To illustrate this point, atmospheric

flow simulations including surface heterogeneities on the order of 10 km can lead to the apparent disappearance of the pre-assumed existing spectral gap between microscale and mesoscale processes [*Kang,* 2009]. Furthermore, variability in sensible heat fluxes between regions representing the same surface type has been documented when attempting to form composite fluxes (i.e., weighted area averaged fluxes for each representative surface type within a landscape). This was evident in agricultural fields analyzed during the Lindenberg Inhomogeneous Terrain Fluxes between Atmosphere and Surface (LITFASS) experiment, where significant differences in sensible heat fluxes were noted between triticale and rye cereals [*Beyrich et al.,* 2006]. Furthermore, the analysis of energy balance closure for three Canadian boreal forests was found to be sensitive to friction velocity, atmospheric stability, and time of day [*Barr et al.,* 2006]. This is important because the distribution of roughness elements plays a central role in controlling and defining friction velocity which can change over short distances within the boreal forest. Since the modeling of turbulent fluxes in complex canopies using satellite remote sensing data input or mesoscale hydroecological models suffers from spatial scale gaps between the model footprint and local measurements, a simple approximation factor for upscaling may not properly resolve local differences in roughness and thermal regimes. Thus, a clearer understanding of local variations in energy exchange within boreal forests is crucial in order to improve knowledge of ecosystem processes and large-scale processes**,** and their connection to climate and atmospheric modeling.

Understanding local variability in the boreal forest is also important for obtaining reliable model parameters. Incorrect parameterization of forest extent, type, and density has led to the overestimation of evapotranspiration rates in weather prediction and climate models [*Sellers et*

al., 1997]. To advance this, studies from BOREAS [*Sellers et al.*, 1997] and Evaporation at Grid and Pixel Scale (EVA-GRIPS) [*Mengelkamp et al*., 2006] emphasized a multiscale approach to processes ranging from 1 to 1000 m^2 in order to improve model representation and parameterization of small-scale interactions. However, there are few studies that document the variability in surface processes in the heterogeneous Alaskan boreal forests and their link to large scales.

In this work, we employ data from an intensive observing period (IOP) spanning from 3 July to 20 September 2013 to quantify the differences in turbulent fluxes and energy partitioning within two domains of the boreal forest less than 1 km apart with distinctly different canopy architectures but under the influence of the same atmospheric boundary layer (ABL) flow conditions. Section 3.2 describes the site and instrumentation, section 3.3 describes the data processing, section 3.4 reports results and discussions, and section 3.5 provides conclusions and some arguments toward improving the current understanding of the degree to which spatial variations in local turbulent energy fluxes contribute to the "ergodicity" of the forest [*Katul et al.*, 2004].

3.2 Selection of Cases, Site Characteristics and Instrumentation

From the summer 2013 IOP, 11 days (528 half hourly periods) were selected for this analysis, consisting of four consecutive days from 12 to 15 July, and seven consecutive days from 27 July to 2 August. This "optimal period" was chosen because of the lack of precipitation as well as the absence of wildfire smoke (a frequent issue owing to large forest fires during that summer). Despite that no days during the IOP have completely clear skies, the days comprising

the optimal period are taken from the two largest spans of data without smoke or precipitation that have the smoothest diurnal patterns of temperature. Furthermore, the ABL flow regime was similar across towers for the optimal period, such that local differences in fluxes are expected to result from surface properties rather than from mesoscale forcing.

The study area is located within a black spruce (*Picea mariana*) boreal forest north of the University of Alaska Fairbanks (UAF). Fairbanks is located in central Alaska (64°49' N, 147°52' W) where seasonality is extreme due to its high latitude and continentality [*Shulski and Wendler*, 2007]. Specifically, the study area is comprised of two domains, both with discontinuous permafrost and an understory of evergreen shrubs, deciduous shrubs, sedges, and moss cover [*Iwata et al.*, 2012]. One domain is characterized by a dense canopy (hereafter referred to as DC), while the other, located approximately 600 m to the west, is characterized by a short and sparse canopy (hereafter referred to as SC) (Figure 3.1). DC has an elevation of 165 m above sea level (asl) and a mean canopy height (h_1) of 4.7 m, with a standard deviation of ±3.14 m [*Starkenburg et al.*, 2013]. The forest density at DC is around 8500 trees ha^{-1}. SC sits at an elevation of about 155 m als, with a mean canopy height (h_2) of 3.0 m and a tree density of 4500 trees ha^{-1} [*Iwata et al.*, 2012]. The ground texture near SC is more irregular due to the prevalence of patchy hummocks [*Iwata et al.*, 2012].

Both domains were instrumented with micrometeorological towers and subsurface sensors (Table 3.1). Each tower has one sonic anemometer at about twice the local mean canopy height to evaluate the turbulence within proximity of the vegetation top (SC 6 m and DC 12 m). DC also has a sonic anemometer in the subcanopy level at 3 m and one at 24 m to provide vertical profiles of turbulent fluxes. In addition to sonic anemometers, SC is also equipped with

four cup anemometers, and both domains employ air temperature and humidity sensors at multiple heights. During the IOP, a Doppler acoustic sounder (sodar) was deployed to characterize the mesoscale flow common to both domains [*Mayfield and Fochesatto,* 2013; *Fochesatto et al.,* 2013; *Malingowski et al.*, 2014].

3.3 Data Processing

After a qualitative review for time intervals containing signal dropouts and non-physical outliers, the eddy covariance data were processed with a comprehensive suite of post-processing corrections and adjustments [*Alfieri et al.*, 2012]. Specifically, the data were cleaned via an iterative despiking procedure adapted from *Goring and Nikora* [2002]. The air temperature from the sonic anemometer was also corrected for humidity effects according to *Liu et al.* [2001]. Then, a two-dimensional coordinate rotation procedure was applied [*Kaimal and Finnigan,* 1994] along with corrections for sensor displacement (i.e., the slight distance between the gas analyzer and the anemometer transducers), and frequency response attenuation [*Massman,* 2000; *Massman and Lee,* 2002]. After the 30 min. block average turbulent fluxes were calculated, they were corrected for heat and water vapor density changes [*Webb et al.*, 1980].

Wind speeds in the study area were often low (i.e., < 3 ms^{-1} on average); therefore the assumption of a stationary flow may not always be realized. Thus, it was necessary to test for stationarity as outlined in *Foken and Wichura* [1996]. This method subdivides the 30 min averaging period into six, 5 min subintervals. The mean of the flux calculated for each of the subintervals is compared to the flux for the whole 30 min period; if they agree to within 30%, stationarity of the flow can be assumed valid. Otherwise, if this difference exceeds 30%, then the

period was flagged as nonstationary and omitted from the analyses of turbulent fluxes discussed herein.

3.4 Results and Discussion

3.4.1 Mesoscale Conditions and Flow Stationarity

For the 11 days of the optimal period, the ABL was generally well developed. Potential temperature soundings revealed a superadiabatic layer below 200 m on most afternoons, and a well-mixed adiabatic layer from 200 m up to heights ranging from 800 to 1800 m [*Fochesatto*, 2014]. Therefore, the depth of the ABL exceeded the horizontal scale of the heterogeneity as defined by the distance between the two towers (600 m). This suggests that any differences found in this study are due mainly to varying surface conditions at the two domains and not to differences in the ABL regimes. Based on the analysis of the sodar data, the wind direction is uniform between 50 and 500 m. Data from the anemometers at both towers confirm that local wind directions above canopy agree both with one another as well as with the mesoscale wind directions derived from the sodar. Specifically, time series of wind speed and direction from sodar and anemometers suggest that there is a diurnal pattern in the wind direction, with the winds tending to be from the east during the morning but shifting to southwesterly later in the day.

Our results show that on average, the percentages of half hour periods in a day that are nonstationary are the following: 35% (DC 24 m), 28% (DC 12 m), 32% (SC 6 m), and 39% (DC 3 m). Nonstationary periods occur mainly during the night and early morning when conditions are often stable and winds are slow and variable in direction. By contrast, the time interval

between 0800 and 1800 had far fewer nonstationary periods (Figure 3.2). Thus, we conclude that in the boreal forest during summer when the ABL is well-developed, daytime periods are more often stationary; overnight periods, however, require additional evaluation. After removing all nonstationary periods, the number of half hour blocks remaining for subsequent analyses were the following: 343 (DC 24 m), 380 (DC 12 m), 361 (SC 6 m), and 324 (DC 3 m).

3.4.2 Differences in Temperature Regimes

Before assessing the turbulent fluxes, a spatial analysis of the thermal regimes at DC and SC was used to determine if general differences between the two domains were present. For this analysis ambient air temperatures at different heights were used (Table 3.1). The results show that despite 18-21 daylight hours, there is a diurnal temperature cycle. Figure 3.3 shows the mean diurnal pattern in the air temperature at various heights at both towers. At DC, the difference between temperatures at 24 m and 3 m at 0400 AKST is approximately 3.5 ºC, while at SC the difference between 8 m and 1 m is nearly 5 ºC. Also, between midnight and 0500 AKST, temperatures at DC 7 and 12 m (1.5 h_1 and 2.6 h_1) are consistently warmer than at SC 4 and 8 m (1.3 h_2 and 2.7 h_2). This implies that there is a temperature difference between SC and DC reflecting the variable canopy density of the forest. Another important consideration is that in deciduous forests, the canopy tends to be warmer (colder) than the ground during daytime (night), such that the temperature profile below and above the canopy will be reversed [*Foken*, 2008a]. However, the canopy of the boreal conifer forest is open, and therefore, the temperature profile is more continuous, which is an important consideration when upscaling and modeling turbulent parameters in different forest species.

Another feature of the boreal forest is the large diurnal temperature swing that occurs despite long daylight hours. Remarkably, temperatures at 1 m in the SC fell to 0 °C on two mornings, despite mid-day high temperatures of 27 °C. Air temperatures from various levels at each tower show that the average difference between the mean daily high and low temperatures is largest for sensors located near the ground (Figure 3.3) and that this difference is larger than the uncertainty of the sensors. For the top sensors at each tower, this diurnal range is 14.3 °C (DC 24 m) and 17.7 °C (SC 8 m). For the bottom sensors, the range is 19.3 °C (DC 3 m) and nearly 24.7 °C (SC 1 m). However, around the middle of the day the temperature differences between sensors become less significant (no more than about 2 °C between all sensors at both towers) indicating a surface layer with a well-established turbulent flux regime. Nevertheless, DC is often slightly warmer than SC for a given height (Figure 3.3). For instance, from 1000 to 1700 AKST, it is typical for the temperature at SC 1 m to be most similar to DC 3 m, while SC 2 m is most similar to DC 12 m and 7 m, and SC 4 m and 8 m are most similar to DC 24 m (Figure 3.3, inset). Therefore, changes in canopy height and density impact the temperature distribution within and above the forest, consequently affecting thermodynamic processes at small scales; thus, upscaling local processes requires accurate spatial data on canopy architecture [*Gruber and Fochesatto*, 2013; *Gruber et al.*, 2014].

3.4.3 Comparison of Turbulent Variables

Figure 3.4 shows the average half-hourly sensible and latent heat flux for the optimal period. Here it is evident that midday flux values tend to be lower at SC than at DC, especially when comparing DC 12 m ($2.6\ h_1$) and SC 6 m ($2\ h_2$). Consideration must be given to the

uncertainty inherent in any intercomparison of eddy covariance derived flux values owing to instrumental bias, random error, and data quality. *Mauder et al.* [2007] indicated good agreement (similar regression coefficients) between sensible heat fluxes based on CSAT3 and the R.M. Young 81000 sonic anemometers. Therefore, interinstrument bias is not a large concern in this analysis. Additionally, comparisons of sensor types and data quality showed accuracies for sensible heat flux values ranging from 5% (or 10 W m^{-2}) to 15% (or 30 W m^{-2}) [*Mauder et al.*, 2006]. To examine the differences found between DC 12 m and SC 6 m, all half-hourly periods when the heat flux at both instruments exceeded 50 W m^{-2} were isolated because these periods correspond with a well-defined flux during unstable conditions when the flux values are larger and more reliable for comparison. In total, 222 half-hourly periods met this condition. For those 222 cases, the additional criterion that the difference between the DC 12 m and SC 6 m fluxes had to exceed 30 W m^{-2} was imposed. After isolating those cases, an additional constraint was imposed that these differences also had to exceed some percentage of the measured flux at both instruments. Results show that the difference exceeded (a) 30% of the measured flux values 63% of the time, (b) 20% of the measured flux values 82% of the time, (c) 15% of the measured flux values 85% of the time, and (d) 10% of the measured flux values 87% of the time. Thus, we conclude that the difference between DC 12 m and SC 6 m is important when considering the spatial heterogeneity of fluxes within a black spruce boreal forest at 2-2.5 times the local mean canopy height.

Figure 3.4 also shows a vertical comparison of the mean diurnal sensible heat flux values from the three instruments at DC. The Monin-Obukhov similarity hypothesis states that over homogeneous, evenly heated terrain and within a stationary flow, surface fluxes are nearly

constant with height in the surface layer [*Arya*, 2001]. However, the boreal forest is far removed from these idealized conditions, especially within the roughness sublayer. Evident in Figure 3.4 is that during midday periods, flux values are generally highest at 12 m, while those at 3 and 24 m are slightly lower and more similar to one another. Clearly, this profile verifies an increased value at heights where the local roughness increases, suggesting complex patterns in the local aggregation of sensible heat fluxes [*Gruber et al.*, 2014].

In addition to sensible heat flux, gas analyzers were available at DC 24 m and SC 6 m, so in those locations turbulent latent heat fluxes could also be calculated. Latent heat flux is considerably lower than the sensible heat flux, as expected (Figure 3.4). For instance, *Chapin et al.* [2000] note that conifer trees have low albedos and transpiration rates, resulting in high sensible heat fluxes; deciduous boreal forests generate 50-80% more evapotranspiration than conifers in summer. Also, despite permafrost retarding drainage, surface moisture is insulated from the atmosphere by an organic moss layer which may further lower the latent heat flux or introduce non-linear relationships that are difficult to evaluate. *Blok et al.* [2011] demonstrated this insulating effect by removing the moss layer (4-5 cm) from the tundra in northeastern Siberia, resulting in increased ground heat flux and increased understory evapotranspiration from the organic layer below. Although their site was characterized as tundra, these implications show that the insulating moss cover can indeed affect the ground-atmosphere energy exchange.

In order to explain the observed differences between sensible heat flux values it is necessary to consider more than just the thermal differences across the landscape noted earlier in section 3.4.2. The mean 30 min wind direction derived from the sonic anemometer data shows that above the canopy, winds were predominantly southwesterly at both towers (Figure 3.5). A

southwesterly flow traveling toward SC experiences lower roughness than a flow traveling toward DC, resulting in a spatial variation of mechanical mixing. This can be seen in the larger friction velocities (u_*) at DC (Figure 3.6). For example, the mean u_* is about the same for SC 6 m as it is for DC 3 m. This is true despite that SC 6 m is above its local mean canopy height where shear stress is expected to be larger, while DC 3 m is below its local mean canopy height. Additionally, wind speeds at SC 6 m are typically higher than DC 3 m, yet still u_* is about the same at both instruments.

In order to evaluate which mechanism dominates production of turbulent fluxes, we consider the rate equation for turbulent kinetic energy (TKE) [*Stull*, 1988]:

$$\frac{\partial\langle e\rangle}{\partial t} = -\langle u'w'\rangle\frac{\partial\langle \boldsymbol{V}\rangle}{\partial z} + \frac{g}{\langle\theta_v\rangle}\langle w'\theta_v'\rangle - \frac{\partial\langle w'e\rangle}{\partial z} - \frac{1}{\langle\rho\rangle}\frac{\partial\langle w'p'\rangle}{\partial z} - \varepsilon \qquad \text{(Eq. 3.1)}$$

where $\langle e\rangle$ is the mean TKE per unit mass given as $0.5\cdot[\langle u'^2\rangle+\langle v'^2\rangle+\langle w'^2\rangle]$. Furthermore, $\frac{\partial}{\partial t}$ is the local time derivative, $\langle u'w'\rangle$ is the mean horizontal momentum flux, $\langle V\rangle$ is the horizontal wind velocity, g is the acceleration due to gravity, θ_v is the virtual potential temperature, p is air pressure, z is height, ρ is the density of air, and ε is the energy dissipation rate. The angled brackets indicate time averaging over 30 min. Of primary interest in this analysis are the first two terms on the right-hand side in Eq. (3.1): shear stress and buoyancy production of TKE. Evaluating these terms over time and taking the diurnal trends at SC 6 m and DC 12 m shows that shear production dominates over buoyancy production above the canopy and that shear production is typically largest at DC (Figure 3.7). This suggests that the more developed canopy at DC boosts mechanical shear locally, in agreement with the higher u_* values at DC (Figure 3.6).

Analysis of the turbulent temperature scale (θ_*) supports the importance of shear production in the sensible heat fluxes of the boreal forest. The temperature scale is defined by [*Arya*, 2001]

$$\theta_* = -H/(\rho \cdot c_p \cdot u_*) \quad \text{(Eq. 3.2)}$$

where H is the sensible heat flux, ρ is the density of air and c_p is the specific heat of air at constant pressure. Eq. (3.2) describes the relationship between the magnitude of the kinematic sensible heat flux and the shear stress associated with mechanical turbulence. All the evaluated cases show similar diurnal trends of mean θ_* (Figure 3.8). Specifically, Figure 3.8 reveals that for midday periods, the mean difference in θ_* horizontally between DC 12 m and SC 6 m is not much different than that vertically among sensors at DC. This suggests that differences in θ_* cannot account for the difference in sensible heat fluxes between the towers, because u_* plays an equally important role at both towers such that the location where u_* is more robust should have the greatest sensible heat flux. This result demonstrates that variations in canopy structure can cause spatial variability in the mechanical turbulence and thus in the local sensible heat flux.

3.4.4 Energy Partitioning

Figure 3.9 shows the four terms of the basic surface energy balance for DC 24 m and SC 6 m: sensible heat flux (H), latent heat flux (LE), ground heat flux (G), and net radiation (R_{NET}). G is small and difficult to assess owing to the moss layer that insulates the mineral soil from the atmosphere and its variability across the landscape (typical daily maxima are 32 and 13 W m^{-2} at DC and SC, respectively). Furthermore, H is typically much larger than LE, while R_{NET} usually peaks near 500 W m^{-2}. To quantify the partitioning of H, LE and G over R_{NET}, we only used the

data from 0800 to 1800 AKST during each day (Table 3.2a). This period is chosen because average sensible heat flux values are above 50 W m^{-2} while average net radiation (R_{NET}) exceeds 100 W m^{-2}, providing more robust data. Figure 3.10 reveals that the higher sensible heat flux at DC results in a larger fraction of H/R_{NET} there; however, this must be tempered by the fact that DC 24 m is about 5.1 h_1, whereas SC 6 m is about 2.0 h_2; therefore, differences in the variability of water vapor density and vertical velocity are not directly comparable for these two instruments. When the same energy ratios are produced from daily cumulative sums rather than half-hourly intervals between 0800 and 1800 AKST, the result is very similar to that shown in Figure 3.10, differing by 4% or less (Table 3.2b). For the same midday period (0800-1800 AKST), we also evaluated the Bowen ratio for DC 24 m and SC 6 m. Table 3.2 reveals high daily average Bowen ratios (over 2.0) at both towers, with the highest at DC 24 m owing to the larger sensible heat flux there. Nonetheless, it is clear that the greatest partitioning of energy in the boreal forest is into sensible heat.

Table 3.3 compares the results of this analysis with data compiled by *Eugster et al.* [2000] and *Euskirchen et al.* [2010] from some spring and summertime studies in boreal forests also using the eddy covariance method. Most boreal forests have a similar G/R_{NET}, typically at or below a 10% ratio. In all but two cases, H/R_{NET} exceeds LE/R_{NET}, and DC 24 m from this analysis has the second highest Bowen ratio. Energy balance closures below 90% reveal the difficulty in accounting for all the scales involved in the development of turbulent fluxes [e.g., *Wilson et al.,* 2002; *Amiro,* 2009]. Differences in closure may also be due to the differences in techniques used to derive that closure. For instance, in Table 3.3, the balance closure shown in row 13 (labeled as row B), is the result of eddy covariance data that had been corrected for

underestimation using an induction factor derived from cospectral analyses [*Eugster and Senn*, 1995; *Chambers and Chapin*, 2003]. Furthermore, the closure shown in row 14 (labeled C) was derived from linear regressions of $H+LE/R_{NET}$-G [*Liu and Randerson*, 2008].

3.5 Conclusions

In conclusion, measurements from two micrometeorological towers located 600 m apart within a black spruce boreal forest in interior Alaska with discontinuous permafrost were selected to evaluate and compare under similar ABL flows in the summer of 2013. One site was located in a denser, taller canopy (DC) and the other in a more open canopy (SC). Testing the stationarity of the atmospheric flow revealed that an average of about 34% of the half-hourly periods in a day are non-stationary, primarily at night or during transitions, reinforcing that stationarity becomes very restrictive in a forest canopy.

It was also found that higher temperatures typify DC, most notably at night, owing to its denser canopy. Vertical gradients of temperature were larger at SC at night, while DC shows a lower diurnal range of temperature variation. This points to the complexity of defining a time for the ABL transition in the turbulent fluxes across the landscape which in turn will complicate the computation of large-scale area average turbulent fluxes.

Sensible heat flux values were larger at DC on average, especially between DC 12 m and SC 6 m where a difference of over 30% of the measured flux value (and over 30 W m^{-2} in magnitude) occurred 60% of the time during midday periods. This was explained by the increased surface roughness and enhanced mechanical mixing at DC, evidenced by the higher friction velocity and greater shear production which dominate in the TKE rate equation.

Comparing sensible heat flux values vertically at DC, we also found that the largest values were at 12 m on average, confirming a complex aggregation of sensible heat within and above the spruce canopy. The resultant energy balance closure was around 64% for SC 6 m and 77% for DC 24 m, with greater values of sensible heat flux at DC primarily contributing to the higher closure fraction.

Thus, we conclude that spatial variations in thermal regime and in sensible heat flux values exist within the complex forests of interior Alaska over short distances, resulting from variations in canopy height and density which control friction velocity and the heating of canopy elements. This study also reveals that upscaling local turbulent heat fluxes to large-scale area average values within the boreal forest is likely to be complex and non-linear owing to the aggregation of energy fluxes in a heterogeneous canopy.

Acknowledgements

This research was supported by the Alaska NASA EPSCoR program award NNX10NO2A, by the Alaska Space Grant Program, and by the "New GK-12 Program: The CASE (Changing Alaska Science Education) for Enhancing Understanding of Climate Change" NSF (DGE-0948029). Data sets for this paper can be requested from G.J. Fochesatto (foch@gi.alaska.edu), Geophysical Institute University of Alaska Fairbanks, for DC and Doppler sodar sites and from Y. Harazono (yharazono@iarc.uaf.edu), International Arctic Research Center University of Alaska Fairbanks, for SC site.

The following authors contributed work on this manuscript as noted:

D. Starkenburg: Collected DC data, processed, and evaluated all data; primary writer/editor

G. J. Fochesatto: Assisted in data processing and guiding research; secondary editor

J. Cristóbal: Assisted in data processing; secondary editor

J. G. Alfieri: Provided processing code for sonic anemometer data; secondary editor

H. Nagano, Y. Harazono: Collected and provided SC data; secondary editors

H. Iwata: Assisted in processing SC water vapor data; secondary editor

A. Prakash, R. Gens, and D. L. Kane: Secondary editors

3.6 References

Alfieri, J. G., W. P. Kustas, J. H. Prueger, L. E. Hipps, S. R. Evett, J. B. Basara, C. M. U. Neale, A. N. French, P. Colaizzi, N. Agam, M. H. Cosh, J. L. Chavez, and T. A. Howell (2012), On the discrepancy between eddy covariance and lysimetry-based surface flux measurements under strongly advective conditions, *Adv. Water Resour.*, *50*, 62-78, doi: 10.1016/j.advwatres.2012.07.008.

Amiro, B. (2009), Measuring boreal forest evapotranspiration using the energy balance residual, *J. Hydrol.*, *336*(1-4), 112-118, doi: 10.1016/j.jhydrol.2008.12.021.

Arya, S. P. (2001), *Introduction to Micrometeorology*, 2nd ed., Academic Press, San Diego.

Barr, A. G., K. Morgenstern, T. A. Black, J. H. McCaughey, and Z. Nesic (2006), Surface energy balance closure by the eddy-covariance method above three boreal forest stands and implications for the measurement of the CO_2 flux, *Agric. Forest Meteorol.*, *140*(1-4), 322-337, doi: 10.1016/j.agrformet.2006.08.007.

Barr, A. G., G. van der Kamp, T. A. Black, J. H. McCaughey, and Z. Nesic (2012), Energy balance closure at the BERMS flux towers in relation to the water balance of the White Gull Creek watershed 1999-2009, *Agric. Forest Meteorol.*, *153*, 3-13, doi: 10.1016/j.agrformet.2011.05.017.

Beyrich, F., J.-P. Leps, M. Mauder, J. Bange, T. Foken, S. Huneke, H. Lohse, A. Ludi, W. M. L. Meijninger, D. Mironov, U. Weisensee, and P. Zittel (2006), Area-averaged surface fluxes over the LITFASS region based on eddy-covariance measurements, *Boundary-Layer Meteorol.*, *121*(1), 33-65, doi: 10.1007/s10546-006-9052-x.

Blok, D., M. M. P. D. Heijmans, G. Schaepman-Strub, J. van Ruijven, F. J. W. Parmentier, T. C. Maximov, and F. Berendse (2011), The cooling capacity of mosses: controls on water and energy fluxes in a Siberian tundra site, *Ecosystems*, *14*(7), 1055-1065, doi: 10.1007/s10021-011-9463-5.

Chambers, S. D., and F. S. Chapin III (2003), Fire effects on surface-atmosphere energy exchange in Alaskan black spruce ecosystems: Implications for feedbacks to regional climate, *J.Geophys. Res.*, *108*(D1), FFR 1-17, doi: 10.1029/2001JD000530.

Chapin III, F. S., A. D. McGuire, J. Randerson, R. Pielke Sr., D. Baldocchi, S. E. Hobbie, N. Roulet, W. Eugster, E. Kasischke, E. B. Rastetter, S. A. Zimov, and S. W. Running (2000), Arctic and boreal ecosystems of western North America as components of the climate system, *Global Change Biol.*, *6*(S1), 211–223, doi: 10.1046/j.1365-2486.2000.06022.x.

Eder, F., F. De Roo, K. Kohnert, R. L. Desjardins, H. P. Schmid, and M. Mauder (2014), Evaluation of two energy balance closure parameterizations, *Boundary-Layer Meteorol.*, *151*(2), 195-219, doi: 10.1007/s10546-013-9904-0.

Eugster, W., W. R. Rouse, R. A. Pielke Sr., J. P. McFadden, D. D. Baldochhi, T. G. F. Kittel, F. S. Chapin III, G. E. Liston, P. L. Vidale, E. Vaganov, and S. Chambers (2000), Land-atmosphere energy exchange in Arctic tundra and boreal forest: available data and feedbacks to climate, *Global Change Biol.*, *6*(S1), 84-115, doi: 10.1046/j.1365-2486.2000.06015.x.

Eugster, W., and W. Senn (1995), A cospectral correction model for measurement of turbulent NO_2 flux, *Boundary-Layer Meteorol.*, *74*(4), 321-340, doi: 10.1007/BF00712375.

Euskirchen, E. S., A. D. McGuire, F. S. Chapin III, and T. S. Rupp (2010), The changing effects of Alaska's boreal forests on the climate system, *Can. J. For. Res.*, *40*(7), 1336-1346, doi: 10.1139/X09-209.

Fochesatto, G.J. (2014), Methodology for determining multilayered temperature inversions. *Atmos. Meas. Tech. Discuss*., *7*(10), 10559-10583, doi: 10.5194/amtd-7-10559-2014.

Fochesatto**,** G. J., J. A. Mayfield, M. A. Gruber, D. Starkenburg and J. Conner (2013), Occurrence of shallow cold flows in the winter atmospheric boundary layer of interior of Alaska, *Meteorol. Atmos. Phys.,* 1-14, doi: 10.1007/s00703-013-0274-4.

Foken, T. (2008a), *Micro-meteorology*, Springer-Verlag, Berlin.

Foken, T. (2008b), The energy balance closure problem: an overview, *Ecol. Appl.*, *18*(6), 1351-1367, doi: 10.1890/06-0922.1.

Foken, T., M. Mauder, C. Liebethal, F. Wimmer, F. Beyrich, J.-P. Leps, S. Raasch, H. A. R. DeBruin, W. M. L. Meijninger, and J. Bange (2010), Energy balance closure for the LITFASS-2003 experiment, *Theor. Appl. Climatol.*, *101*(1-2), 149-160, doi: 10.1007/s00704-009-0216-8.

Foken, T., and B. Wichura (1996), Tools for quality assessments of surface-based flux measurements, *Agric. Forest Meteorol.*, *78*(1-2), 83-105, doi: 10.1016/0168-1923(95)02248-1.

Goring, D. G., and V. I. Nikora (2002), Despiking acoustic Doppler velocimeter data, *J. Hydraul. Eng.*, *128*(1), 117-126, doi:10.1061/(ASCE)0733-9429(2002)128:1(117).

Gruber, M. A. and G. J. Fochesatto (2013), A new sensitivity analysis and solution method for scintillometer measurements of area-average turbulent fluxes, *Boundary-Layer Meteorol.*, *149*(1), 65–83, doi: 10.1007/s10546-013-9835-9.

Gruber, M. A., G. J. Fochesatto, O. K. Hartogensis, and M. Lysy (2014), Functional derivatives applied to error propagation of uncertainties in topography to large-aperture scintillometer-derived heat fluxes, *Atmos. Meas. Tech.*, *7*(7), 2361-2371, doi: 10.5194/amt-7-2361-2014.

Iwata, H., Y. Harazono, and M. Ueyama (2012), The role of permafrost in water exchange of a black spruce forest in Interior Alaska, *Agric. Forest Meteorol.*, *161*, 107-115, doi: 10.1016/j.agrformet.2012.03.017.

Kaimal, J. C., and J. J. Finnigan (1994), *Atmospheric Boundary Layer Flows: Their Structure and Measurement*, Oxford University, New York.

Kang, S.-L. (2009), Temporal oscillations in the convective boundary layer forced by mesoscale surface heat-flux variations, *Boundary-Layer Meteorol.*, *132*(1), 59-81, doi: 10.1007/s10546-009-9391-5.

Kasischke, E. S., S. J. Goetz, J. S. Kimball, and M. M. Mack (2010), The Arctic-Boreal Vulnerability Experiment (ABoVE): A concise plan for a NASA-sponsored field campaign, <http://cce.nasa.gov/terrestrial_ecology/pdfs/ABoVE%20Final%20Report.pdf>.

Katul, G., D. Cava, D. Poggi, J. Albertson, and L. Mahrt (2004), Stationarity, homogeneity, and ergodicity in canopy turbulence, in *Handbook of micrometeorology: A guide for surface*

flux measurement and analysis, edited by X. Lui, W. Massman and B. Law, Kluwer Academic Publishers, Dordrecht, Netherlands.

Leblanc, S. G., J. M. Chen, R. Fernandes, D. W. Deering, and A. Conley (2005), Methodology comparison for canopy structure parameters extraction from digital hemispherical photography in boreal forests, *Agric. Forest Meteorol.*, *129*(3-4), 187-207, doi: 10.1016/j.agrformet.2004.09.006.

Liu H., G. Peters, and T. Foken (2001), New equations for sonic temperature variance and buoyancy heat flux with an omnidirectional sonic anemometer, *Boundary-Layer Meteorol.*, *100*(3), 459–468, doi: 10.1023/A:1019207031397.

Liu H., and J. T. Randerson (2008), Interannual variability of surface energy exchange depends on stand age in a boreal forest fire chronosequence, *J. Geophys. Res.*, *113*(G01006), 1-13, doi: 10.1029/2007JG000483.

Mahrt, L (1998), Flux sampling errors for aircraft and towers, *J. Atmos. Oceanic Technol.*, *15*(2), 416-429, doi: 10.1175/1520-0426(1998)015<0416:FSEFAA>2.0.CO;2.

Malingowski J., D. Atkinson, G. J. Fochesatto, J. Cherry, and E. Stevens (2014), An observational study of radiation temperature inversions in Fairbanks, Alaska, *Polar Science*, *8*(1), 24–39, doi: 10.1016/j.polar.2014.01.002.

Mayfield J. A., and G. J. Fochesatto (2013), The layered structure of the winter atmospheric boundary layer in the interior of Alaska, *J. Appl. Meteor. Climatol.*, *52*(4), 953-973, doi: 10.1175/JAMC-D-12-01.1.

Massman W.J. (2000), A simple method for estimating frequency response corrections for eddy covariance systems, *Agric. Forest Meteorol.*, *104*(3), 185–198, doi: 10.1016/S0168-1923(00)00164-7.

Massman W.J., and X. Lee (2002), Eddy covariance flux corrections and uncertainties in long term studies of carbon and energy exchanges, *Agric. Forest Meteorol.*, *113*(1), 121–144, doi: 10.1016/S0168-1923(02)00105-3.

Mauder, M., C. Liebethal, M. Gockede, J.-P. Leps, F. Beyrich, and T. Foken (2006), Processing and quality control of flux data during LITFASS-2003, *Boundary-Layer Meteorol.*, *121*(1), 67-88, doi: 10.1007/s10546-006-9094-0.

Mauder, M., S. P. Oncley, R. Vogt, T. Weidinger, L. Ribeiro, C. Bernhofer, T. Foken, W. Kohsiek, H. A. R. De Bruin, and H. Liu (2007), The energy balance experiment EBEX-2000. Part II: Intercomparison of eddy-covariance sensors and post-field data processing methods, *Boundary-Layer Meteorol.*, *123*(1), 29-54, doi: 10.1007/s10546-006-9139-4.

Mengelkamp, H.-T., F. Beyrich, G. Heinemann, F. Ament, J. Bange, F. Berger, J. Bösenberg, T. Foken, B. Hennemuth, C. Heret, S. Huneke, K.-P. Johnsen, M. Kerschgens, W. Kohsiek, J.-P. Leps, C. Liebethal, H. Lohse, M. Mauder, W. Meijninger, S. Raasch, C. Simmer, T. Spieb, A. Tittebrand, J. Uhlenbrock, and P. Zittel (2006), Evaportaion over a heterogeneous land surface: The EVA-GRIPS Project, *Bull. Amer. Meteor. Soc.*, *87*(6), 775-786, doi: http://dx.doi.org/10.1175/BAMS-87-6-775.

Sellers, P. J., F. G. Hall, R. D. Kelly, A. Black, D. Baldocchi, J. Berry, M. Ryan, K. J. Ranson, P. Crill, D. Lettenmaier, H. Margolis, J. Cihlar, J. Newcomer, D. Fitzjarrald, P. G. Jarvis, S. T. Gower, D. Halliwell, D. Williams, B. Goodison, D. E. Wickland, and F. E. Guertin

(1997), BOREAS in 1997: experiment overview, scientific results, and future directions, *J. Geophys. Res.-Atmos.*, *102*(D24), 28731-28769, doi: 10.1029/97JD03300.

Shulski, M., and G. Wendler (2007), *The Climate of Alaska*, 216 pp., University of Alaska, Fairbanks.

Starkenburg, D., G. J. Fochesatto, A. Prakash, J. Cristóbal, R. Gens, and D. L. Kane (2013), The role of coherent flow structures in the sensible heat fluxes of an Alaskan boreal forest, *J. Geophys. Res.-Atmos.*, *118*(15), 8140-8155, doi: 10.1002/jgrd.50625.

Stull, R. B. (1988), *An Introduction to Boundary Layer Meteorology*, Kluwer Academic, Dordrecht, Netherlands.

Webb E. K., G. L. Pearman, and R. Leuning (1980), Correction of flux measurements for density effects due to heat and water vapour transfer, *Q. J. R. Meteorol. Soc.*, *106*(447), 85–100, doi: 10.1002/qj.49710644707.

Wilson, K., A. Goldstein, E. Falge, M. Aubinet, D. Baldocchi, P. Berbigier, C. Bernhofer, R. Ceulemans, H. Dolman, C. Field, A. Grelle, A. Ibrom, B. E. Law, A. Kowalski, T. Meyers, J. Moncrieff, R. Monson, W. Oechel, J. Tenhunen, R. Valentini, and S. Verma (2002), Energy balance closure at FLUXNET sites, *Agric. Forest Meteorol.*, *113*(1-4), 223-243, doi: 10.1016/S0168-1923(02)00109-0.

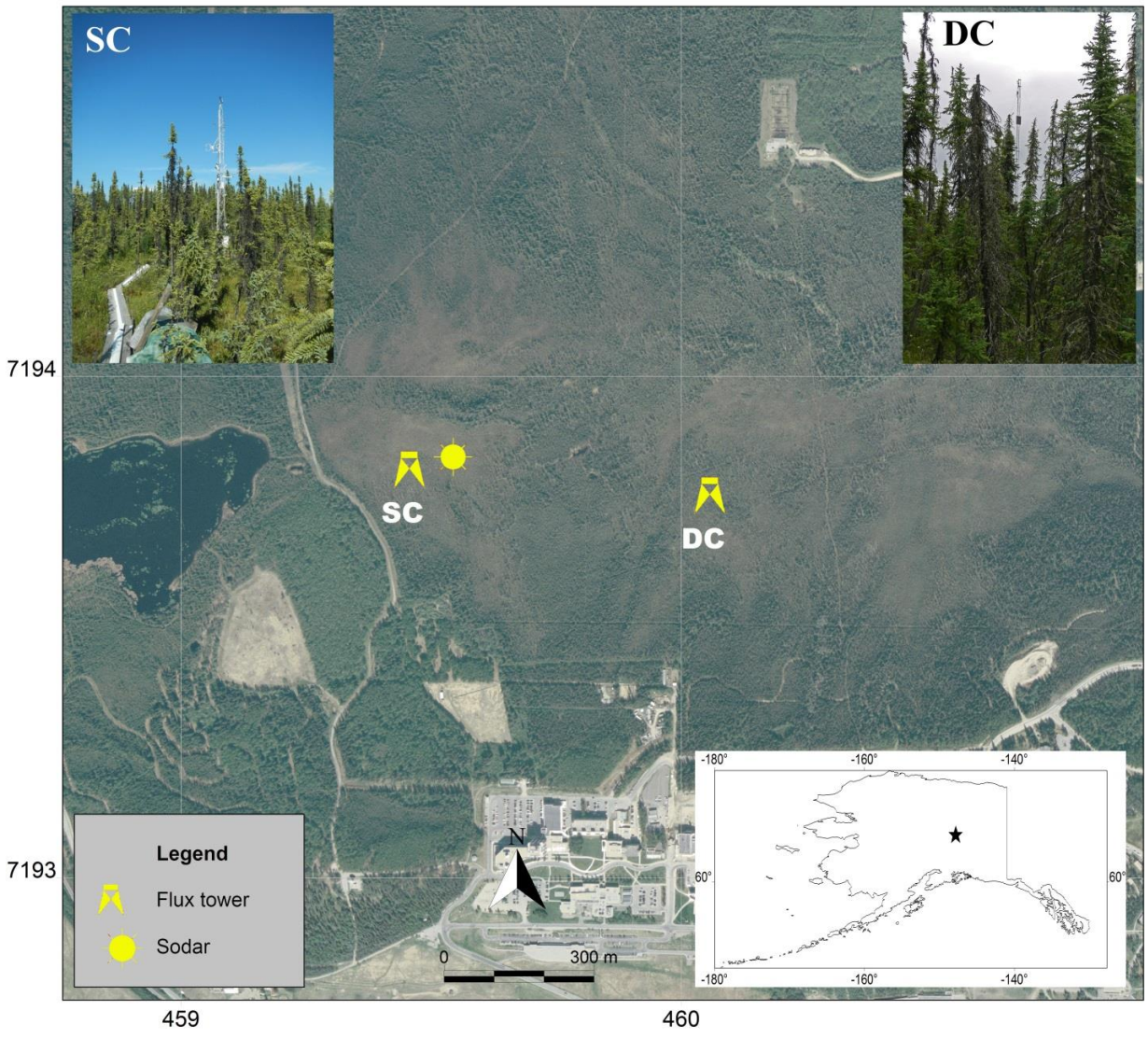

Figure 3.1 The black spruce boreal forest north of the University of Alaska Fairbanks (UAF). Flux tower near the center of the image is DC, while that to the west is SC. Solid yellow circle indicates the location of a Doppler sodar. Coordinates are in km in UTM-06 N Datum NAD-83.

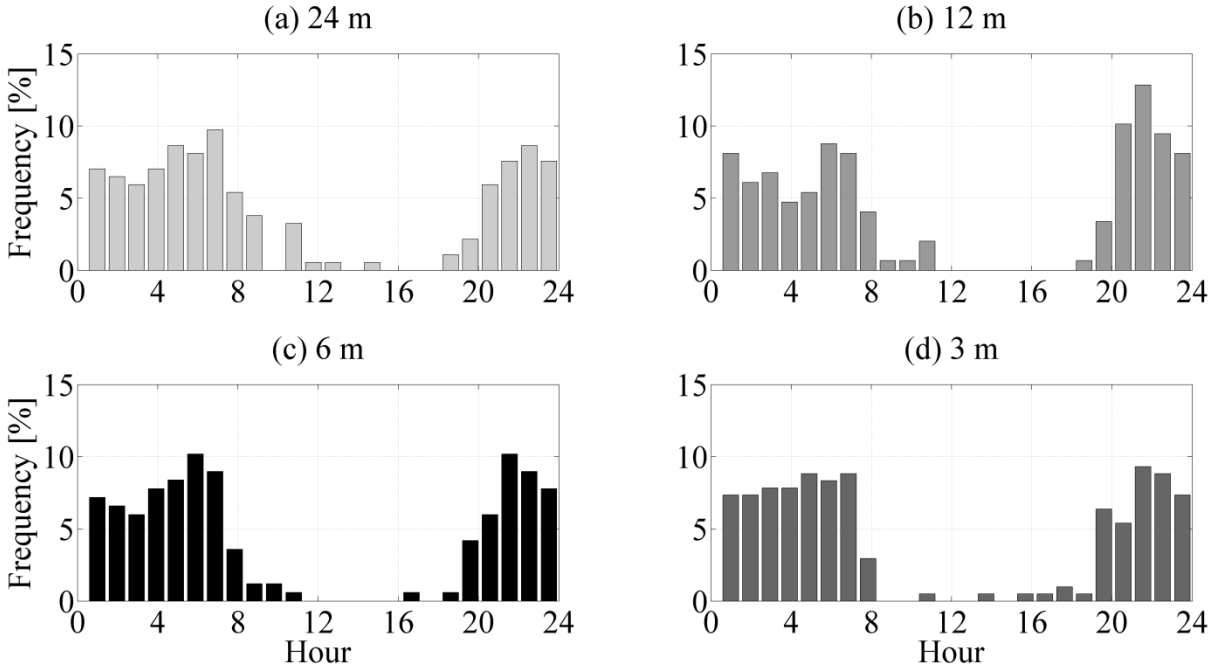

Figure 3.2 Times with nonstationary flows. Total number of data samples was 528 half-hour periods for each instrument. Bin size is one hour (i.e., 24 bins).

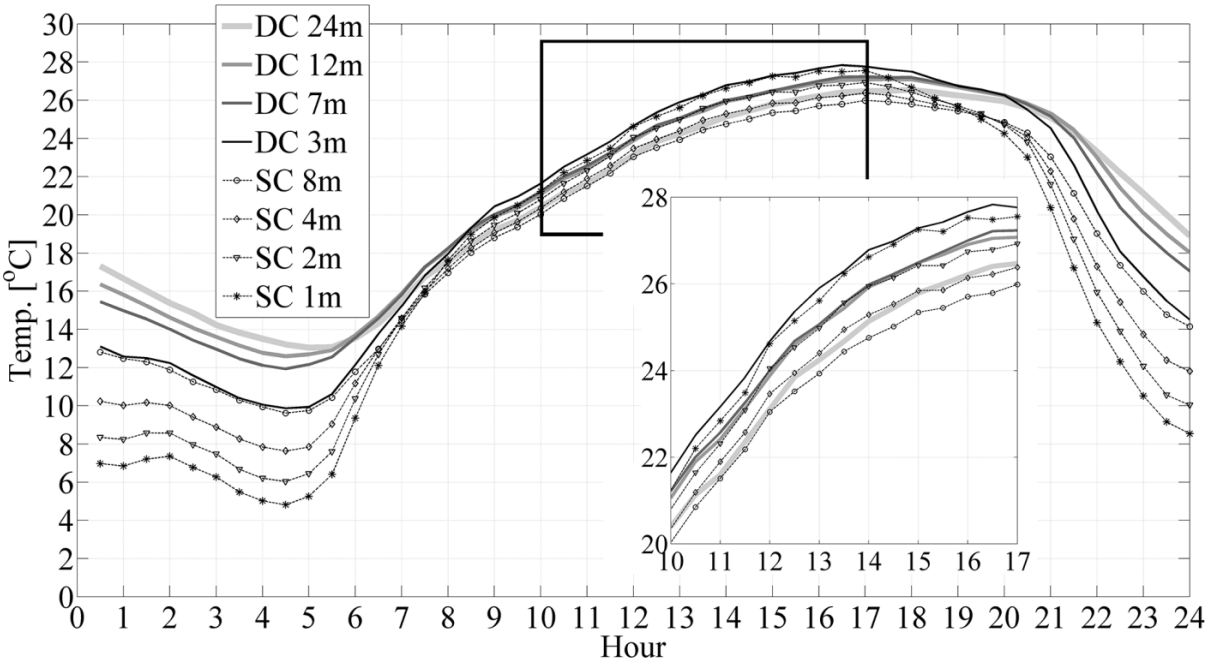

Figure 3.3 Mean diurnal temperature cycles for DC and SC. Black rectangle indicates inset, which shows enlargement of 1000-1700 AKST.

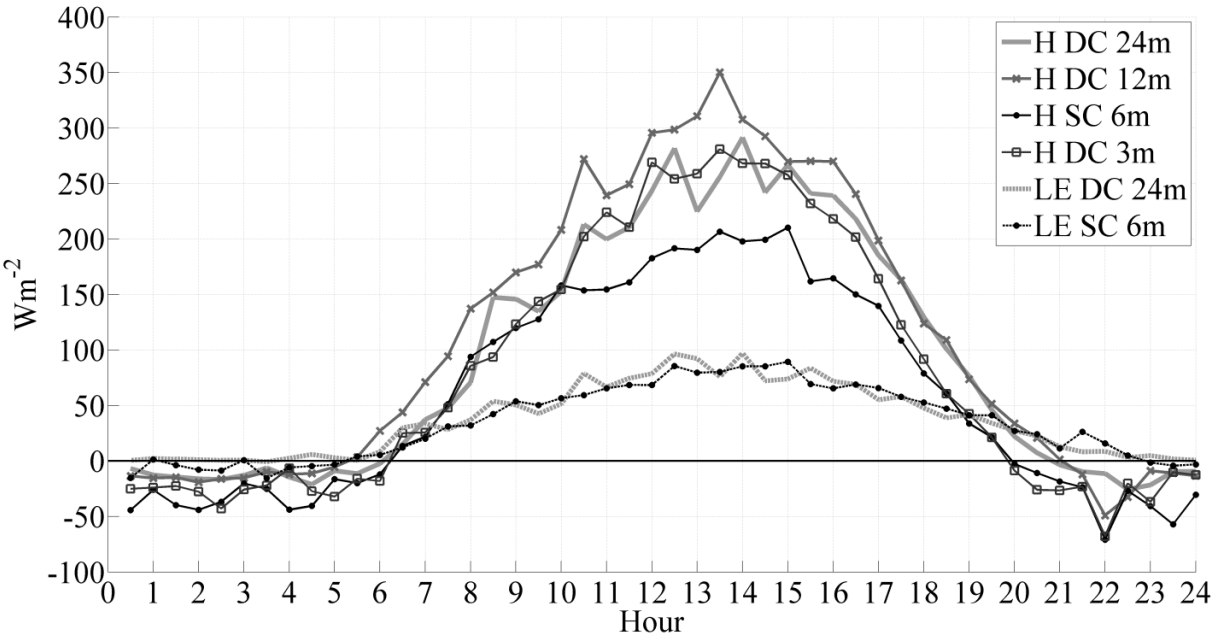

Figure 3.4 Mean sensible (H) and latent (LE) heat fluxes evaluated from sonic anemometer data at DC (24, 12 and 3 m) and also at SC (6 m) over the optimal period. Horizontal line at 0 W m^{-2} is shown for reference.

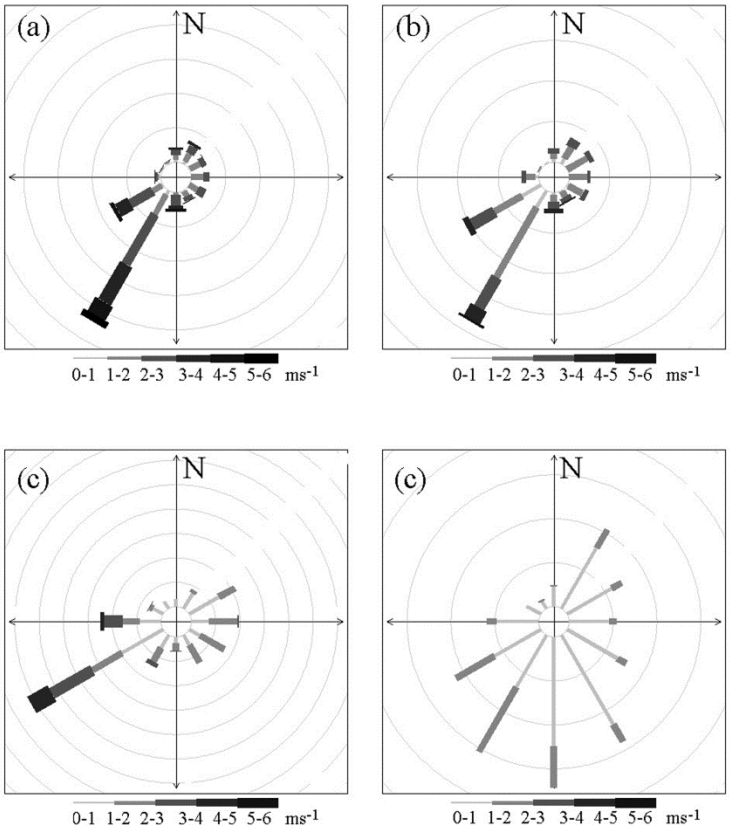

Figure 3.5 Wind rose diagrams for (a) DC 24 m, (b) DC 12 m, (c) SC 6 m, and (d) DC 3 m.

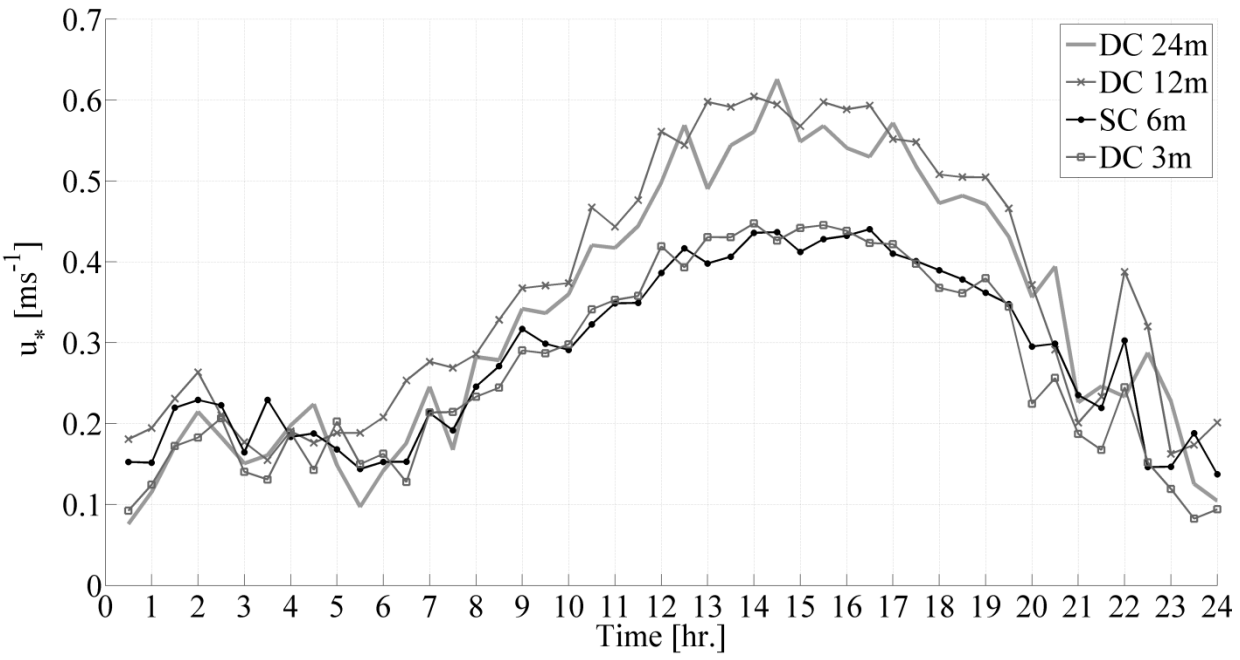

Figure 3.6 Mean friction velocity for DC (24, 12 and 3 m) and SC (6 m) over the optimal period (note that the secondary peak at 2200 AKST is due to a small sample size of stationary periods during nighttime).

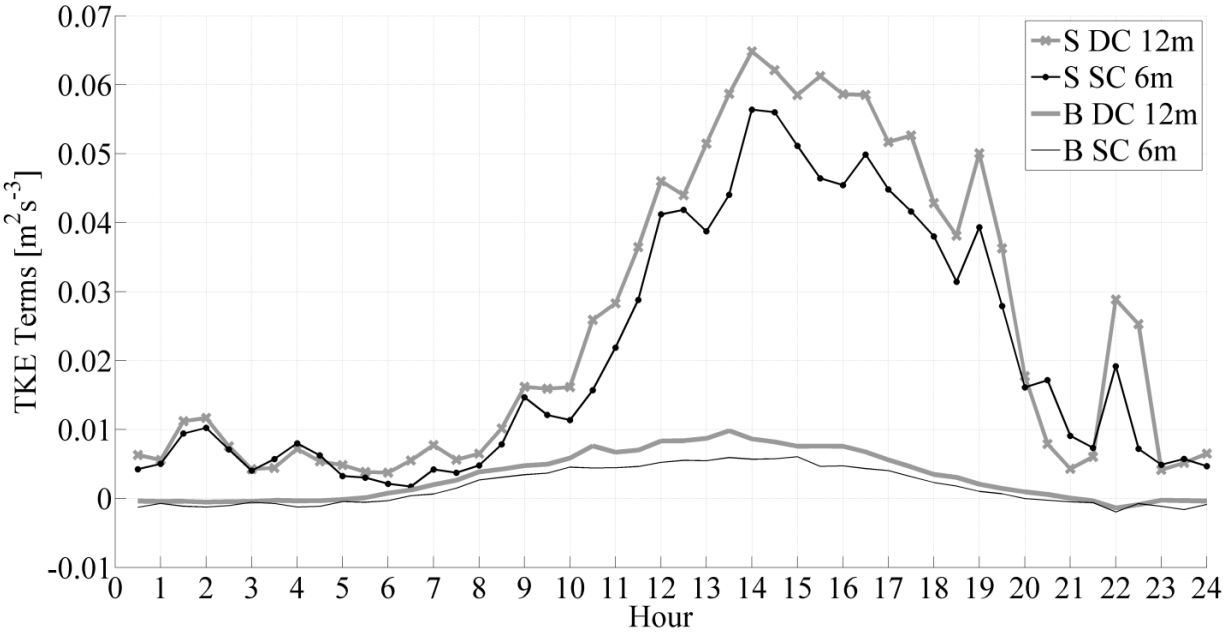

Figure 3.7 Mean shear stress production (S) and buoyancy production (B) for DC 12 m and SC 6 m over the optimal period (note that the secondary peak at 2200 AKST is due to a small sample size of stationary periods during nighttime).

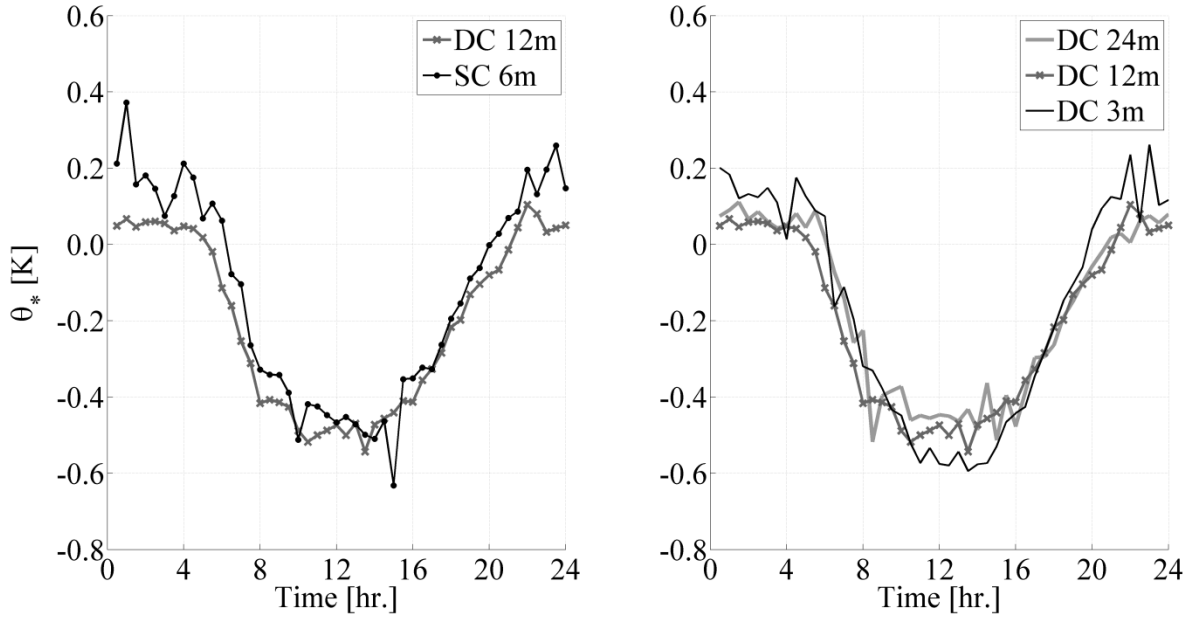

Figure 3.8 Mean temperature scale (θ_*) for DC 24, 12 and 3 m and also for SC 6 m. Panel (a) shows only DC 12 and SC 6 m to emphasize the horizontal variation between towers, while (b) shows all instruments at DC to reveal the vertical variation locally at one tower.

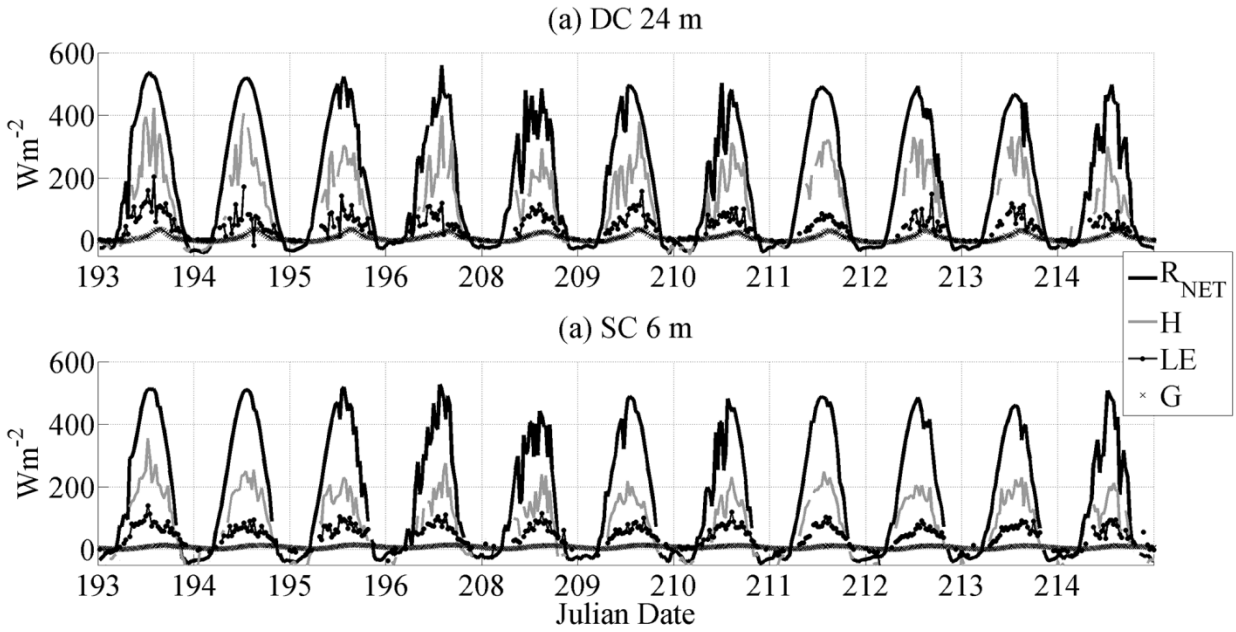

Figure 3.9 Terms of the surface energy balance: net radiation (R_{NET}), sensible heat flux (H), latent heat flux (LE) and ground heat flux (G) for (a) the tower location at DC 24 m, and (b) at SC 6 m.

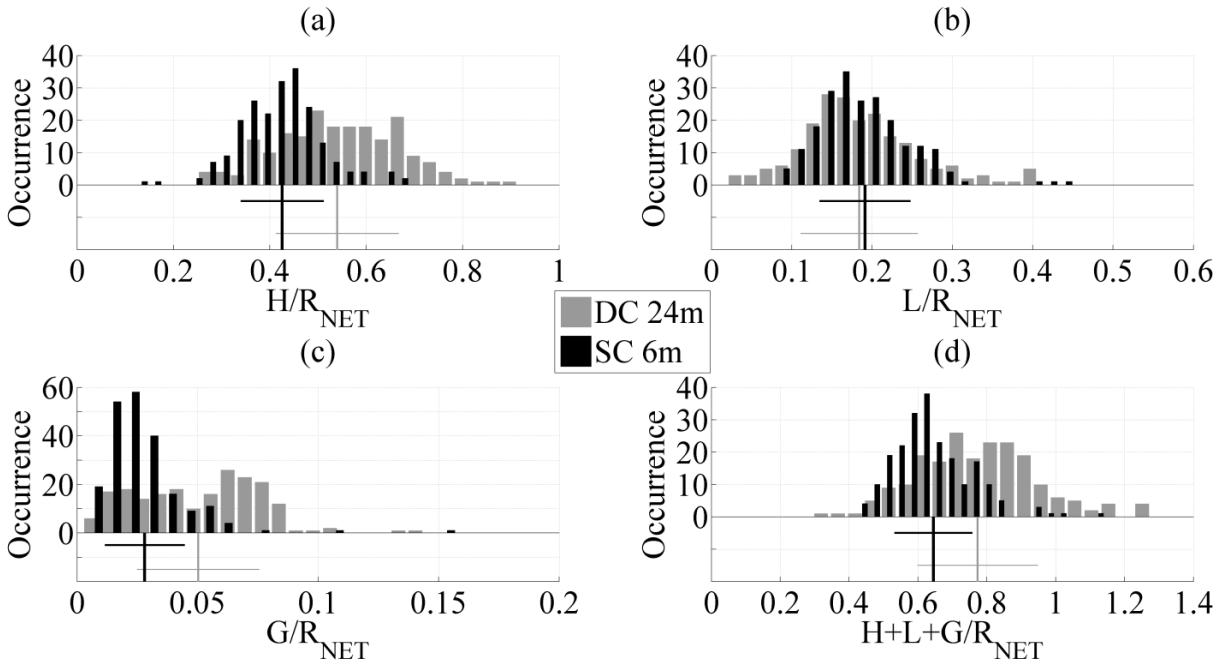

Figure 3.10 Energy partitioning for DC and SC for half hourly periods from 0800 to 1800 AKST, showing: (a) sensible heat flux over R_{NET}, (b) latent heat flux over R_{NET}, (c) ground heat flux over R_{NET}, (d) energy balance closure. Sample size is: 203 (214) for DC (SC). Bin size is 20. Vertical (horizontal) lines under the histograms are means (standard deviation). Nonstationary periods are removed.

Table 3.1 Instrumentation at: (a) SC and (b) DC. Italics indicate instrumentation below ground.

(a) SC – International Arctic Research Center (UAF)

Mounting Height [m]	Instrument	Model	Variable Measured
10	wind vane	Yokogawa Denshikiki, A-802	wind direction
8	cup anemometer	Makino Applied Instruments AF750	wind speed
	temperature/RH probe	Vaisala HMP155Z	air temperature/RH
6	3D sonic anemometer	Campbell Scientific CSAT3	u,v,w and sonic temp
	gas analyzer	Li-Cor LI-7500	H_2O vapor density
4.9	net radiometer	Kipp & Zonen CNR 4	shortwave up and down
4	cup anemometer	Makino Applied Instruments AF750	wind speed
	temperature/RH probe	Vaisala HMP155Z	air temperature/RH
2	cup anemometer	Makino Applied Instruments AF750	wind speed
	temperature/RH probe	Vaisala HMP155Z	air temperature/RH
	barometer	Vaisala PTB101	barometric pressure
1	temperature/RH probe	Vaisala HMP155Z	air temperature/RH
1	Doppler sodar	Remtech PA0	mesoscale wind flow
0 to -0.1	*TDR sensor*	*CS616 Campbell Scientific*	*volumetric water content*
-0.1	*heat flux plate (4)*	*REBS, HFT3-L*	*ground heat flux*
	thermocouple thermometer		*subsoil temperature*
-0.1 to -0.2	*TDR sensor*	*CS616 Campbell Scientific*	*volumetric water content*
-0.2	*thermocouple thermometer*		*subsoil temperature*
-0.2 to -0.3	*TDR sensor*	*CS616 Campbell Scientific*	*volumetric water content*
0 to -0.3	*TDR sensor*	*CS616 Campbell Scientific*	*volumetric water content*
-0.8	*thermocouple thermometer*		*subsoil temperature*
-1.3	*thermocouple thermometer*		*subsoil temperature*

(b) DC – Geophysical Institute (UAF)

Mounting Height [m]	Instrument	Model	Variable Measured
24	3D sonic anemometer	Campbell CSAT3	u,v,w and sonic temp
	gas analyzer	EC-150 Campbell Scientific	H_2O vapor density
	net radiometer	NR01 Hukseflux	solar radiation
	temperature sensor	107-L Campbell Scientific	air temperature
12	3D sonic anemometer	RMYoung 81000	u,v,w and sonic temp
	temperature/RH probe	Vaisala HMP45	air temperature/RH
7	thermistor	107-L Campbell Scientific	air temperature
3	3D sonic anemometer	RMYoung 81000	u,v,w and sonic temp
	temperature/RH probe	Vaisala HMP45	air temperature/RH
	barometer	Vaisala CS106	barometric pressure
-0.06	*thermistor (2)*	*107-L Campbell Scientific*	*subsoil temperature*
-0.12	*thermistor (2)*	*107-L Campbell Scientific*	*subsoil temperature*
	soil moisture sensor	*CS616-L Campbell Scientific*	*volumetric water content*
-0.13	*heat flux plate (2)*	*HFP01-L Hukseflux*	*ground heat flux*
-0.16	*soil moisture sensor*	*CS616-L Campbell Scientific*	*volumetric water content*
-0.23	*heat flux plate (2)*	*HFP01-L Hukseflux*	*ground heat flux*

Table 3.2 Energy partitioning of DC 24 m and SC 6 m for (a) stationary half-hourly values between 0800-1800 AKST, and (b) daily cumulative sums of all stationary periods for each of the 11 days. First column is the domain, second column is the sample size (n), third column is sensible heat over R_{NET}, fourth column is latent heat over R_{NET}, fifth column is ground heat flux over R_{NET}, sixth column is Bowen ratio, seventh column is closure fraction. Values in parentheses and italics are ±1 standard deviation. (Note that for (b), the sample size is the total number of stationary half hours for all 11 days, but the standard deviation is that of the 11 daily means).

(a) Half-hourly (0800-1800 AKST)

Partition	**n**	**H/R_{NET}**	**LE/R_{NET}**	**G/R_{NET}**	**BR**	**$H+LE+G/R_{NET}$**
DC 24 m	203	0.54 *(0.13)*	0.18 *(0.07)*	0.05 *(0.03)*	3.32 *(2.30)*	0.77 *(0.17)*
SC 6 m	214	0.43 *(0.09)*	0.19 *(0.06)*	0.03 *(0.02)*	2.38 *(0.69)*	0.64 *(0.11)*

(b) Daily Cumulative Sum

Partition	**n**	**H/R_{NET}**	**LE/R_{NET}**	**G/R_{NET}**	**BR**	**$H+LE+G/R_{NET}$**
DC 24 m	342	0.52 *(0.04)*	0.19 *(0.03)*	0.05 *(0.01)*	2.82 *(0.53)*	0.76 *(0.05)*
SC 6 m	354	0.39 *(0.04)*	0.20 *(0.03)*	0.03 *(0.01)*	2.03 *(0.38)*	0.62 *(0.04)*

Table 3.3 Energy partitioning. Rows 1-2 (bold): Energy partitioning of DC and SC for daily cumulative sums as in table 2b, except now including the mean daily value of shortwave downwelling radiation (SW↓) and net radiation (R_{NET}) both in W m^{-2}. Rows 3-11: similar values from other boreal forest sites as compiled by *Eugster et al.*, [2000]. Rows 12-14 (italics): similar values from other Alaskan boreal forests compiled by *Euskirchen et al.*, [2010]. (Note that daily mean values of SW↓ and R_{NET} for the current paper are derived from all available data, while H/R_{NET}, LE/R_{NET}, G/R_{NET}, and $H+LE+G/R_{NET}$ have nonstationary periods removed; also, BR in this table is the ratio of column 4 over column 5, and $H+LE+G/R_{NET}$ for the values from other authors are calculated here as the sum of columns 4, 5 and 6).

Partition	**SW↓**	**R_{NET}**	**H/R_{NET}**	**LE/R_{NET}**	**G/R_{NET}**	**BR**	**$H+LE+G/R_{NET}$**
DC 24 m	**268**	**181**	**0.52**	**0.19**	**0.05**	**2.74**	**0.76**
SC 6 m	**271**	**167**	**0.39**	**0.20**	**0.03**	**1.95**	**0.62**
Bfc1	-	143	0.47	0.42	0.09	1.12	0.98
Bfc2	-	-	0.58	0.38	-	1.53	-
	-	-	0.53	0.45	-	1.18	-
	-	-	0.53	0.37	-	1.43	-
Bfc3	-	144	0.43	0.54	0.03	0.80	1.00
Bfc4	-	66	0.41	0.55	0.02	0.75	0.98
Bfp1	-	121	0.48	0.38	0.01	1.26	0.87
Bfp3	194	107	0.52	0.23	0.10	2.26	0.85
Bfp5	-	196	0.64	0.17	0.19	3.76	1.00
A	-	-	*0.40*	*0.37*	-	*1.08*	-
B	-	-	*0.52*	*0.35*	*0.08*	*1.49*	*0.95*
C	-	-	*0.53*	*0.24*	*0.01*	*2.21*	*0.78*

Bfc1 - Black Spruce (Prince Albert, Saskatchewan, Canada)
Bfc2 - Black Spruce (Prince Albert, Saskatchewan, Canada)
Bfc3 - P. sylvestris, P. abies (Norunda, Sweden)
Bfc4 - P. sylvestris, P. abies (Flakaliden, Sweden)
Bfp1 - Jack pine (Nipawin, Saskatchewan, Canada)
Bfp3 - Jack pine
Bfp5 - Scots pine (Jadraås, Sweden)

A - 14 years postfire (black spruce and small shrubs) - Summer
B - 80-85 years postfire (black spruce forest) - Summer
C - 80-85 years postfire (black spruce forest) – Spring

Chapter 4 Multiscale Sensible Heat Fluxes above a Heterogeneous Canopy in an Alaskan Black Spruce Boreal Forest[1]

Abstract

This paper compares eddy covariance (EC) derived sensible heat fluxes above a heterogeneous black spruce boreal forest canopy at a micrometeorological tower 24 m above ground level, to those derived from a large aperture scintillometer (LAS) whose beam is centered near the tower at an average height of 36 m, and over a path length of 1423 m. This analysis focuses on unstable daytime periods from June, July and August of 2013. Results suggest that sensible heat flux values derived from the sonic anemometer (H_{EC}) are above 50 W m^{-2} primarily between 0700 to 2000 Alaska Standard Time. This timing agrees with the minima in the mean diurnal pattern of C_n^2 from the LAS, and is used to define daytime in this analysis. For the high flux regime (daytime periods where H_{EC} > 50 W m^{-2}), we find that H_{EC} and the large-scale flux from the LAS (H_{LAS}) correlate with R^2 = 0.68, while H_{EC} captures about 82% of H_{LAS} on average. The magnitude of H_{EC} and H_{LAS} are both strongly sensitive to incoming solar radiation, with H_{LAS} having a better correlation and regression slope, suggesting that the local measurements are adjusting also to surface and/or flow conditions above a heterogeneous surface. Evaluation of the magnitude of the ratio of H_{EC}/H_{LAS} for days with varying amounts of solar radiation suggests that while radiation affects the magnitude of H_{LAS} and H_{EC} independently, it does not affect their ratio. For daytime periods with lower fluxes (H_{EC} between

[1] Starkenburg, D., G. J. Fochesatto, J. Cristóbal, A. Prakash, R. Gens, J. G. Alfieri, and D. L. Kane. Prepared for submission to *J. Geophys. Res. Atmos.*

10 and 50 W m^{-2}), H_{EC} captures about 69% of H_{LAS} on average. However, the local and large-scale fluxes during this low flux regime correlate poorly with incoming solar radiation (R^2 = 0.42 for H_{LAS} and R^2 = 0.15 for H_{EC}), and with one another (R^2 = 0.27), suggesting that local heterogeneities are not well-integrated into the large-scale flux. Therefore, low flux periods should be considered separately for the purposes of upscaling. For the high flux regime, a finer resolution of upscaling can be provided based on the mean diurnal pattern of H_{EC}/H_{LAS} and the Obukhov length (L). Namely, as the boundary layer becomes less unstable in late afternoon (the magnitude of L increases), H_{EC}/H_{LAS} increases, supporting that the eddy covariance technique can capture more of the large-scale flux when the boundary layer is more shear-driven (less buoyancy driven).

4.1 Introduction

4.1.1 Local and Larges-scale Turbulent Energy Fluxes

Surface-atmosphere interactions are central to understanding current and future trends in weather and climate. Large-scale surface fluxes are the quantities often required for model input and/or validation [*Beyrich et al.*, 2002; *Hartogensis et al.*, 2003; *Ward et al.*, 2014]. However, this research is challenging because it involves the analysis of turbulence data which is best understood only under specific surface and atmospheric boundary layer (ABL) flow conditions, and often limited to specific levels within the ABL [*Arya*, 1988; *Holton*, 1992; *Arya*, 1999; *Santoso and Stull*, 1998, 2001]. Such ideal conditions are not always representative of the local surface properties and climate regime being evaluated. Even within what might be classified as the same surface type, local flux values can vary considerably [*Beyrich et al.*, 2006; *Alfieri and*

Blanken, 2012; *Starkenburg et al.,* 2015]. Quantifying the relationship between local and large-scale fluxes and their effect on the flow regime has been the motivation for numerous field campaigns [*André et al.,* 1988; *Chehbouni et al.,* 2000; *Mengelkamp et al.,* 2006].

Fortunately, a large and growing global network of flux towers are available for making local measurements of turbulent fluxes [*Xiao et al.*, 2012, and citations therein], and methods to interpret these results at the larger scale have been developed, including empirical methods, data-assimilation methods, and/or satellite remote sensing models [*Samain et al.*, 2012a; *Xiao et al.*, 2012; *Ueyama et al.*, 2014]. Comparisons of local to large-scale fluxes over a variety of landscapes from agricultural land and forests to urban environments abound in the literature [*Chehbouni et al.,* 2000; *Beyrich et al.*, 2002, 2006; *Ezzahar et al.,* 2009; *Brunsell et al.,* 2011; *Evans et al.* 2012; *Salmond et al.,* 2012; *Ward et al.,* 2014]. However, data sets in high latitude locations such as interior Alaska are still lacking owing to remoteness, extreme weather, and experimental conditions which make instrumentation logistically arduous to install and maintain. This is particularly troublesome, given that that the higher latitudes are especially vulnerable to a warming climate [*Hinzman and Kane,* 1992, and citations therein; *Bekryaev et al.,* 2010]. The large aperture scintillometer (LAS) provides an advantage over eddy covariance (EC) towers in that it can obtain representative samples of turbulence data over larger areas [*Hartogensis et al.*, 2003; *Hemakumara et al.*, 2003; *Guyot et al.*, 2009]. However, the LAS is costly and less amenable for remote locations. Thus, estimations of the landscape scale flux via satellite remote sensing is an attractive option, but in order to be successful, the relationship between the local and large-scale fluxes over a heterogeneous boreal forest canopy must be properly quantified.

4.1.2 Instrumentation and Measurement Techniques

Eddy covariance (EC) is a common method for evaluating sensible heat flux (H) from sonic anemometer data. Sonic anemometers use ultrasonic calibrated signals to evaluate sonic air temperature (θ_s) as well as the *u*, *v*, and *w* components of the total wind vector based on deviations from the speed of sound detected by the acoustic signal. The covariance of the turbulent component of vertical velocity (w') and sonic temperature (θ_s') provides a direct measurement of the vertical transport of temperature by small eddies, but requires a long averaging time (typically 30 minutes) to allow a large number of eddies to be sampled by the anemometer so as to provide a statistically robust value of H at the local scale. Even then, this sampled turbulence only represents the larger landscape scale for homogeneous surfaces under stationary flows within a constant flux layer [*Arya*, 1988]. If turbulence is intermittent [*Coulter and Doran*, 2002; *Acevedo et al.*, 2006] and/or confined to shallow layers [*Fochesatto et al.*, 2013], traditional EC methods may underestimate turbulent energy fluxes. The EC method also cannot adequately evaluate fluxes under larger scale updrafts, whose mean vertical velocities are averaged out during the Reynolds decomposition process [*Mahrt*, 1998].

Another method for deriving H over a large area is the LAS, which is comprised of an emitter and a receiver installed across the landscape under study. The emitter uses an eye-safe pulsed light emitting diode array configured in a dual channel electromagnetic signal aimed across the landscape, directly facing the receiver. Sensible heat fluxes (i.e., microscale changes in temperature due to the turbulence field) cause changes to the refractive index of air (n), which are detected as variations in the laser intensity due to light scintillation collected at the receiver.

From these measured fluctuations of signal intensity one obtains the turbulence refractive index structure function (C_n^2) which is then converted to the turbulent structure parameter of temperature (C_T^2) in the optical range, and ultimately to H [*Anandakumar,* 1999]. The long beam path of the LAS (500 m to 5 km) can take a large and instantaneous sample of the distributed boundary layer turbulence, which provides turbulence statistics over scales larger than traditional EC techniques [*Beyrich et al.,* 2002; *Meijninger et al.* 2002]. Studies have shown that H derived from the LAS compares well with the mean of the aggregated local EC fluxes even over patchy, heterogeneous landscapes [*Beyrich et al.,* 2002; *Ezzahar et al.* 2009; *Evans et al.* 2012]. Indeed, for the case of large secondary circulations induced by surface type heterogeneity [*Kang* 2009] and terrain heterogeneity [*Foken et al.* 2010], measurement systems with larger footprints such as the LAS may be preferred in order to improve the energy balance closure [*Foken et al.* 2010]. It has also been shown that the LAS is versatile enough to provide reliable heat flux data even when the beam path is slanted, and/or has a variable height above the ground along its path length [*Hartogensis et al.* 2003], as long as certain conditions are maintained so that the physical framework allowing the LAS observations to be converted into H remain valid.

The objective of this work is to determine the relationship of local turbulent fluxes of H to large-scale area-averaged ABL turbulent fluxes. Local scale fluxes are obtained by EC while large-scale ABL fluxes are retrieved by means of a LAS system installed across the boreal forest canopy. The analysis of the present observations concern only unstable daytime summer periods during June, July and August of 2013. Owing to abrupt changes in canopy height, uneven heating and a slow mean wind speed [*Starkenburg et al.,* 2015], combined with frequent disconnection between sub and above canopy flows [*Starkenburg et al.,* 2013], there is a need to

study the relationship between local and large-scale values of H in complex heterogeneous boreal forest canopies over discontinuous permafrost. Following this introduction, Section 4.2 describes the study site while Section 4.3 reviews the instrumentation and signal processing. Section 4.4 compares local and large-scale H values for unstable periods during the summer of 2013. Section 4.5 summarizes the most important results of this work.

4.2 Site Description

Fairbanks is a high-latitude continental region located in central Alaska (64°49'N, 147°52'W) with extreme seasonality [*Shulski and Wendler*, 2007]. The study site for this analysis is described in *Starkenburg et al*. [2013], but is briefly summarized here for convenience. Specifically, the data are taken in and above a black spruce boreal forest near the Geophysical Institute of the University of Alaska Fairbanks (UAF) at an altitude of 165 m above sea level (Figure 4.1). The overstory in the study area is predominantly black spruce (*Picea mariana*), with a 60% cover density. The understory is composed of small trees, shrubs (*Vaccinium sp., Betula nana, Alnus incana*), and mosses (*Sphagnum sp*.) [*Kitamoto et al.*, 2007]. Soil profiles reveal an organic layer which ranges from 13 to 26 cm deep, underneath which a mineral layer is present. The site is underlain by discontinuous permafrost [*Iwata et al.*, 2010]. The mean canopy height (h) is 4.7 m, with a standard deviation of ±3.14 m around the EC micrometeorological tower as measured from transects spaced apart on a 200 m x 200 m grid. The variability in canopy height and tree density observed in this forest results from abrupt changes in permafrost, complex soil profiles and drainage, and can result in significant spatial

variations in mechanical mixing and sensible heat flux values [*Starkenburg et al.*, 2013; *Starkenburg et al.*, 2015].

4.3 Instrumentation and Signal Processing

4.3.1 Sonic Anemometer (EC)

Micrometeorological measurements of turbulent fluxes were carried out by a Campbell Scientific CSAT3 at 24 m (5.1 h) at a frequency of 20 Hz. As described in *Starkenburg et al.* [2015], the anemometer data were processed with a comprehensive suite of post-processing corrections and adjustments [*Alfieri et al.*, 2012]. Specifically, the data were cleaned via a despiking algorithm adapted from *Goring and Nikora* [2002]. The air temperature from the sonic anemometer was corrected for humidity effects according to *Liu et al.* [2001]. Then, a two-dimensional coordinate rotation procedure was applied [*Kaimal and Finnigan,* 1994], along with corrections for sensor displacement (i.e., the slight distance between the gas analyzer and the anemometer transducers), and frequency response attenuation [*Massman*, 2000; *Massman and Lee,* 2002]. After the 30 min block average turbulent sensible heat fluxes from the sonic anemometer were calculated, they were corrected for heat and water vapor density changes [*Webb et al.*, 1980].

4.3.2 Large Aperture Scintillometer (LAS)

A LAS (the Scintec BLS900 boundary layer scintillometer) was installed so that its beam was centered near the meteorological tower where the sonic anemometer is located (Figure 4.1). The mean beam height of the LAS is 36 m above ground, and spans a 1423 m transect at a slight

slope (1.56° sight line) (Figure 4.2). The scintillation detected by the LAS is spatially weighted to a footprint whose area is maximized near the center of the transect, as defined by the horizontal path weighting function, *W(x')*, which is used to obtain the optical path weighting function *G(x')*, via:

$$W(x') = 2.163 \cdot \left(2 \cdot \frac{J_1(y)}{y}\right)^2 \quad \text{(Eq. 4.1)}$$

$$y = 2.283 \cdot \pi \cdot (x' - 0.5) \quad \text{(Eq. 4.2)}$$

$$G(x') = W(x') / \int_0^1 W(x')dx' \quad \text{(Eq. 4.3)}$$

Here, x' is the relative path position along the beam transect ($0 \leq x' \leq 1$), $J_1(y)$ is the first order Bessel function of the first kind, and *y* is a function of x' with 0.5 being the normalized beam path center location [*Hartogensis,* 2003; *Scintec BLS Manual*, 2008].

Optical intensities (*I*) of the LAS beam were collected at 30 second time intervals to yield one minute average values of the optical turbulence of refractive index, C_n^2. C_n^2 is calculated as a direct measurement by consideration of the aperture diameter of the LAS receiver (*D* = 0.15 m), the path length for the experiment (*L*= 1423 m), and the variance of the natural log of the signal intensity [*Tatarski*, 1961]:

$$C_n^2 = 1.12 \cdot D^{7/3} \cdot L^{-3} \cdot \sigma^2 \left(\ln \frac{\sigma(I)}{\langle I \rangle}\right) \quad \text{(Eq. 4.4)}$$

where the angled brackets ⟨⟩ denote the mean. The C_n^2 data were then inspected for spikes and dropouts using a median filter on a sliding window of length 3 points (3 minutes), in order to identify spurious values. Similarly, the diagnostic error code from the LAS instrument was evaluated to isolate time frames which may have experienced an instrumental malfunction. Next,

C_n^2 was converted to the structure parameter of temperature, C_T^2 ($K^2\ m^{-2/3}$), through the following equations [*Hartogensis*, 2003; *Scintec BLS Manual*, 2008]:

$$C_T^2 = C_n^2 \cdot \left(\frac{T^4}{p^2}\right) \cdot \alpha_1^{-2} \cdot [1 + (0.03/\beta)]^{-2} \quad \text{(Eq. 4.5)}$$

$$\alpha_1 = \alpha_2 \cdot \left(1 + \frac{\lambda_0^2}{\lambda^2}\right) \quad \text{(Eq. 4.6)}$$

Here, β is the Bowen ratio (i.e., the ratio of sensible over latent heat flux), *T* is air temperature in degrees K, and *p* is air pressure in Pa. The term α_1 is a wavelength dependent proportionality factor defined as a function of: a constant α_2 = 0.776 x 10^{-6} K·Pa^{-1}; the wavelength of the LAS beam, λ = 0.880 μm; and a second constant λ_0 = 7.53 x 10^{-3} μm^2. Additionally, since we require a single beam height despite that the height varies along the path, an effective height (z_{eff}) for the LAS beam is calculated. For neutral conditions [*Hartogensis et al.*, 2003]:

$$z_{eff} = \left[\int_0^1 (z(x')^{-\frac{2}{3}} \cdot G(x'))dx'\right]^{-3/2} \quad \text{(Eq. 4.7)}$$

Here, z(x′) is the actual beam height above the ground along the beam path and in this case, a displacement height (d) is evaluated as 2/3 of the mean canopy height of 4.7 m, such that z(x′) = z(x′) - d. Finally, to derive H requires solving the set of Monin-Obukhov similarity equations that relate these variables to a universal function of stability, $f_T(\varsigma)$ [*Wyngaard et al.*, 1971]:

$$C_T^2 \cdot \frac{(z_{eff})^{\frac{2}{3}}}{\theta_*^2} = f_T(\varsigma) \quad \text{(Eq. 4.8)}$$

$$\theta_* = -\frac{H}{\rho \cdot c_p \cdot u_*} \quad \text{(Eq. 4.9)}$$

$$L = u_*^2 \cdot \frac{T}{\kappa \cdot g \cdot \theta_*} \quad \text{(Eq. 4.10)}$$

$$f_T(\varsigma) = \begin{cases} c_1(1 - c_2 \cdot \varsigma)^{-2/3} & \text{if } \varsigma < 0 \text{ (unstable)} \\ c_1(1 + c_3 \cdot \varsigma^{2/3}) & \text{if } \varsigma > 0 \text{ (stable)} \end{cases} \quad \text{(Eq. 4.11)}$$

Here, ρ is air density; c_p is the specific heat capacity of air at constant pressure (1004 J kg^{-1} K^{-1}); κ is the dimensionless von Kármán constant (equal to 0.4); g is gravitational acceleration (9.8 m s^{-2}); θ_* is the temperature scale; u_* is the velocity scale (or friction velocity, in m s^{-1}), based on the wind field evaluated at the 24 m sonic anemometer; and L is the Obukhov length (a measure of dynamic stability, in m). Equation 4.11 describes $f_T(\varsigma)$ which is a universal function of stability, where $\varsigma = z_{eff}/L$ is the dimensionless stability parameter, and c_1 = 4.9, c_2 = 6.1 and c_3 = 2.2 are empirically derived constants [*Wyngaard et al.*, 1971; *Andreas,* 1988]. Next, the set of Monin-Obukhov similarity equations are combined algebraically to yield an analytical expression for the stability parameter [*Gruber and Fochesatto,* 2013]:

$$\varsigma = V(\varsigma) \equiv M^{\frac{1}{3}} \cdot (1 - c_2 \cdot \varsigma)^{\frac{1}{3}} \cdot (1 + d(-\varsigma)^{\frac{2}{3}}) \qquad \text{(Eq. 4.12)}$$

Here, d = 0.46 is an empirically derived constant [*Andreas*, 1988], and M is a dummy variable which combines the terms in Equations 4.8 to 4.10 with C_n^2 and the turbulent dissipation rate (see *Gruber and Fochesatto* [2013] for a detailed derivation). To drive the convergence of the analytical solution, the atmospheric static stability is evaluated based on the sign of the eddy covariance derived heat flux, such that if $H_{EC} > 5$ W m^{-2} conditions are unstable, or if $H_{EC} \leq 5$ W m^{-2} conditions are stable [*Samain et al.,* 2012b]. We chose this method for determining static stability over the use of the vertical temperature difference (ΔT) between ambient air temperature sensors, owing to the uncertainty in the actual times of stability transitions found in ΔT for the different sensors at the tower (see Section 4.4). Once u_* and θ_* are known, then the sensible heat flux from the LAS (H_{LAS}) can be evaluated [*Arya*, 1988]:

$$H_{LAS} = \rho \cdot c_p \cdot u_* \cdot \theta_* \qquad \text{(Eq. 4.13)}$$

4.4 Results and Discussion

The period under study comprises the summer months of June, July and August of 2013. According to the Alaska Climate Research Center [*ACRC*, 2015], June 2013 was the 3rd warmest in 108 years, being 3.6°C above the monthly mean of 15.8°C. July and August were also warm, with monthly mean temperatures of 1 and 1.8°C above average, respectively. The season was fairly dry, with June and July receiving less than half the expected 34.8 and 54.9 mm of precipitation, respectively. August was wetter, receiving 7% more than the mean of 47.8 mm. As is typical for Fairbanks, the mean wind was low for all months, ranging from 1.8 to 2.6 m s^{-1}. For these three months, mean 30 min H were evaluated according to the methodology outlined in Section 4.3. Of the 92 days during this summer (4,416 half-hourly periods), the sonic anemometer had data for 4,018 periods, and the LAS for 3,528 periods. No spikes were detected in this series of LAS data, and about 0.1% of the data were reported as having an instrumental malfunction, during which times enough of the actual value of C_n^2 was missing such that no resultant heat flux was recorded for those half-hourly periods.

From the time series of multiscale sensible heat flux values, only unstable periods were selected, since it is widely known that flux measurements derived from EC and the LAS during ABL transitions and stable stratification require additional consideration [*Beyrich et al.*, 2002; *Acevedo et al.*, 2006]. To ensure an unstable regime, we first flagged all periods where sensible heat flux from the sonic anemometer (H_{EC}) exceeds 50 W m^{-2} [*Prueger et al.*, 2004], which allows an exploration of the local and large-scale fluxes outside the influence of local variations. Figure 4.3 shows that the times when $H_{EC} > 50$ W m^{-2} are primarily between 0700 to 2000 Alaska Standard Time (AKST). Corroborating this, the mean diurnal curve of C_n^2 for the

summer of 2013 shows that the minima in C_n^2 occur at about 0630 and 2000 AKST, suggesting that on average, the large-scale ABL regime was unstable between these times [*Wesely and Alcaraz*, 1973; *Samain et al.*, 2012b] (Figure 4.4). For comparison, Figure 4.5 shows the mean diurnal curves of ΔT for air temperature sensors located at 24, 12, 7 and 3 m on the central micrometeorological tower. In Figure 4.5, the times at which ΔT crosses the horizontal line of neutral stability indicates where the stability regime of the ABL is transitioning. Based on which depth of the ABL is evaluated (e.g. 24-12 m vs. 12-3 m), the time of the ABL transition varies widely (~ 2.5 hours), even at this one location within the forest, pointing to the difficulty in using a locally derived ΔT as a means for evaluating stability over a heterogeneous canopy and prompting further studies regarding the structure and timing of ABL transitions [e.g., *Sorbjan*, 1997; *Fochesatto et al.*, 2001a, b].

Based on this study of stability, we use the fact that most of the data for which $H_{EC} > 50$ W m^{-2} occur between the times marking the minima in C_n^2 (i.e., ~ 0700 to 2000 AKST). Accordingly, we isolated the data for each available day that occurred between 0700 and 2000 AKST, and then from that data we retained only cases where $H_{EC} > 50$ W m^{-2} and where both the EC and LAS had simultaneous data. From this set, and in order to assure data under similar weather conditions, we also removed cases where the National Weather Service reported rain, smoke, or fog at the Fairbanks International Airport (the closest reliable meteorological station, ~ 6 km from our study site), since such weather conditions may affect the accuracy of H [*Beyrich et al.*, 2002]. The resulting data set (hereafter known as the high flux regime) represents about 32% of the EC data and 37% of the LAS data that were originally available for the summer of 2013. Table 4.1 gives an overview of the available data for this time.

Next, it is instructive to observe the complexity of the surface and the flow regime as indicated in Figure 4.6. This figure shows an optimal curve of downwelling shortwave radiation (SW↓), indicating the presence of relatively clear skies. Despite this, the curves of H from both instruments show quite a bit of variation from one half-hourly period to the next, revealing that even when the incoming energy is robust and consistent, the interaction of the boundary layer flow with the canopy still results in a more complex diurnal pattern of H than of SW↓. This result alone is a quantification of the complexity of the surface and the flow, and can be taken as a measure of the degree of departure of this data from the ideal conditions of the Monin-Obukhov Similarity hypothesis where local and landscape scale fluxes are similar and constant with height [*Arya*, 1988].

An important aspect of data in the summer of interior Alaska is the prevalence of at least some clouds most of the time, despite some days having quite smooth curves for SW↓. This raises the question as to the dependence of the relationship between the local and large-scale values of H to SW↓. As expected, the magnitude of SW↓ is proportional to the magnitude of H for both instruments (Figure 4.7). The regression slope is higher for H_{LAS} data (0.58) as compared to H_{EC} data (0.46). Furthermore, the coefficient of determination is larger between SW↓ and H_{LAS} ($R^2 = 0.83$) than between SW↓ and H_{EC} ($R^2 = 0.71$). This is important because it shows that the effect of solar radiation on the large-scale flux is more direct and less complicated by local heterogeneities, supporting an expected increase in energy balance closure at the large-scale.

One concern that is often discussed in comparisons between EC and LAS data is instrument footprint. Specifically, the LAS can take a larger instantaneous sample of the surface

layer and thus represents a larger source area for the flux values being measured. The sonic anemometer at the tower obviously cannot sample the same volume of the flow, but the tower is located near the center of the LAS beam so that regardless of wind speed and direction, all instruments should have strongly overlapping footprints most of the time. Evaluating the relationship of the ratio of the local to the large-scale flux (H_{EC}/ H_{LAS}) as a function of 30 min mean wind direction derived from the sonic anemometer reveals that no discernable relationship exists (Figure 4.8). This is not surprising given the relatively low winds in Fairbanks, combined with the heterogeneous canopy, conditions which do not promote strong, pronounced fetches. Thus, we conclude that the relationship between the fluxes in the present study is not strongly dependent on wind direction and that other than the actual size of the footprint, analysis of footprint shapes and overlaps will not likely explain the differences we observe, and furthermore, will not provide a meaningful clustering of the data.

Results for the high flux regime data show that the sensible heat flux from the LAS (H_{LAS}) was larger on average than H_{EC}, with R^2 = 0.68 and a regression slope of 0.71 (Figure 4.9). For the high flux regime, the mean and median value of the ratio of H_{EC}/H_{LAS} is 0.82 and 0.80, suggesting that on average H_{EC} captures about 82% of H_{LAS} (Figure 4.10). Next, we investigated whether varying amounts of solar radiation affect H_{EC}/H_{LAS} for the high flux regime. To do so, we took the mean curve of SW↓ for each of the available days and noted that the value exceeded 200 W m^{-2} between 0830 and 1830 AKST. Integrating this section of the mean curve of SW↓ between these times provides a single benchmark value that we use as a model (SW_{MOD}) to test radiation levels for the individual days. Specifically, we calculate the ratio of the integral of SW↓ between 0830 and 1830 AKST on each day (SW_{OBS}), and compare this to SW_{MOD}.

Then, imposing the rule that SW_{OBS}/SW_{MOD} must be less than a certain threshold value allows us to evaluate the data for only days with a certain degree of incoming radiation (Table 4.2). For example, eliminating days where SW_{OBS}/SW_{MOD} is less than 1.0 is moderately restrictive, leaving 858 available half-hourly periods out of the original 1287 (i.e., about 67% of the data) for analysis. Table 4.2 reveals that for a range of thresholds from 0.4 to 1.5, the R value between H_{EC} and H_{LAS}, along with the mean and median of the ratio H_{EC}/H_{LAS}, hardly change. This result shows that while SW↓ affects the magnitude of H_{LAS} and H_{EC} independently, it does not affect their ratio.

As a further investigation, we also isolated the lower flux values from the daytime periods (i.e., where $10 < H_{EC} \leq 50$ W m^{-2}). There are 255 half-hourly periods that meet this criteria, hereafter known as the low flux regime. The low flux regime represents periods when the flux values are low but still mostly within the sonic anemometer's uncertainty [*Mauder et al.*, 2006]. For the low flux regime, the relationship between H_{LAS} and H_{EC} is much weaker, with $R^2 = 0.27$ (Figure 4.11). The mean and median of the ratio H_{EC}/H_{LAS} is 0.69 and 0.66, suggesting that H_{EC} captures about 69% of H_{LAS} (Figure 4.12). However, for this low flux regime the correlation of the flux data to SW↓ is much poorer than for the high flux regime data (Figure 4.13), suggesting that local heterogeneities are not well-integrated into the large-scale flux, and should therefore be considered separately for the purposes of upscaling local to landscape scale flux values.

Returning to the high flux regime where the relationship between the local and large-scale fluxes is most robust, we take the mean diurnal curve of the ratio of H_{EC}/H_{LAS} and also that for the Obukhov length (L), in order to assess whether or not there is any dependence on the

relationship between the two flux values and dynamic stability over the period 0700 to 2000 AKST (Figure 4.14). What is noticeable is a trend in which H_{EC}/H_{LAS} increases through the afternoon while the magnitude of L increases (i.e., L becomes less unstable). This suggests that in addition to the mean relationship between H_{EC}/H_{LAS}, there is a finer resolution in which this ratio can be adjusted based on the dynamic stability. Logically, as L becomes less unstable in the latter part of the day, the boundary layer becomes more shear-driven and less buoyancy-driven. Since the eddy covariance technique will average out any mean in the vertical velocity [*Mahrt*, 1998], the sonic anemometer may not capture all the flux during highly unstable periods when low frequency buoyant plumes contribute more to the total flux. Thus, the ratio H_{EC}/H_{LAS} improves when the boundary layer is less unstable. Figure 4.14c shows a second order polynomial fitting of the mean diurnal values of H_{EC}/H_{LAS} to L, in which $R^2 = 0.66$ and with a root mean square error of 21.88 m^{-1}. Note that when L becomes very low in magnitude, the curve flattens, suggesting that the relationship between the flux ratios and stability breaks down for both instruments in this region.

4.5 Conclusions

To date, little has been done to compare local and large-scale area averaged sensible heat fluxes in interior Alaska. This analysis evaluates and compares the 30 min mean sensible heat fluxes above a heterogeneous black spruce boreal forest canopy from a sonic anemometer 24 m above ground level, to those derived from a large aperture scintillometer whose beam is centered near the tower at an average height of 36 m above ground, over a path length of 1423 m, and with a slant angle of about 1.56°. To compare the local fluxes from the anemometer (H_{EC}) to the

large-scale flux values from the LAS (H_{LAS}), we first cluster the data by taking only unstable daytime periods with higher flux values as defined by $H_{EC} > 50$ W m^{-2}. Doing so reveals that most of these cases occur between 0700 and 2000 AKST, which is also the time bracketed by the minima in the mean diurnal pattern of C_n^2 from the LAS. Attempting to assess stability in the ABL by considering the vertical temperature difference (ΔT) between the air temperature sensors at the micrometeorological tower reveals that there can be as much as a 2.5 hour difference in the stability transition time, based on which level of the surface layer is considered. This points to the difficulty in using local measurements during the transition periods to determine whether the ABL is stable or unstable.

After taking all data between 0700 and 2000 AKST where $H_{EC} > 50$ W m^{-2}, and extracting periods where precipitation, fog or smoke was reported, we obtain the high flux regime, which is roughly 32 to 37% of the originally available EC and LAS data, respectively. For the high flux regime data, we find that H_{EC} and the large-scale flux from the LAS (H_{LAS}) correlate with $R^2 = 0.68$, while H_{EC} captures about 82% of H_{LAS} on average. The magnitude of H_{EC} and H_{LAS} are both strongly sensitive to incoming solar radiation, with H_{LAS} having the best correlation and regression slope, suggesting that local measurements must also adjust to surface and/or flow heterogeneity in addition to responding to changes in solar radiation. Evaluation of the ratio of H_{EC}/H_{LAS} for days with varying amounts of solar radiation suggests that while radiation affects the magnitude of H_{LAS} and H_{EC} independently, it does not affect their ratio.

We also isolate daytime periods between 0700 and 2000 AKST with lower fluxes (H_{EC} between 10 and 50 W m^{-2}). This dataset is known as the low flux regime, and represents only about 6 to 7% of the originally available EC and LAS data, respectively. For the low flux regime,

H_{EC} captures about 69% of H_{LAS} on average, but the correlation between the fluxes is much poorer (R^2 = 0.27). These low flux periods also correlate poorly with incoming solar radiation (R^2 = 0.42 for H_{LAS} and R^2 = 0.15 for H_{EC}). During such low flux regimes, local heterogeneities may not be well integrated into the large-scale flux, resulting in poorer agreement between H_{EC} and H_{LAS}. As a result, low flux daytime periods should be considered separately for the purposes of upscaling flux values in the boreal forest. For the high flux regime, a finer resolution of upscaling can be provided based on the mean diurnal pattern of H_{EC}/H_{LAS} and the Obukhov length (L). Namely, as the boundary layer becomes less unstable in late afternoon, H_{EC}/H_{LAS} increases, suggesting that the eddy covariance technique can capture more of the large-scale flux when the boundary layer is more shear-driven (less buoyancy driven).

Acknowledgements

This research was supported by the Alaska NASA EPSCoR program award NNX10NO2A, by the Alaska Space Grant Program, and by the "New GK-12 Program: The CASE (Changing Alaska Science Education) for Enhancing Understanding of Climate Change" NSF (DGE-0948029).

The following authors contributed work on this manuscript as noted:

D. Starkenburg: Collected, processed, and evaluated data; primary writer/editor

G. J. Fochesatto: Assisted in collecting data, scripting codes, guiding research; secondary editor

J. Cristóbal: Assisted in collecting, providing and processing data; secondary editor

J. Alfieri: Provided code for EC data processing; secondary editor

A. Prakash, R. Gens, and D. L. Kane: Secondary editors

4.6 References

Acevedo, O. C., O. L. L. Moraes, G. A. Degrazia, and L. E. Medeiros (2006), Intermittency and exchange of scalars in the nocturnal surface layer, *Boundary-Layer Meterol., 119*(1), 41-55, doi: 10.1007/s10546-005-9019-3.

ACRC (2015), Alaska Climate Research Center; cited 2015, http://akclimate.org/.

Alfieri, J. G., and P. D. Blanken, (2012), How representative is a point? The spatial variability of surface energy fluxes across short distances in a sand-sagebruch ecosystem, *J. Arid Environ., 87*, 42-49, doi: 10.1016/j.jaridenv.2012.04.010.

Alfieri, J. G., Kustas, W. P., Prueger, J. H., Hipps, L. E., Evett, S. R., Basara, J. B., Neale, C. M. U., French, A. N., Colaizzi, P., Agam, N., Cosh, M. H., Chavez, J. L., and T. A. Howell, (2012), On the discrepancy between eddy covariance and lysimetry-based surface flux measurements under strongly advective conditions, *Adv. Water Resour., 50*, 62-78, doi: 10.1016/j.advwatres.2012.07.008.

Anandakumar, K., (1999), Sensible heat flux over a wheat canopy: optical scintillometer measurements and surface renewal analysis estimations, *Agric. and Forest. Meteorol., 96*(1-3), 145-156, doi: 10.1016/S0168-1923(99)00026-X.

André, J. C., J.-P. Goutorbe, A. Perrier, F. Becker, P. Bessemoulin, P. Bougeault, Y. Brunet, W. Brutsaert, T. Carlson, R. Cuenca, et al. (1988), Evaporation over land surfaces: First results from HAPEX-MOBILHY special observing period, *Ann. Geophys., 6*, 477–492, https://hal.archives-ouvertes.fr/hal-01011981.

Andreas, E. L. (1988), Estimating C_n^2 over snow and sea ice from meteorological data, *J. Opt. Soc. Am. A, 5*(4), 481-495, doi: 10.1364/JOSAA.5.000481.

Arya, S. P., (1988), *Introduction to Micrometeorology*, Academic Press, San Diego.

Arya, S. P., (1999), Comments on "Wind and temperature profiles in the Radix Layer: the bottom fifth of the convective boundary layer", *J. Atmos. Sci.*, *38*(4), 493-494, doi: 10.1175/1520-0450(1999)038<0493:COWATP>2.0.CO;2.

Bekryaev, R.V., Polyakov, I.V., and A. Alexeev (2010), Role of polar amplification in long-term surface air temperature variations and modern Arctic warming, *J. Climate*, *23*(14), 3888-3906, doi: 10.1175/2010JCLI3297.1.

Beyrich, F., H. A. R. De Bruin, W. M. L. Meijninger, J. W. Schipper, and H. Lohse (2002), Results from one-year continuous operation of a large aperture scintillometer over a heterogeneous land surface, *Boundary-Layer Meterol.*, *105*(1), 85-97, doi: 10.1023/A:1019640014027.

Beyrich, F., J.-P. Leps, M. Mauder, J. Bange, T. Foken, S. Huneke, H. Lohse, A. Ludi, W. M. L. Meijninger, D. Mironov, U. Weisensee, and P. Zittel (2006), Area-averaged surface fluxes over the LITFASS region based on eddy-covariance measurements, *Boundary-Layer Meteorol.*, *121*(1), 33-65, doi: 10.1007/s10546-006-9052-x.

Brunsell, N. A., J. M. Ham, and K. A. Arnold (2011), Validating remotely sensed land surface fluxes in heterogeneous terrain with large aperture scintillometry, *Int. J. Remote Sens.*, *32*(21), 6295-6314, doi: 10.1080/01431161.2010.508058.

Chehbouni, A., Watts, C., Lagouarde, J.-P., Kerr, Y.H., Rodriguez, J.-C., Bonnefond, J.-M., Santiago, F., Dedieu, G., Goodrich, D.C., and C. Unkrich (2000), Estimation of heat and momentum fluxes over complex terrain using a large aperture scintillometer, *Agric. and Forest Meteorol.*, *105*(1-3), 215-226, doi: 10.1016/S0168-1923(00)00187-8.

Coulter, R.L., and J.C. Doran (2002), Spatial and temporal occurrences of intermittent turbulence during CASES-99, *Boundary-Layer Meterol.*, *105*(2), 329-349, doi: 10.1023/A:1019993703820.

Evans, J. G., D. D. McNeil, J. W. Finch, T. Murray, R. J. Harding, H. C. Ward, and A. Verhoef (2012), Determination of turbulent heat fluxes using a large aperture scintillometer over undulating mixed agricultural terrain, *Agric. and Forest Meteorol.*, *166*, 221-233, doi: 10.1016/j.agrformet.2012.07.010.

Ezzahar, J., A. Chehbouni, J. Hoedjes, D. Ramier, N. Boulain, S. Boubkraoui, B. Cappelaere, L. Descroix, B. Mougenot, and F. Timouk (2009), Combining scintillometer measurements and an aggregation scheme to estimate area-averaged latent heat flux during the AMMA experiment, *J. Hydrol.*, *375*(1-2), 217-226, doi: 10.1016/j.jhydrol.2009.01.010.

Fochesatto, J., P. Drobinski, C. Flamant, D. Guédalia, C. Sarrat, P.H. Flamant, and J. Pelon (2001a), Observational and Modeling of the Atmospheric Boundary Layer Nocturnal-Diurnal Transition During the ESQUIF Experiment, In: *Advances in Laser Remote Sensing*, Dabas, A., C. Loth, and J. Pelon (Eds.), 439-442, Paris, 2001.

Fochesatto, J., .P Drobinski, C. Flamant, D. Guedalia, C. Sarrat, P. Flamant, and J. Pelon (2001b), Evidence of Dynamical coupling between the residual layer and the developing convective boundary layer, *Boundary-Layer Meteorol.*, *99*(3), 451-464, doi: 10.1023/A:1018935129006.

Fochesatto, G. J., J. A. Mayfield, M. A. Gruber, D. Starkenburg and J. Conner (2013), Occurrence of shallow cold flows in the winter atmospheric boundary layer of interior of Alaska, *Meteorol. Atmos. Phys.,* 1-14, doi: 10.1007/s00703-013-0274-4.

Foken, T., M. Mauder, C. Liebethal, F. Wimmer, F. Beyrich, J.-P. Leps, S. Raasch, H. A. R. DeBruin, W. M. L. Meijninger, and J. Bange (2010), Energy balance closure for the LITFASS-2003 experiment, *Theor. Appl. Climatol.*, *101*(1-2), 149-160, doi: 10.1007/s00704-009-0216-8.

Goring, D. G., and V. I. Nikora (2002), Despiking acoustic Doppler velocimeter data, *J. Hydraul. Eng.*, *128*(1), 117-126, doi:10.1061/(ASCE)0733-9429(2002)128:1(117).

Gruber, M. A. and G. J. Fochesatto (2013), A new sensitivity analysis and solution method for scintillometer measurements of area-average turbulent fluxes, *Boundary-Layer Meteorol.*, *149*(1), 65–83, doi: 10.1007/s10546-013-9835-9.

Guyot, A., Cohard, J.M., Anquetin, S., Galle, S., and C.R. Lloyd (2009), Combined analysis of energy and water balances to estimate latent heat flux of a sudanian small catchment, *J. Hydrol.*, *375*(1-2), 227-240, doi: 10.1016/j.jhydrol.2008.12.027.

Hartogensis, O. K., Watts, C. J., Rodriguez, J. C., and H. A. R. De Bruin (2003), Derivation of an effective height for scitnillometers: La Poza experiment in Northwest Mexico, *J. Hydrometeorol.*, *4*(5), 915-928, doi: 10.1175/1525-7541(2003)004<0915:DOAEHF>2.0.CO;2.

Hemakumara, H. M., Chandrapala, L., and A. F. Moene (2003), Evapotranspiration fluxes over mixed vegetations areas measured from large aperture scintillometer, *Agr. Water Management*, *58*(2), 109-122, doi: 10.1016/S0378-3774(02)00131-2.

Hinzman, L. D., and D. L. Kane (1992), Potential Response of an Arctic Watershed during a Period of Global Warming, *J. Geophys. Res.*, *97*(03), 2811-2820, doi: 10.1029/91JD01752.

Holton, J. R., (1992), *An Introduction to Dynamic Meteorology*, 3rd ed., Academic Press, San Diego.

Iwata, H., Y. Harazono, and M. Ueyama (2010), Influence of source/sink distributions on flux–gradient relationships in the roughness sublayer over an open forest canopy under unstable conditions, *Boundary-Layer Meterol.*, *136*(3), 391-405, doi: 10.1007/s10546-010-9513-0.

Kaimal, J. C., and J. J. Finnigan (1994), *Atmospheric Boundary Layer Flows: Their Structure and Measurement*, Oxford University, New York, NY.

Kang, S.-L. (2009), Temporal oscillations in the convective boundary layer forced by mesoscale surface heat-flux variations, *Boundary-Layer Meteorol.*, *132*(1), 59-81, doi: 10.1007/s10546-009-9391-5.

Kitamoto, T., M. Ueyama, Y. Harazono, T. Iwata, and S. Yamamoto (2007), Applications of NOAA/AVHRR and observed fluxes to estimate 3 regional carbon fluxes over black spruce forests in Alaska, *J. Agr. Meteorol.*, *63*(4), 171-183.

Liu H., G. Peters, and T. Foken (2001), New equations for sonic temperature variance and buoyancy heat flux with an omnidirectional sonic anemometer, *Boundary-Layer Meteorol.*, *100*(3), 459–468, doi: 10.1023/A:1019207031397.

Mahrt, L (1998), Flux sampling errors for aircraft and towers, *J. Atmos. Oceanic Technol.*, *15*(2), 416-429, doi: 10.1175/1520-0426(1998)015<0416:FSEFAA>2.0.CO;2.

Massman W.J. (2000), A simple method for estimating frequency response corrections for eddy covariance systems, *Agric. Forest Meteorol.*, *104*(3), 185–198, doi: 10.1016/S0168-1923(00)00164-7.

Massman W.J., and X. Lee (2002), Eddy covariance flux corrections and uncertainties in long term studies of carbon and energy exchanges, *Agric. Forest Meteorol.*, *113*(1-4) 121–144, doi: 10.1016/S0168-1923(02)00105-3.

Mauder, M., C. Liebethal, M. Gockede, J.-P. Leps, F. Beyrich, and T. Foken (2006), Processing and quality control of flux data during LITFASS-2003, *Boundary-Layer Meteorol.*, *121*(1), 67-88, doi: 10.1007/s10546-006-9094-0.

Meijninger, W. M. L., O. K. Hartogensis, W. Kohsiek, J. C. B. Hoedjes, R. M. Zuurbier, and H. A. R. DeBruin (2002), Determination of area-averaged sensible heat fluxes with a large aperture scintillometer over a heterogeneous surface—Flevoland field experiment, *Boundary-Layer Meteorol.*, *105*(1), 37-62, doi: 10.1023/A:1019647732027.

Mengelkamp, H.-T., F. Beyrich, G. Heinemann, F. Ament, J. Bange, F. Berger, J. Bösenberg, T. Foken, B. Hennemuth, C. Heret, S. Huneke, K-P. Johnsen, M. Kerschgens, W. Kohsiek, J-P. Leps, C. Liebethal, H. Lohse, M. Mauder, W. Meijninger, S. Raasch, C. Simmer, T. Spieß, A. Tittebrand, J. Uhlenbrock, and P. Zittel (2006), Evaporation Over A Heterogeneous Land Surface: The EVA-GRIPS project, *Bull. Amer. Meteor. Soc.*, *87*(6), 775–786, doi: 10.1175/BAMS-87-6-775.

Prueger, J. H., Kustas, W. P., Hipps, L. E., and J. L. Hatfield, (2004), Aerodynamic parameters and sensible heat flux estimates for a semi-arid ecosystem, *J. Arid Environ.*, *57*(1), 87-100, doi: 10.1016/S0140-1963(03)00090-9.

Salmond, J.A., Roth, M., Oke, T.R., Christen, A., and J.A. Voogt (2012), Can surface-cover tiles be summed to give neighborhood fluxes in cities?, *J. Appl. Meteor. Climatol.*, *51*(1), 133-149, doi: 10.1175/JAMC-D-11-078.1.

Samain, B., G. W. H. Simons, M. P. Voogt, W. Defloor, N.-J. Bink, and V. Pauwels (2012a), Consistency between hydrological model, large aperture scintillometer and remote sensing based evapotranspiration estimates for a heterogeneous catchment, *Hydrol. Earth Syst. Sci.*, *16*(7), 2095 - 2107, doi: 10.5194/hess-16-2095-2012.

Samain, B., Defloor, W., and V.R.N. Pauwels (2012b), Continuous time series of catchment-averaged sensible heat flux from a large aperture scintillometer: efficient estimation of stability conditions and importance of fluxes under stable conditions, *J. Hydrometeorol.*, *13*(2), 423-442, doi: 10.1175/JHM-D-11-030.1.

Santoso, E., and R. Stull (1998), Wind and temperature profiles in the Radix Layer: the bottom fifth of the convective boundary layer, *J. Appl. Meteorol.*, *37*, 545-558, doi: 10.1175/1520-0450(1998)037<0545:WATPIT>2.0.CO;2.

Santoso, E., and R. Stull (2001), Similarity equations for wind and temperature profiles in the Radix Layer, at the bottom of the convective boundary layer, *J. Atmos. Sci.*, *58*(11), 1446-1464, doi: 10.1175/1520-0469(2001)058<1446:SEFWAT>2.0.CO;2.

Scintec BLS Manual (2008), Scintec AG, Rottenburg, Germany (version 1.49)

Shulski, M., and G. Wendler (2007), *The Climate of Alaska*, University of Alaska, Fairbanks.

Sorbjan, Z. (1997), Decay of convective turbulence revisited, *Boundary-Layer Meteorol.*, *82*(3), 501-515, doi: 10.1023/A:1000231524314.

Starkenburg, D., G. J. Fochesatto, A. Prakash, J. Cristóbal, R. Gens, and D. L. Kane (2013), The role of coherent flow structures in the sensible heat fluxes of an Alaskan boreal forest, *J. Geophys. Res.-Atmos.*, *118*(15), 8140-8155, doi: 10.1002/jgrd.50625.

Starkenburg, D., G. J. Fochesatto, J. Cristóbal, A. Prakash, R. Gens, J. G. Alfieri, H. Nagano, Y. Harazono, H. Iwata, and D. L. Kane (2015), Temperature regimes and turbulent heat fluxes across a heterogeneous canopy in an Alaskan boreal forest, *J. Geophys. Res. Atmos.*, *120*(4), 1348-1360, doi: 10.1002/2014JD022338.

Tatarski, V. (1961), *Wave Propagation in a Turbulent Medium*, McGraw-Hill, New York, NY.

Ueyama, M., K. Ichii, H. Iwata, E. S. Euskirchen, D. Zona, A. V. Rocha, Y. Harazono, C. Iwama, T. Nakai, W. C. Oechel (2014), Change in surface energy balance in Alaska due to fire and spring warming, based on upscaling eddy covariance measurements, *J. Geophys. Res.-Biogeo.*, *119*(10), 1947-1969, doi: 10.1002/2014JG002717.

Ward, H.C., Evans, J.G., and C.S.B. Grimmond (2014), Multi-scale sensible heat fluxes in the suburban environment from large-aperture scintillometry and eddy covariance, *Boundary-Layer Meterol.*, *152*(1), 65-89, doi: 10.1007/s10546-014-9916-4.

Webb E.K., Pearman G.L., Leuning R. (1980), Correction of flux measurements for density effects due to heat and water vapour transfer, *Q. J. R. Meteorol. Soc.*, *106*(447) 85–100, doi: 10.1002/qj.49710644707.

Wesely, M. L., and E. C. Alcaraz (1973), Diurnal cycles of the refractive index structure function coefficient, *J. Geophys. Res.*, *78*(27), 6224-6232, doi: 10.1029/JC078i027p06224.

Wyngaard, J.C., Izumi, Y., and S.A. Collins (1971), Behavior of the refractive-index-structure parameter near the ground, *J. Optical Soc. of America*, *61*(12), 1646-1650, doi: http://dx.doi.org/10.1364/JOSA.61.001646.

Xiao, J., J. Chen, K. J. Davis, and M. Reichstein (2012), Advances in upscaling of eddy covariance measurements of carbon and water fluxes, *J. Geophys. Res.-Biogeo.*, *117*(G1), doi: 10.1029/2011JG001889.

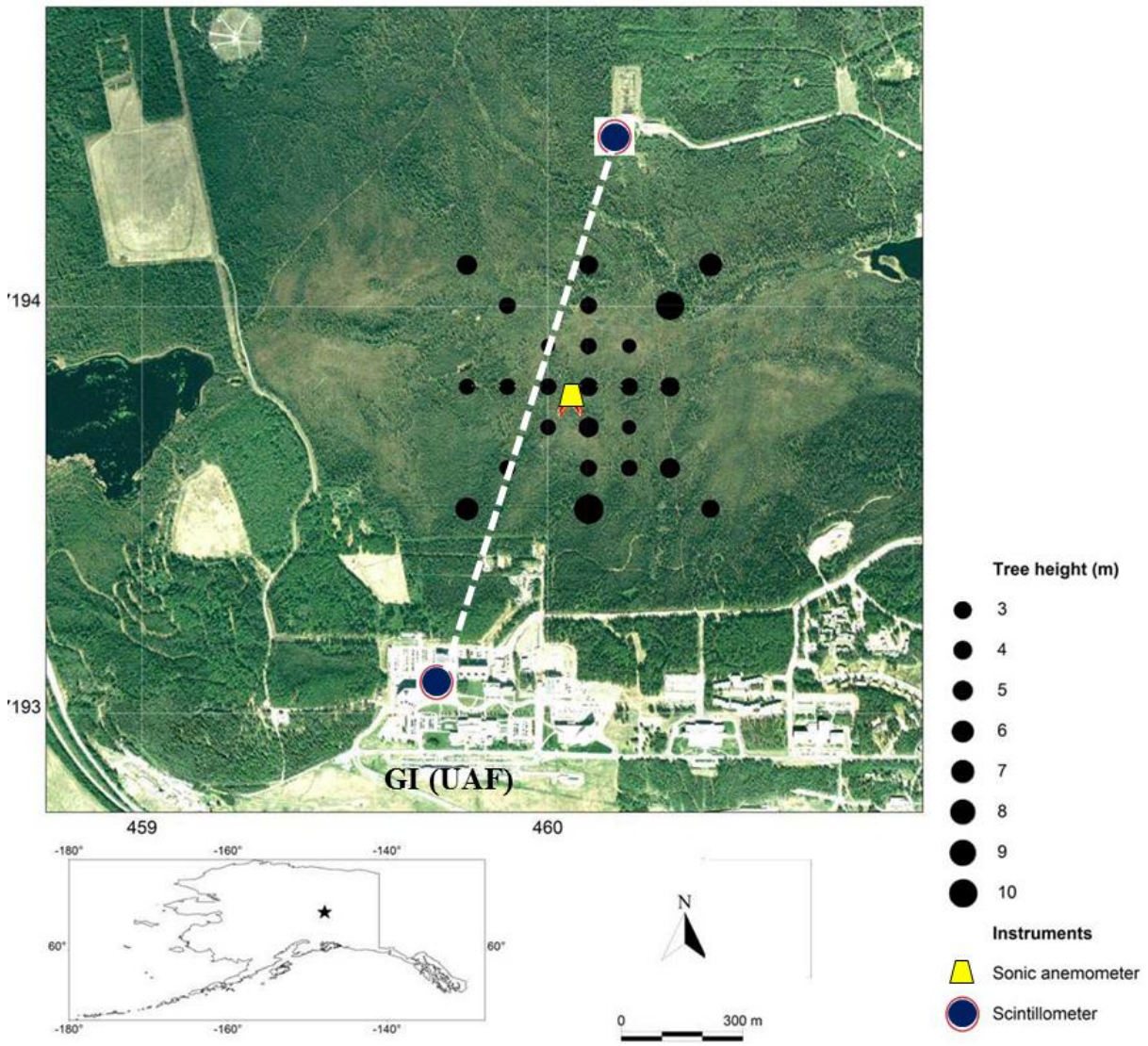

Figure 4.1 Aerial map of the study site. Black circles represent mean canopy height at various transects; yellow trapezoid is the location of the micrometeorological tower; purple circles and white dashed line represent the large aperture scintillometer equipment and beam path, respectively. The campus at the south central region of the map is the Geophysical Institute (GI) at the University of Alaska Fairbanks (UAF).

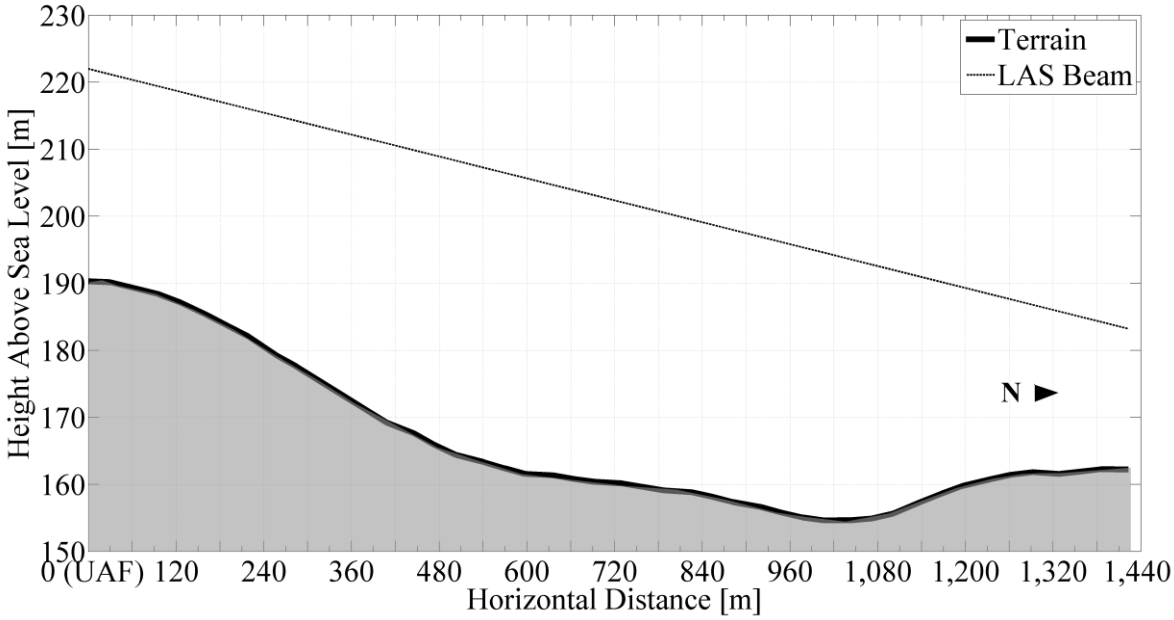

Figure 4.2 Topographic cross section showing terrain (gray shading) and the height of the LAS beam (slanted line); vertical scale on the y-axis is greater than the horizontal scale on the x-axis for clarity. The LAS emitter is on the right side, and the receiver on the left side (marked as "UAF" on the x-axis).

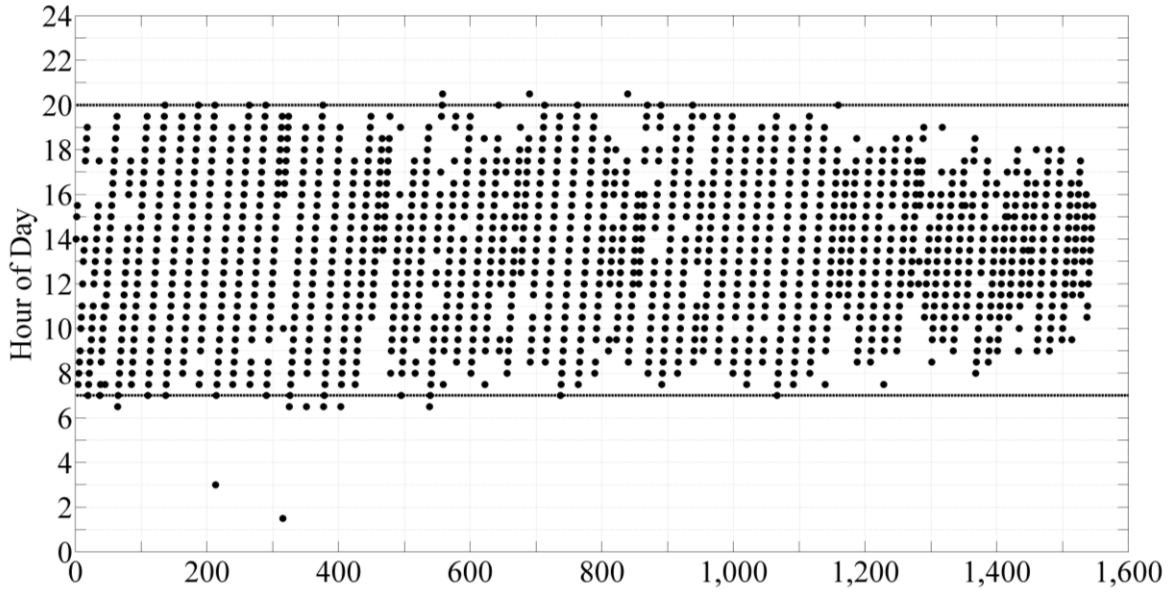

Figure 4.3 Time of occurrence of H_{EC} > 50 W m^{-2}. The x-axis is the number of each measurement (i.e., each point represents one 30 min flux measurement).

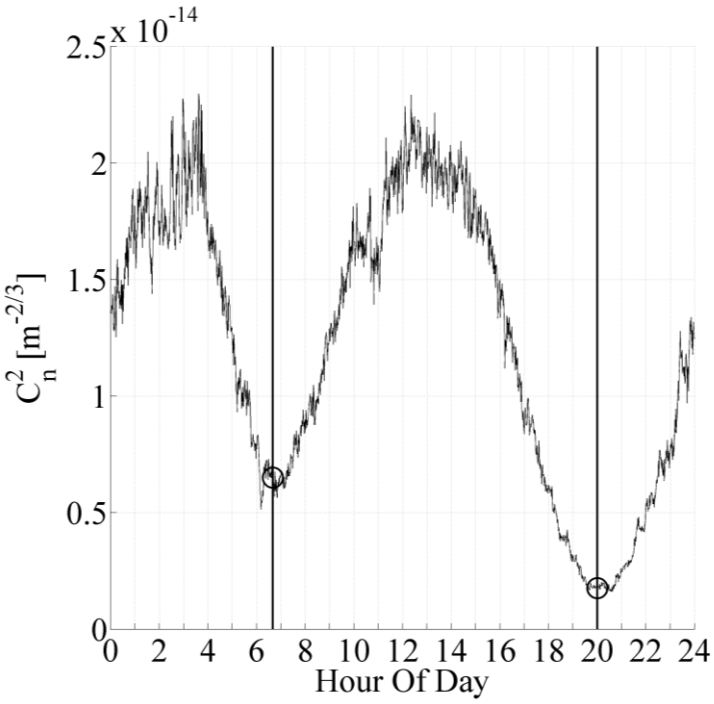

Figure 4.4 Mean diurnal curve of C_n^2 for all available data; black circles and vertical lines mark periods where the large-scale ABL is believed to transition its stability regime.

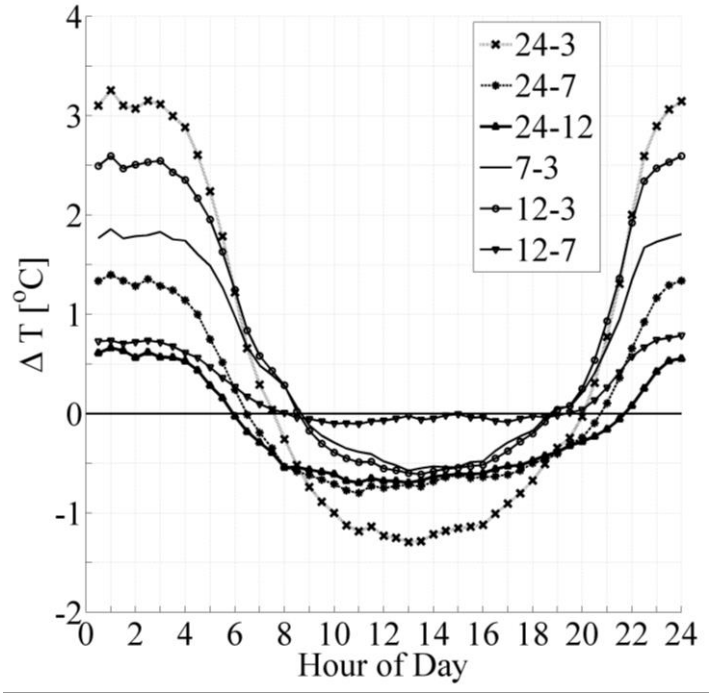

Figure 4.5 Mean diurnal pattern of the ΔT for all available data, as derived from the air temperature sensors at 24, 12, 7 and 3 m on our micrometeorological tower for available data in summer of 2013. Horizontal line is the point of neutral stability. Note that at this local scale, it takes ~ 2.5 hrs. for sub- and above-canopy flows to adjust to the new ABL state.

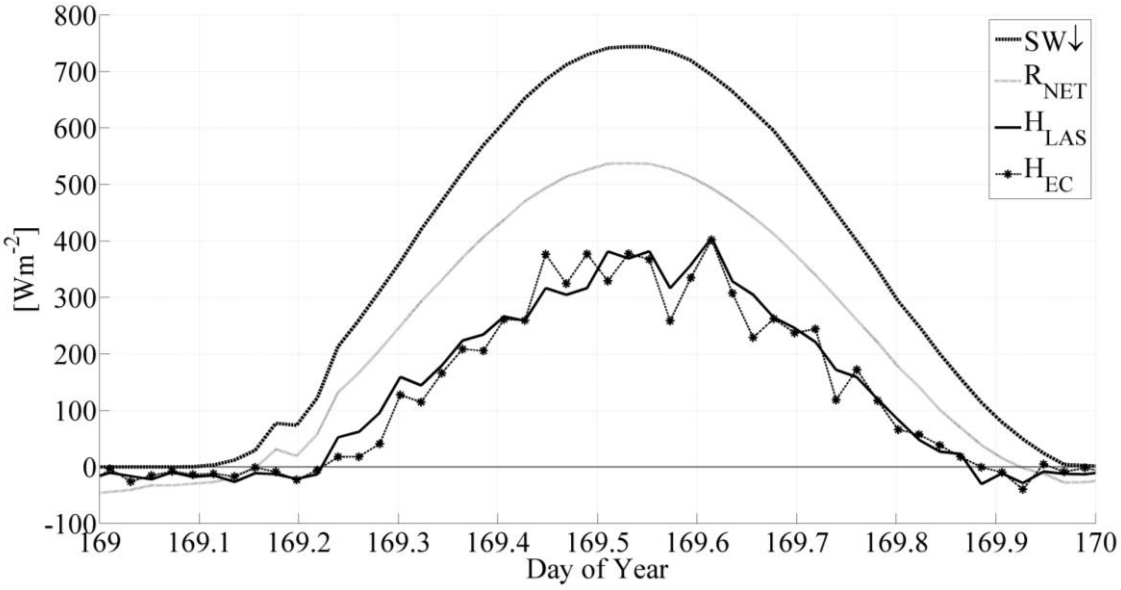

Figure 4.6 Flux values for an ideal summer day in the boreal forest, (June 18, 2013). The horizontal line indicates a flux of 0 W m^{-2} for reference.

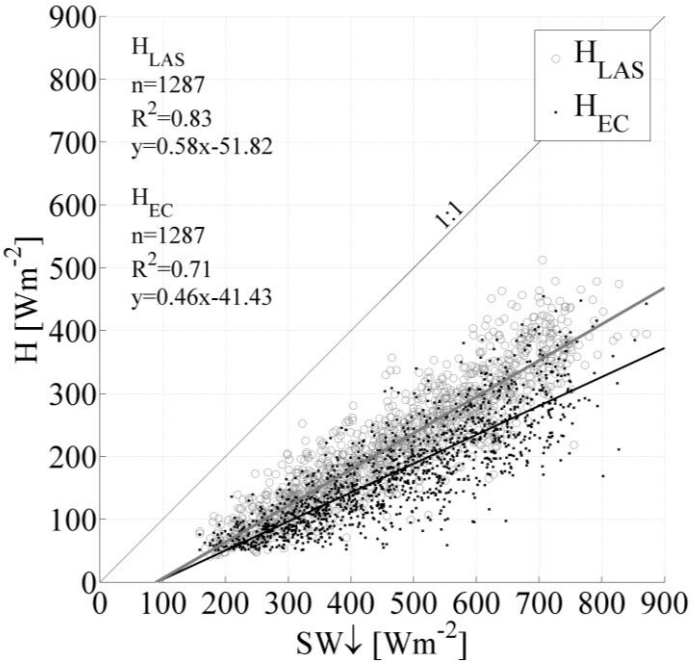

Figure 4.7 H_{LAS} and H_{EC} plotted against SW↓ for high flux regime data.

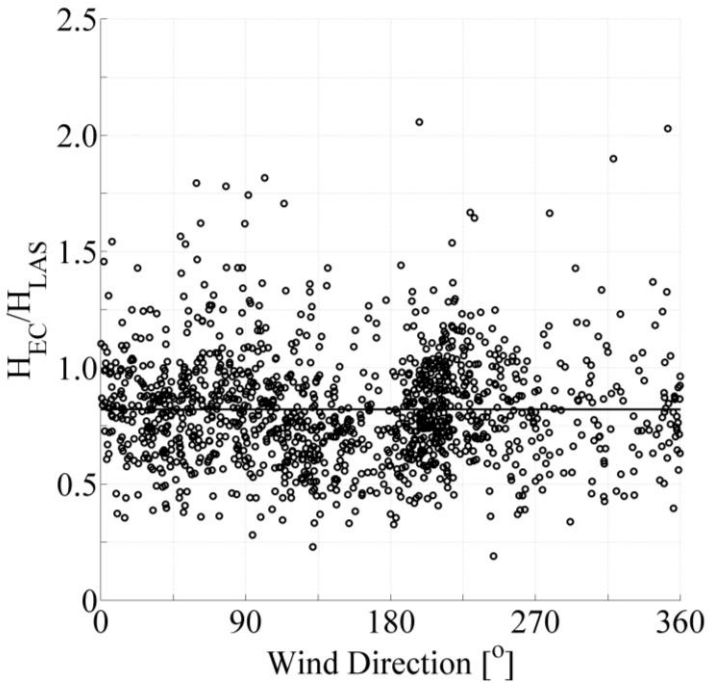

Figure 4.8 The ratio of H_{EC}/H_{LAS} as a function of wind direction measured from the sonic anemometer for high flux regime data. Horizontal line is the mean of H_{EC}/H_{LAS}.

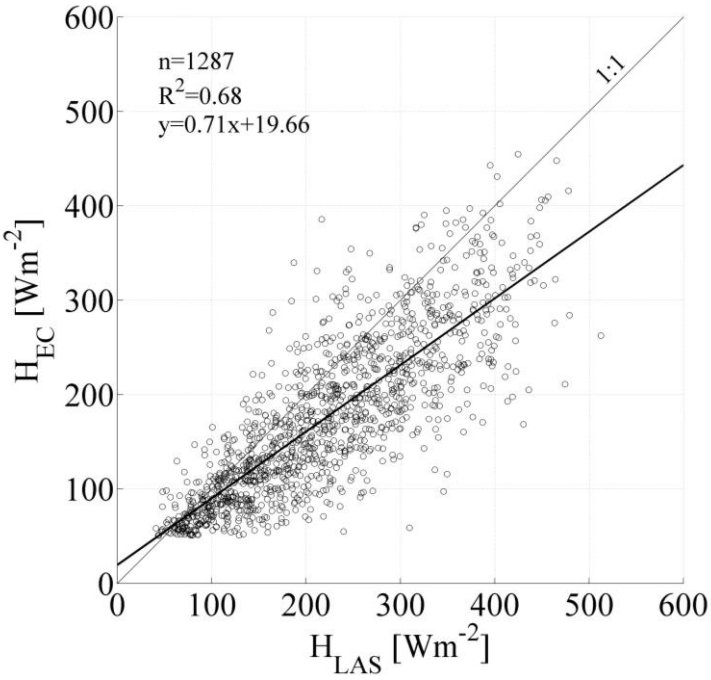

Figure 4.9 Scatter plot of H_{LAS} and H_{EC} for high flux regime. Sample size is 1287 half-hour periods.

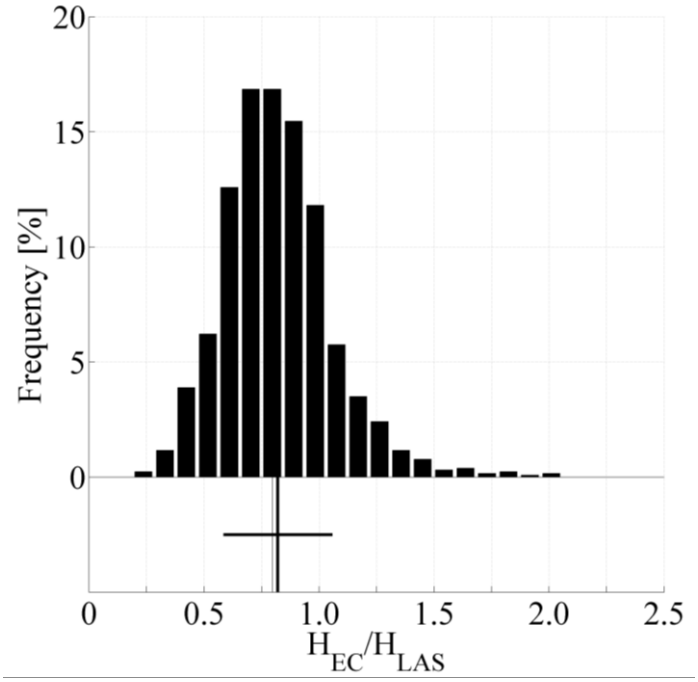

Figure 4.10 Histogram of H_{LAS}/H_{EC} for high flux regime. Thick (thin) vertical line is the mean (median), and the horizontal line is ± one standard deviation.

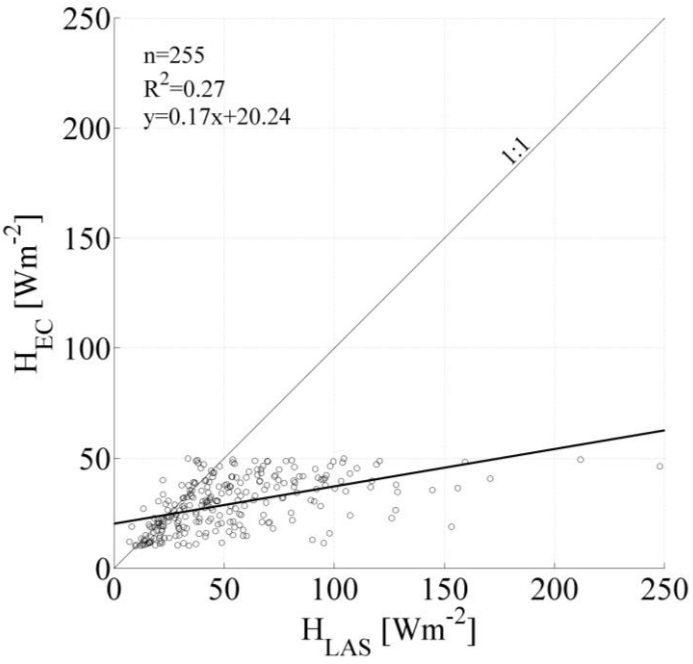

Figure 4.11 Scatter plot of H_{LAS} and H_{EC} for low flux regime.

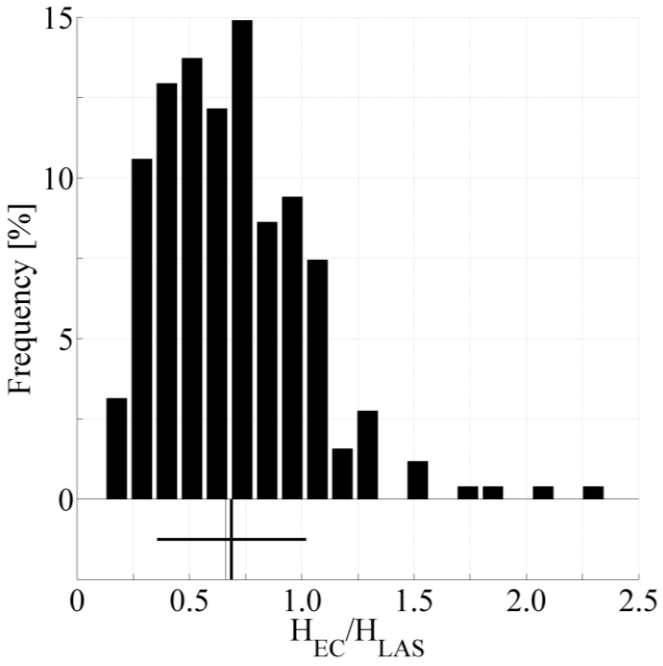

Figure 4.12 Histogram of H_{LAS}/H_{EC} for low flux regime. Thick (thin) vertical line is the mean (median), and the horizontal line is ± one standard deviation.

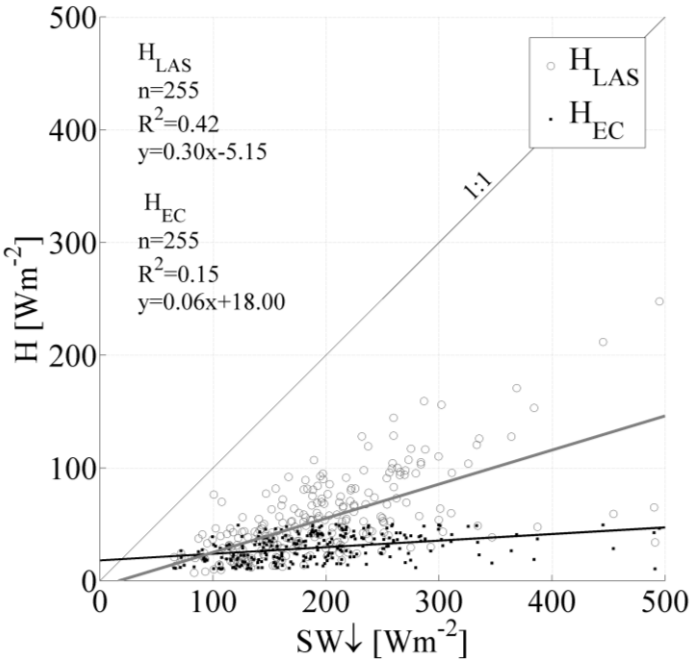

Figure 4.13 H_{LAS} and H_{EC} plotted against SW↓ for low flux regime data.

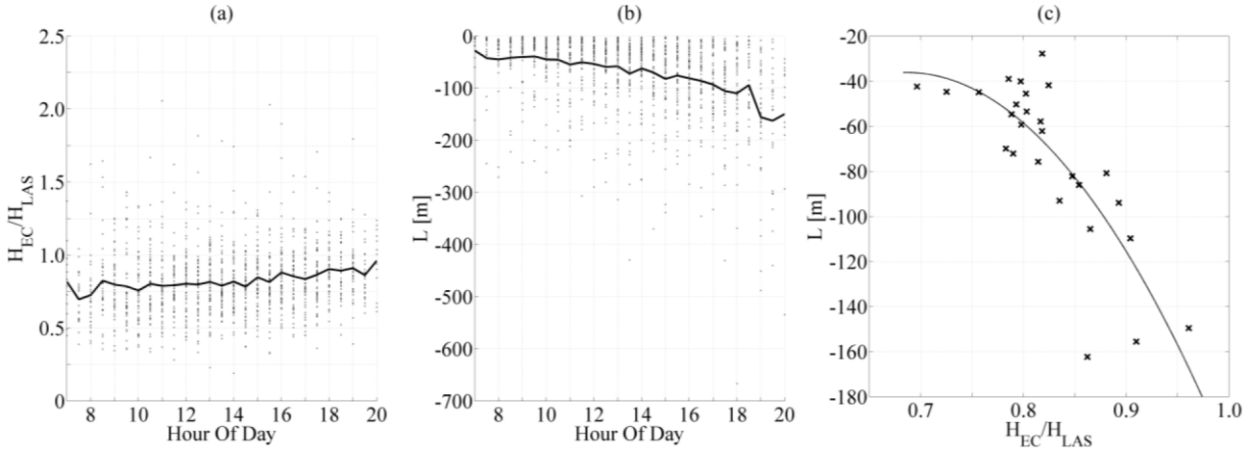

Figure 4.14 Mean diurnal pattern of H_{EC}/H_{LAS} (a), mean diurnal pattern of Obukhov length (b), and the relationship between them fitted with a second order curve (c) for the high flux regime. In panel (a) and (b), the black dots are all available data, while the solid curves are the mean diurnal pattern.

Table 4.1 Available half-hour periods for H_{EC} and H_{LAS}. Columns 1 is the description of the meteorological conditions; columns 2 and 4 are the number of half-hour periods that meet the description in column1 for HEC and HLAS, respectively; columns 3 and 5 are the percentages of the total available data; last rows indicate the periods that constitute high flux regime and low flux regime data as described in the text.

	H_{EC}		**H_{LAS}**	
Total Available Data (Half-hour Periods)	4018		3528	
Total Periods with Precipitation	333	*8.3%*	308	*8.7%*
Total Periods with Smoke	204	*5.1%*	188	*5.3%*
Total Periods with Fog	7	*0.2%*	2	*0.1%*
High Flux Regime	1287	*32.0%*	1237	*36.5%*
Low Flux Regime	255	*6.3%*	255	*7.2%*

Table 4.2 Results of solar radiation analysis. Row 1 is the threshold of the ratio SW_{OBS}/SW_{MOD} that is being used; Row 2 shows the total number of half-hour periods available based on that threshold; Rows 3 is the correlation coefficient (R) of H_{LAS} to H_{EC}, and Rows 4-8 show statistical information about the ratio of H_{EC}/H_{LAS}, including the mean, the median, the standard deviation (σ), the maximum (max) and the minimum (min) values.

Threshold	**0.4**	**0.5**	**0.6**	**0.7**	**0.8**	**0.9**	**1.0**	**1.1**	**1.2**	**1.3**	**1.4**	**1.5**
Periods Used	1283	1268	1220	1169	1056	953	858	732	630	439	292	150
R	0.82	0.82	0.81	0.81	0.80	0.80	0.80	0.79	0.79	0.84	0.85	0.87
mean (H_{EC}/H_{LAS})	0.82	0.82	0.82	0.82	0.82	0.83	0.83	0.83	0.83	0.82	0.82	0.85
median (H_{EC}/H_{LAS})	0.80	0.80	0.80	0.80	0.80	0.81	0.81	0.81	0.81	0.81	0.83	0.86
σ (H_{EC}/H_{LAS})	0.24	0.24	0.24	0.24	0.24	0.23	0.23	0.24	0.23	0.20	0.20	0.17
max (H_{EC}/H_{LAS})	2.06	2.06	2.06	2.06	2.03	2.03	2.03	2.03	1.82	1.82	1.79	1.54
min (H_{EC}/HLAS)	0.19	0.19	0.19	0.19	0.19	0.19	0.19	0.19	0.19	0.28	0.36	0.39

Chapter 5 Conclusions

The nature of the turbulent sensible heat flux regime in a black spruce boreal forest of interior Alaska was investigated at three scales: (a) locally at one micrometeorological tower below and above canopy, via the analysis of coherent structures; (b) horizontally between two micrometeorological towers 600 m apart and in distinctly different canopy architectures, through the thermal regime and the magnitude of the sensible heat flux; and (c) across the landscape scale (~ 1.4 km), by comparing large-scale area-averaged fluxes derived from scintillometry to local values from eddy covariance in order to assess the feasibility of upscaling over a heterogeneous boreal forest canopy for unstable summer daytime periods.

At the local study, a version of the Stokes parameters was employed to obtain a quantitative evaluation of the significant degree of wave-like behavior within the sub and above canopy flows in the boreal forest. This has critical implications for boundary layer studies because waves can have complex interactions with turbulence [*Finnigan et al.*, 1984]. Wave-like behavior is also important for energy exchange analyses since waves are a sign of stable stratification, a condition wherein drainage flows can remove carbon dioxide fluxes before they can be measured above the forest [*Grace et al.*, 1996]. In addition, less than a quarter of the coherent structures detected below and above the boreal forest canopy were synchronous, suggesting a lack of coupling between these levels such that energy fluxes measured below canopy may not always propagate to upper levels.

The horizontal study revealed that different thermal regimes, different stability transition times, and significant variations in sensible heat fluxes occur as a function of canopy architecture

even under consistent boundary layer conditions. Furthermore, the largest local flux value was not from the highest instrument with the greatest footprint area, but rather from the instrument closer to the canopy where its proximity to greater shear and canopy heating resulted in the highest sensible heat flux on average. These results suggest that any studies requiring ground observations for model validation need to consider where observation towers are located within the black spruce forest. Since landscape scale fluxes are the mean (not the sum) of all local fluxes, local observations should be situated with this in mind.

The large-scale study revealed the complexity in determining the time where stability transitions (from stable to unstable, or vice-versa). Taking the vertical temperature difference from various sensors at one tower showed as much as a 2.5 hour discrepancy in defining the unstable daytime period, which is significant for studies that focus on times when the boundary layer transitions. For the boreal forest, a time window of 0700 to 2000 Alaska Standard Time was determined by the minima in the mean diurnal cycle of C_n^2. This same time window was shown to agree with the majority of the periods with a vigorous, unstable flux regime where the local flux exceeds 50 W m^{-2} [*Prueger et al.*, 2004]. Ultimately, the large-scale study concluded that upscaling the local to the large-scale sensible heat flux for seasonal averages is feasible in the boreal forest, but only under prescribed meteorological conditions when fluxes are large and unstable such that local fluxes are well integrated into the landscape scale. Under such conditions, the local flux captures about 82% of the large-scale flux, and this relationship remains even when the amount of incoming solar radiation varies due to cloud cover. Data under weaker flux regimes require additional consideration, as the local and large-scale fluxes have a much poorer relationship to one another and to incoming solar radiation. For the high flux

regime, a finer resolution of upscaling can be provided based on the mean diurnal pattern of H_{EC}/H_{LAS} and the Obukhov length (L). Namely, as the boundary layer becomes less unstable in late afternoon, H_{EC}/H_{LAS} increases, supporting that the eddy covariance technique can capture more of the large-scale flux when the boundary layer is more shear-driven (less buoyancy driven) [*Mahrt*, 1998].

Overall, this multi-scale analysis provides three levels of critical information for the investigation of turbulent energy exchanges within and above the heterogeneous black spruce boreal forest of Alaska. Satellite remote sensing models often require ground observations at the local scale (~ 100 m) and/or the regional scale (~1 km) to validate results. This study suggests a ratio of 0.82 for the local to large-scale flux, with the local flux from the sonic anemometer being comparable to a LANDSAT pixel and the flux derived from the large aperture scintillometer being comparable to that from a MODIS pixel (Figure 5.1). In addition, when model results differ from observations, a physical explanation based on a thorough understanding of the turbulent energy exchange is required. This study suggests that the location within and above the heterogeneous canopy where the local observations are taken must be carefully chosen, and cautions that in the subarctic, winds are often low and the flow is complex, such that fluxes measured below canopy may not always propagate to above canopy levels. Therefore, disagreement between models and observations must be carefully reviewed with the precise meteorological and surface conditions before such discrepancies are reported or discussed, and before model performance is rated.

Owing to the lack of studies employing scintillometers in the boreal forest, it is recommended that future studies in this location be designed similarly to studies done over

patchy terrain in lower latitudes. For instance, across sections of different land surface types, multiple micrometeorological towers can be employed so that their aggregated flux values can be directly compared to the large area-average mean value derived from a scintillometer [e.g., *Beyrich et al.*, 2002, 2006; *Ezzahar et al.*, 2009]. In this vein, different micrometeorological towers located within areas of distinctly different canopy architectures of the spruce forest, but arranged along the path of the scintillometer beam, would enable a more robust comparison of the area-averaged value from each tower (weighted by its source area contribution) to the scintillometer value. This would assist in benchmarking the local and large-scale fluxes by providing a measure of the degree to which each instrument was performing within the context of the entire forest area and all of its variation. In addition, and at a finer scale, sonic anemometers at multiple heights along each tower would enable more measurements of the complex vertical profile of local sensible heat fluxes. This would also enable a comparison of the cospectra of the turbulent components (e.g. $w'\theta'$ and $u'w'$) at various heights above ground, the differences in which may give insight into the height at which the surface layer above the vegetation canopy begins to behave more like that expected over a smoother surface (i.e., more consistent with the Monin-Obukhov Similarity hypothesis). This height could then be compared to a calculated blending height, and would provide information on the optimum height at which the tallest sonic anemometer and the scintillometer beam should be located such that local differences in fluxes are being integrated [*Wieringa,* 1976; *Meijninger et al.,* 2002]. In locations where inhomogeneities are less pronounced and the turbulence is driven by mechanical shear, the height in which the landscape flux can be attained can be lower.

It is also recommended that studies employing tower measurements and scintillometers within the boreal forest be located across latitudinal climate and ecological zones (e.g., Delta Junction, Fairbanks, Fort Yukon, Arctic Village, and Toolik in Alaska). This would enable the ability to track temporal changes in meteorological and ecological parameters as climate shifts occur. In particular, the zone of transition between taiga and tundra is a highly sensitive ecotone where spatial and temporal surface energy exchange processes should be monitored at the local and the large-scale, especially if vegetation canopies expand poleward [*Serreze and Barry,* 2005 (and citations contained therein)]. Not only might the energy exchange between the surface and the atmosphere change over time due to climate warming, but the surface roughness will change as well, which means that despite each experimental site being static in location, its surface properties would be dynamically evolving. Such a study could be accompanied by an attendant temporal satellite image analysis to compliment the surface observations and continue to advance models that forecast climate change for the subarctic and the arctic.

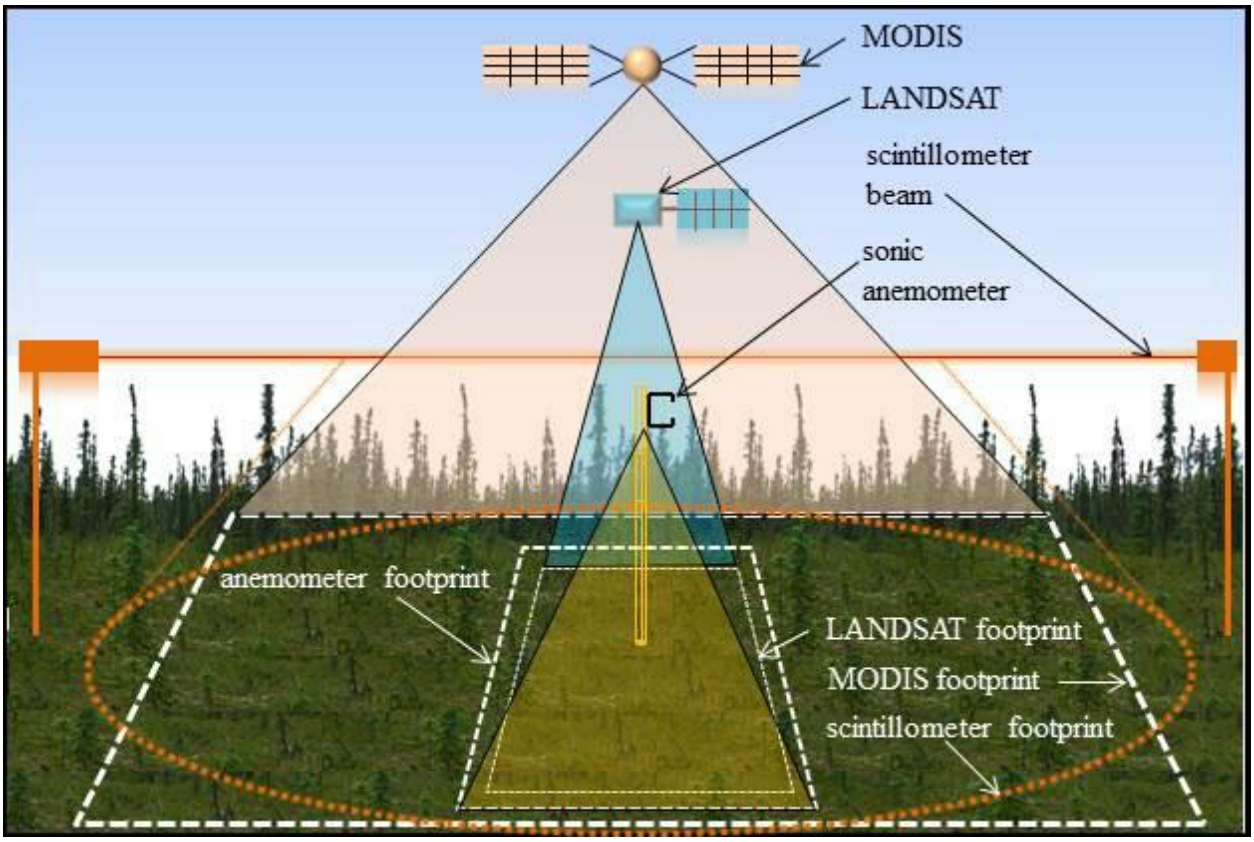

Figure 5.1 Local and large-scale flux measurements compared with satellites of similar scales (diagram is not to scale).

References Cited

Acevedo, O. C., O. L. L. Moraes, G. A. Degrazia, and L. E. Medeiros (2006), Intermittency and exchange of scalars in the nocturnal surface layer, *Boundary-Layer Meterol., 119*(1), 41-55, doi: 10.1007/s10546-005-9019-3.

Arya, S. P. (1988), *Introduction to micrometeorology*, Academic Press, San Diego, CA.

Barr, A. G., K. Morgenstern, T. A. Black, J. H. McCaughey, and Z. Nesic (2006), Surface energy balance closure by the eddy-covariance method above three boreal forest stands and implications for the measurement of the CO_2 flux, *Agric. Forest Meteorol., 140*(1-4), 322-337, doi: 10.1016/j.agrformet.2006.08.007.

Beyrich, F., H. A. R. De Bruin, W. M. L. Meijninger, J. W. Schipper, and H. Lohse (2002), Results from one-year continuous operation of a large aperture scintillometer over a heterogeneous land surface, *Boundary-Layer Meterol., 105*(1), 85-97, doi: 10.1023/A:1019640014027.

Beyrich, F., J.-P. Leps, M. Mauder, J. Bange, T. Foken, S. Huneke, H. Lohse, A. Ludi, W. M. L. Meijninger, D. Mironov, U. Weisensee, and P. Zittel (2006), Area-averaged surface fluxes over the LITFASS region based on eddy-covariance measurements, *Boundary-Layer Meteorol., 121*(1), 33-65, doi: 10.1007/s10546-006-9052-x.

Bonan, G. B., and H. H. Shugart (1989), Environmental factors and ecological processes in boreal forests, *Annu. Rev. Ecol. Syst., 20*(1), 1-28, doi: 10.1146/annurev.es.20.110189.000245.Duffy, P. A., J. Epting, J. M. Graham, T. S. Rupp, and A. D. McGuire (2007), Analysis of Alaskan burn severity patterns using remotely sensed data, *Int. J. Wildland Fire, 16*(3), 277-284, doi: 10.1071/WF06034.

Chapin III, F. S., A. D. McGuire, J. Randerson, R. Pielke Sr., D. Baldocchi, S. E. Hobbie, N. Roulet, W. Eugster, E. Kasischke, E. B. Rastetter, S. A. Zimov, and S. W. Running (2000), Arctic and boreal ecosystems of western North America as components of the climate system, *Global Change Biology*, *6*(S1), 211–223, doi: 10.1046/j.1365-2486.2000.06022.x.

Chapin III, F. S., M. Sturm, M. C. Serreze, J. P. McFadden, J. R. Key, A. H. Lloyd, A. D. McGuire, T. S. Rupp, A. H. Lynch, J. P. Schimel, J. Beringer, W. L. Chapman, H. E. Epstein, E. S. Euskirchen, L. D. Hinzman, G. Jia, C.-L. Ping, K. D. Tape, C. D. C. Thompson, D. A.Walker, and J. M. Welker (2005), Role of land-surface changes in Arctic summer warming, *Science*, *310*(5748), 657-660, doi: 10.1126/science.1117368.

Chapin III, F. S., M. W. Oswood., K. Van Cleve., L. A. Viereck, and D. L. Verbyla (2006), *Alaska's Changing Boreal Forest,* Oxford University, New York, N.Y.

Duffy, P. A., J. Epting, J. M. Graham, T. S. Rupp, and A. D. McGuire (2007), Analysis of Alaska burn severity patterns using remotely sensed data, *Int. J. Wildland Fire*, *16*(3), 277-284, doi: 10.1071/WF06034.

Eder, F., F. De Roo, K. Kohnert, R. L. Desjardins, H. P. Schmid, and M. Mauder (2014), Evaluation of two energy balance closure parameterizations, *Boundary-Layer Meteorol.*, *151*(2), 195-219, doi: 10.1007/s10546-013-9904-0.

Ezzahar, J., A. Chehbouni, J. Hoedjes, D. Ramier, N. Boulain, S. Boubkraoui, B. Cappelaere, L. Descroix, B. Mougenot, and F. Timouk (2009), Combining scintillometer measurements and an aggregation scheme to estimate area-averaged latent heat flux during the AMMA experiment, *J. Hydrol.*, *375*(1-2), 217-226, doi: 10.1016/j.jhydrol.2009.01.010.

Finnigan, J. J., F. Einaudi, and D. Fua (1984), The interaction between an internal gravity wave and turbulence in the stably-stratified nocturnal boundary layer, *J. Atmos. Sci.*, *41*(16), 2409-2436, doi: 10.1175/1520-0469(1984)041<2409:TIBAIG>2.0.CO;2.

Fleming, M. D. (1997), A statewide vegetation map of Alaska using phenological classification of AVHRR data, in Proceedings of the Second Circumpolar Arctic Vegetation Mapping Workshop and the CAVM-North America Workshop, pp. 25-26, Arendal, Norwary.

Foken, T. (2008), The energy balance closure problem: an overview, *Ecol. Appl.*, *18*(6), 1351-1367, doi: 10.1890/06-0922.1.

Foken, T., M. Mauder, C. Liebethal, F. Wimmer, F. Beyrich, J.-P. Leps, S. Raasch, H. A. R. DeBruin, W. M. L. Meijninger, and J. Bange (2010), Energy balance closure for the LITFASS-2003 experiment, *Theor. Appl. Climatol.*, *101*(1-2), 149-160, doi: 10.1007/s00704-009-0216-8.

Grace, J., Y. Malhi, J. Lloyd, J. McIntyre, A. C. Miranda, P. Meir, and H. S. Miranda (1996), The use of eddy covariance to infer the net carbon dioxide uptake of Brazilian rain forest, *Glob. Change Biol.*, *2*(3), 209-217, doi: 10.1111/j.1365-2486.1996.tb00073.x.

Hinzman, L.D., and D.L. Kane (1992), Potential Response of an Arctic Watershed during a Period of Global Warming, *Journal of Geophysical Research*, *97*(03), 2811-2820, doi: 10.1029/91JD01752.

Holton, J. R. (1992), *An Introduction to Dynamic Meteorology*, 3rd ed., Academic Press, San Diego, CA.

Johnson, E. A. (1996), *Fire and Vegetation Dynamics: Studies from the North American Boreal Forest*, Cambridge University Press, New York.

Jorgenson, M. T., C. H. Racine, J. C. Walters, and T. E. Osterkamp (2001), Permafrost degradation and ecological changes associated with a warming climate in central Alaska, *Climate Change*, *48*(4), 551-579, doi: 10.1023/A:1005667424292.

Jorgenson, M. T., Y. L. Shur, and E. R. Pullman (2006), Abrupt increase in permafrost degradation in Arctic Alaska, *Geophys. Res. Lett.*, *33* (L02503), 1-4, doi: 10.1029/2005GL024960.

Kimball, J. S., M. Zhao, K. C. McDonald, and S.W. Running (2006), Satellite remote sensing of terrestrial net primary production for the Pan-Arctic Basin and Alaska, *Mitigation and Adaptation Strategies for Global Climate Change*, *11*(4), 783-804, doi: 10.1007/s11027-005-9014-5.

Mahrt, L (1998), Flux sampling errors for aircraft and towers, *J. Atmos. Oceanic Technol.*, *15*(2), 416-429, doi: 10.1175/1520-0426(1998)015<0416:FSEFAA>2.0.CO;2.

Mauder, M., C. Liebethal, M. Gockede, J.-P. Leps, F. Beyrich, and T. Foken (2006), Processing and quality control of flux data during LITFASS-2003, *Boundary-Layer Meteorol.*, *121*(1), 67-88, doi: 10.1007/s10546-006-9094-0.

Mayfield, J. A., and G. J. Fochesatto (2013), The layered structure of the winter atmospheric boundary layer in the interior of Alaska, *J. Appl. Meteorol. Climatol.*, *52*(4), 953-973, doi: 10.1175/JAMC-D-12-01.1.

Meijninger, W. M. L., O. K. Hartogensis, W. Kohsiek, J. C. B. Hoedjes, R. M. Zuurbier, and H. A. R. De Bruin (2002), Determination of area-averaged sensible heat fluxes with a large aperture scintillometer over a heterogeneous surface – Flevoland field experiment, *Boundary-Layer Meteorol.*, *105*(1), 37-62, doi: 10.1023/A:1019647732027.

Osterkamp, T. E., L. Viereck, Y. Shur, M. T. Jorgenson, C. Racine, A. Doyle, and R. D. Boone (2000), Observations of thermokarst and its impact on boreal forests in Alaska, *Arct. Antarc. Alp. Res.*, *32*(3), 303-315, doi: 10.2307/1552529.

Osterkamp, T. E., M. T. Jorgenson, E. A. G. Shuur, Y. L. Shur, M. Z. Kanevskiy, J. G. Vogel, and V. E. Tumskoy (2009), Physical and ecological changes associated with warming permafrost and thermokarst in interior Alaska, *Permafrost Periglac.*, *20*(3), 235-256, doi: 10.1002/ppp.656.

Prueger, J. H., Kustas, W. P., Hipps, L. E., and J. L. Hatfield, (2004), Aerodynamic parameters and sensible heat flux estimates for a semi-arid ecosystem, *J. Arid Environ.*, *57*(1), 87-100, doi: 10.1016/S0140-1963(03)00090-9.

Randerson, J. T., H. Liu, M. G. Flanner, S. D. Chambers, Y. Jin, P. G. Hess, G. Pfister, M. C. Mack, K. K. Treseder, L. R. Welp, F. S. Chapin, J. W. Harden, M. L. Goulden, E. Lyons, J. C. Neff, E. A. G. Schuur, and C. S. Zender (2006), The impact of boreal forest fire on climate warming, *Science, 314*(5802), 1130-1132, doi: 10.1126/science.1132075.

Rawlins, M.A., M. Steele, M.M. Holland, J.C. Adam, J.E. Cherry, J.A. Francis, P.Y. Groisman, L.D. Hinzman, T.G. Huntington, D.L. Kane, J.S. Kimball, R. Kwok, R.B. Lammers, C.M. Lee, D.P. Lettenmaier, K.C. McDonald, E. Podest, J.W. Pundsack, B. Rudels, M.C. Serreze, A. Shiklomanov, O. Skagseth, T.J. Troy, C.J. Vorosmarty, M. Wensnahan, E.F. Wood, R. Woodgate, D. Yang, K. Zhang, T. Zhang, (2010), Analysis of the Arctic System for Freshwater Cycle Intensification: Observations and Expectations, *Journal of Climate*, *23*, doi: 10.1175/2010JCLI3421.1.

Samain, B., G. W. H. Simons, M. P. Voogt, W. Defloor, N.-J. Bink, and V. Pauwels (2012), Consistency between hydrological model, large aperture scintillometer and remote sensing based evapotranspiration estimates for a heterogeneous catchment, *Hydrol. Earth Syst. Sci.*, *16*(7), 2095 - 2107, doi: 10.5194/hess-16-2095-2012.

Sellers, P. J., F. G. Hall, R. D. Kelly, A. Black, D. Baldocchi, J. Berry, M. Ryan, K. J. Ranson, P. Crill, D. Lettenmaier, H. Margolis, J. Cihlar, J. Newcomer, D. Fitzjarrald, P. G. Jarvis, S. T. Gower, D. Halliwell, D. Williams, B. Goodison, D. E. Wickland, and F. E. Guertin (1997), BOREAS in 1997: experiment overview, scientific results, and future directions, *J. Geophys. Res.-Atmos.*, *102*(D24), 28731-28769, doi: 10.1029/97JD03300.

Serreze, M. C., and R. G. Barry (2005), *The Arctic Climate System*, Cambridge University Press, Cambridge, United Kingdom.

Shulski, M., and G. Wendler (2007), *The Climate of Alaska*, University of Alaska, Fairbanks, AK.

Stull, R. B. (1988), *An Introduction to Boundary Layer Meteorology*, Kluwer Academic, Dordrecht, Netherlands.

Ueyama, M., Y. Harazono, and K. Ichii (2010), Satellite-based modeling of the carbon fluxes in mature black spruce forests in Alaska: a synthesis of the eddy covariance data and satellite remote sensing data, *Earth Interactions*, *14*(13), 1-27, doi: 10.1175/2010EI319.1.

Ueyama, M., K. Ichii, H. Iwata, E. S. Euskirchen, D. Zona, A. V. Rocha, Y. Harazono, C. Iwama, T. Nakai, W. C. Oechel (2014), Change in surface energy balance in Alaska due to fire and spring warming, based on upscaling eddy covariance measurements, *J. Geophys. Res.-Biogeo.*, *119*(10), 1947-1969, doi: 10.1002/2014JG002717.

Ward, H.C., J. G. Evans, and C.S.B. Grimmond (2014), Multi-scale sensible heat fluxes in the suburban environment from large-aperture scintillometry and eddy covariance, *Boundary-Layer Meterol.*, *152*(1), 65-89, doi: 10.1007/s10546-014-9916-4.

Wendler, G., and M. Shulski (2009), A century of climate change for Fairbanks, Alaska, *Arctic*, *62*(3), 295-300, stable URL: http://www.jstor.org/stable/40513307.

Wieringa, J. (1976), An objective exposure correction method for average wind speeds measured at a sheltered location, *Quart. J. R. Met. Soc.*, *102*(431), 241-253, doi: 10.1002/qj.49710243119.

Wilmking, M., G. P. Juday, V. A. Barber, and H. S. J. Zald (2004), Recent climate warming forces contrasting growth responses of white spruce at treeline in Alaska through temperature thresholds, *Glob. Change Biol. 10*(10), 1724-1736, doi: 10.1111/j.1365-2486.2004.00826.x.

Woo, M.K., D.L. Kane, S.K. Carey, and D. Yang (2008), Progress in Permafrost Hydrology in the New Millennium, *Permafrost and Periglacial Processes*, *19*(2), 237-254, doi: 10.1002/ppp.613.

Wyngaard, J.C., Izumi, Y., and S.A. Collins (1971), Behavior of the refractive-index-structure parameter near the ground, *J. Optical Soc. of America*, *61*(12), 1646-1650, doi: http://dx.doi.org/10.1364/JOSA.61.001646.

Xiao, J., J. Chen, K. J. Davis, and M. Reichstein (2012), Advances in upscaling of eddy covariance measurements of carbon and water fluxes, *J. Geophys. Res.-Biogeo.*, *117*(G1), doi: 10.1029/2011JG001889.

Appendix: Co-author Permission

This research was supported by the Alaska NASA EPSCoR program award NNX10NO2A, by the Alaska Space Grant Program, by the "New GK-12 Program: The CASE (Changing Alaska Science Education) for Enhancing Understanding of Climate Change" NSF (DGE-0948029), as well as by travel grants from the College of Natural Science and Mathematics and the Graduate School of the University of Alaska Fairbanks. We also thank the contributions of the following co-authors, whose permission to use this work is contained on the following pages:

USDA
United States Department of Agriculture
Agricultural Research Service

March 12, 2015

Derek Starkenburg
University of Alaska Fairbanks
Department of Atmospheric Sciences
Fairbanks, AK 99775

Mr. Starkenburg:

Although I am honored to be included as a co-author on the two manuscripts, *Temperature regimes and turbulent heat fluxes across a heterogeneous canopy in an Alaskan boreal forest* and *Multiscale Sensible Heat Fluxes above a Heterogeneous Canopy in an Alaskan Black Spruce Boreal Forest* that you have submitted for publication, the research they describe was developed and driven by you. As such, I would have no objection to their inclusion in your doctoral thesis; on the contrary, I strongly encourage you to include these papers as they reflect your hard work and effort to contribute toward our understanding of turbulent exchange processes in boreal forests. And, inasmuch as it is needed, you have my consent to do so.

If either you or any of the faculty and staff of the University of Alaska Fairbanks has additional questions concerning this matter, or if there is anything further that I can do on your behalf, please feel free to let me know.

Best Regards,

Joseph G. Alfieri

Hydrology and Remote Sensing Laboratory
Building 007, Room 104, BARC-West
10300 Baltimore Avenue
Beltsville, Maryland 20705

Dear Derek

I agree to use the contents of the paper entitled "Temperature regimes and turbulent heat fluxes across a heterogeneous canopy in an Alaskan boreal forest" into your thesis document of the UAF Graduate School.

Best Regards
Yoshinobu Harazono
International Arctic Research Center, UAF
930 Koyukuk Dr.
Fairbanks AK, 99775
1-907-474-5515
harazono2009GL@gmail.com
yharazono@alaska.edu

Dear Derek,

You have my permission to put the manuscript entitled /"Temperature regimes and turbulent heat fluxes across a heterogeneous canopy in an Alaskan boreal forest"/ into your compiled thesis document for use by the UAF Graduate School.
Congratulation for completing your PhD work!

Sincerely,
Hiroki Iwata
March 13th, 2015
Hiroki IWATA (岩田 拓記)
E-mail: hiwata(at)shinshu-u.ac.jp
Tel.: 0263-37-2502
Department of Environmental Sciences, Faculty of Science
Shinshu University
3-1-1 Asahi, Matsumoto, Nagano, 390-8621

Dear Derek,

I agree to put the manuscript entitled "Temperature regimes and turbulent heat fluxes across a heterogeneous canopy in an Alaskan boreal forest" into your thesis for use by the UAF Graduate School.
Sincerely yours,
Hirohiko Nagano

Hirohiko Nagano
Visiting Research Scholar
International Arctic Research Center
University of Alaska, Fairbanks
Akasofu Bldg. #207-A, Koyukuk Dr. 930
Fairbanks, Alaska, USA 99775-7340

Tel: +1-907-474-7337
email:
naganohirohiro@yahoo.co.jp
hnagano@alaska.edu